DOI: 10.1002/anie.201201200

Photocatalysis with Visible Light

Semiconductor Photocatalysis—Mechanistic and Synthetic Aspects

*Horst Kisch**

Keywords:
electron transfer · photocatalysis · photochemistry · semiconductors · synthetic methods

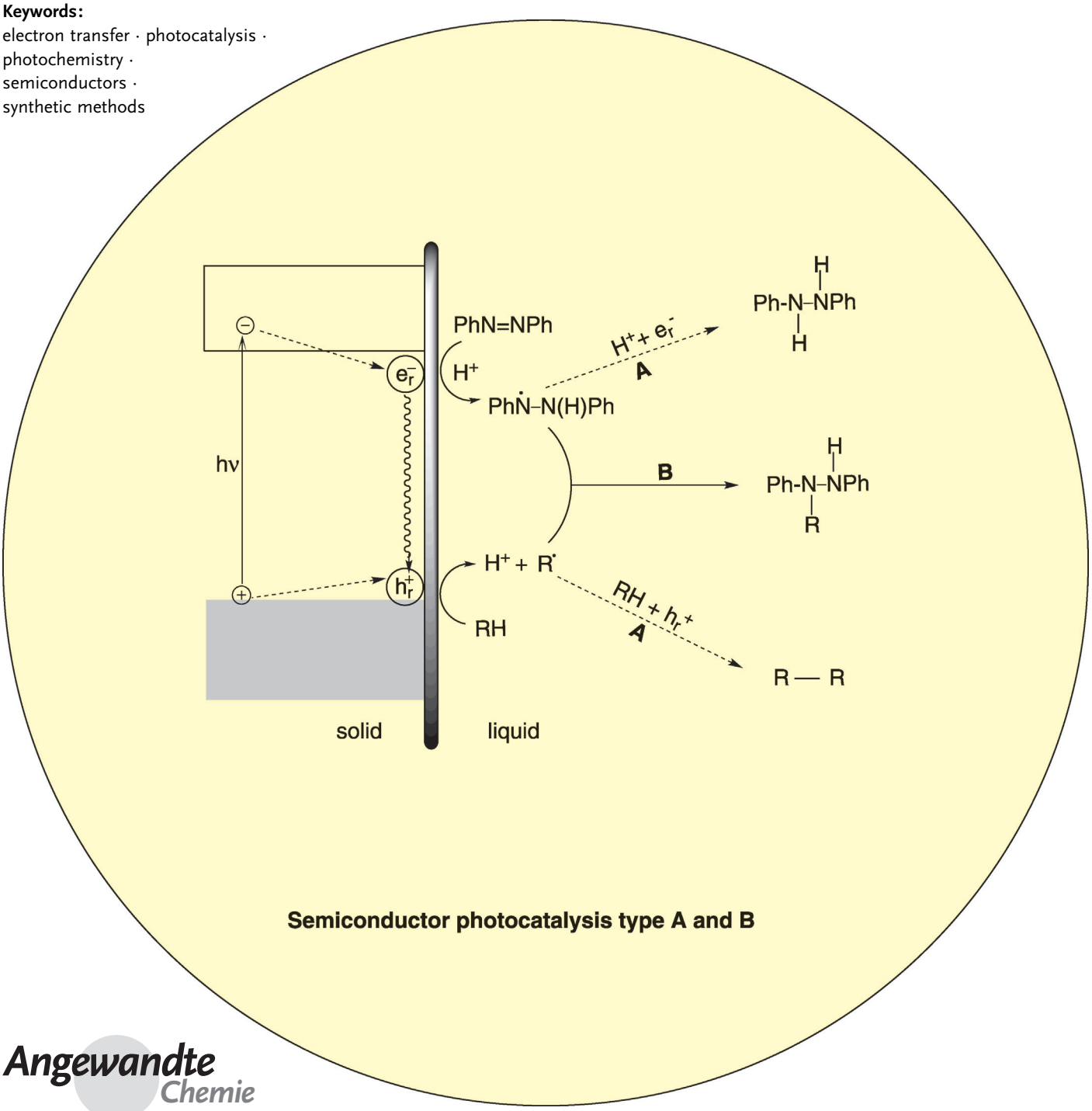

Semiconductor photocatalysis type A and B

Preceding work on photoelectrochemistry at semiconductor single-crystal electrodes has formed the basis for the tremendous growth in the three last decades in the field of photocatalysis at semiconductor powders. The reason for this is the unique ability of inorganic semiconductor surfaces to photocatalyze concerted reduction and oxidation reactions of a large variety of electron-donor and -acceptor substrates. Whereas great attention was paid to water splitting and the exhaustive aerobic degradation of pollutants, only a small amount of research also explored synthetic aspects. After introducing the basic mechanistic principles, standard experiments for the preparation and characterization of visible light active photocatalysts as well as the investigation of reaction mechanisms are discussed. Novel atom-economic C–C and C–N coupling reactions illustrate the relevance of semiconductor photocatalysis for organic synthesis, and demonstrate that the multidisciplinary field combines classical photochemistry with electrochemistry, solid-state chemistry, and heterogeneous catalysis.

From the Contents

1. Introduction

The photochemistry of transition-metal complexes and semiconductor surfaces has received increasing attention to address the problem of chemical utilization of solar energy. Research into this topic started in the 1970s, declined in the 1990s, and restarted at the turn of the new century. Many review articles were published that dealt with relevant areas such as homogeneous metal complexes,[1] photoelectrochemistry at semiconductor electrodes,[2] and semiconductor photocatalysis at colloids[3] or powder suspensions.[4] The majority of studies in general photocatalysis research—homogeneous and heterogeneous—is concerned with the splitting of water into hydrogen and oxygen, the "holy grail" of photochemistry. This process was already predicted in 1874 by Jules Verne in his book "The Mysterious Island": *Yes, my friends, I believe that water will one day be employed as fuel, that hydrogen and oxygen which constitute it will furnish an inexhaustible source of heat and light. Water will be the coal of the future.*" In 1911 Wilhelm Ostwald wrote that "*mankind should cover a maximum part of its energy demand from solar energy.*"[5] In contrast to this artificial cleavage of water, in photosynthesis, that is, biological water cleavage, organic matter is produced instead of hydrogen by C–C coupling through carbon dioxide fixation. The key steps of this heterogeneous photocatalytic process are photoinduced charge separation, charge trapping, and interfacial electron exchange with water. A major part of the research in the field of semiconductor photocatalysis deals with aerobic photooxidation reactions that allow complete degradation of pollutants present in air and water. Different to water splitting, this type of photocatalysis is already utilized practically for air purification.[6] In contrast to these cleavage and degradation reactions, only a small amount of literature is concerned with bond-forming synthetic processes analogous to C–C coupling in photosynthesis. The use of solar energy to drive organic syntheses was already proposed by Ciamician in 1912: "*On the arid lands there will spring up industrial colonies without smoke and without smokestacks; forests of glass tubes will extend over the plants and glass buildings will rise everywhere*; *inside of these will take place the photochemical processes that hitherto have been the guarded secret of the plants*, *but that will have been mastered by human industry which will know how to make them bear even more abundant fruit than nature*, *for nature is not in a hurry and mankind is.*"[7,8]

Recent reviews deal with general photocatalysis of organic reactions, with the semiconductor-photocatalyzed organic transformations affording well-known products.[9] This Review is primarily concerned with synthetically useful bond formations that occur by excitation with visible light of semiconductor powders suspended in a liquid solution of substrates. Only in one case is the semiconductor present as a thin film. After a general introduction to semiconductor photocatalysis, including some characteristic examples for the preparation and characterization of photocatalysts, the areas of nitrogen fixation, C–H activation, and novel atom-economic organic reactions are discussed. All these processes contain as basic reaction steps the formation of N–H, C–S, C–C, and C–N bonds. The mechanistic discussion is aimed at proving experimentally the postulated key steps relevant to chemical synthesis. It may serve as a basic guideline for newcomers to the field of semiconductor photocatalysis. An attempt is also made to categorize the numerous previously

[*] Prof. Dr. H. Kisch
Department Chemie und Pharmazie
Universität Erlangen-Nürnberg
Egerlandstrasse 1, 91058 Erlangen (Germany)
E-mail: kisch@chemie.uni-erlangen.de

observed photocatalytic processes into two simple reaction classes, which are independent of the detailed mechanism.

2. Basic Aspects

The general principle of the conversion of light into chemical energy is summarized by Equations (1)–(7) for the sensitization of the redox reaction $A + D = A_{red} + D_{ox}$ by a transition-metal complex. The three key steps are photoinduced charge separation [Eqs. (1) and (2)] and electron exchange with donor and acceptor substrates D and A to afford primary redox products [Eqs. (3) and (4)], which are converted into stable final products [Eqs. (5) and (6)]. In the case of solar energy storage the overall reaction has to be endergonic, whereas for solar energy utilization it is in general exergonic. Although many systems undergo the first reaction step, only a few also enable the crucial electron-exchange steps because charge recombination is highly favored [Eq. (2)]. Even if these two critical steps proceed [Eqs. (3) and (4)], efficient back electron transfer (BET) between the primary redox products [Eq. (7)] prevents in most cases successive reactions to generate the final redox products [Eqs. (5) and (6)].

$$[M]-L \xrightarrow{h\nu} [M]^{\bullet+}-L^{\bullet-} \quad (1)$$

$$[M]^{\bullet+}-L^{\bullet-} \rightarrow [M]-L + h\nu/\text{heat} \quad (2)$$

$$[M]^{\bullet+}-L^{\bullet-} + A \rightarrow [M]^{\bullet+}-L + A^{\bullet-} \quad (3)$$

$$[M]^{\bullet+}-L + D \rightarrow [M]-L + D^{\bullet+} \quad (4)$$

$$A^{\bullet-} \rightarrow A_{red} \quad (5)$$

$$D^{\bullet-} \rightarrow D_{ox} \quad (6)$$

$$A^{\bullet-} + D^{\bullet+} \rightarrow A + D \quad (7)$$

Thus, the basic problem in the conversion of light into chemical energy is how to inhibit charge recombination and BET processes. In homogeneous systems, the problem is partially solved by making one of the redox steps, for example, Equation (4), so fast that it successfully competes with charge recombination. A typical example is the evolution of hydrogen upon irradiating an aqueous solution of a tris(bipyridyl)ruthenium(II) complex in the presence of methylviologen (*N*,*N*′-dimethyl-4,4′-dipyridinium, MV^{2+}, which corresponds to A) and a reducing agent such as triethylamine (which corresponds to D). In this system, the radical cation generated in the reaction step according to Equation (4) undergoes a fast and irreversible decomposition [Eq. (6)], thereby rendering the BET [(Eq. 7)] too slow to successfully compete with the formation of A_{red} [(Eq. (5)], which corresponds to the reduction of water by the reduced methylviologen.[10] The function of the transition-metal complex in this system is to photosensitize two consecutive homogeneous electron-exchange reactions with a donor and an acceptor.

The reaction sequence discussed above differs significantly from photosensitization by a semiconductor (in general, just termed photocatalysis), a reaction system wherein a solid photocatalyst simultaneously sensitizes two heterogeneous redox reactions. By analogy with Equations (1–7), the basic reaction steps may be summarized in a simplified way according to Equations (8)–(10).

$$SC \xrightarrow{h\nu} SC(e_r^-, h_r^+) \quad (8)$$

$$SC(e_r^-, h_r^+) \rightarrow SC + h\nu/\text{heat} \quad (9)$$

$$SC(e_r^-, h_r^+) + A + D \rightarrow SC + A^{\bullet-} + D^{\bullet+} \quad (10)$$

The absorption of light generates, amongst unreactive species, reactive electron–hole pairs trapped at the semiconductor surface. It is expected that the distance between these redox centers should be larger than in a molecular sensitizer and, therefore, charge recombination may become slow enough to allow the desired interfacial electron transfer (IFET) at the solid/liquid or solid/gas interface. The consecutive electron-exchange reactions in the homogeneous case [Eqs. (3) and (4)] become concerted in the heterogeneous system [Eq. (10)]. The subsequent reaction steps are described by Equations (5)–(7).

In principle, one expects that, similar to a molecule, the exited semiconductor may also undergo energy transfer [Eqs. (11) and (12)]. Experimental evidence for the formation of singlet oxygen was indeed reported.[11] Instead of energy transfer, singlet oxygen may also be formed by hole oxidation of superoxide [Eq. (13)] generated through the reduction of oxygen by the reactive electron.[11a,b]

$$SC \xrightarrow{h\nu} SC(e^-, h^+) \quad (11)$$

$$SC(e^-, h^+) + O_2 \xrightarrow{h\nu} SC + {}^1O_2 \quad (12)$$

$$O_2^- + h_r^+ \rightarrow {}^1O_2 \quad (13)$$

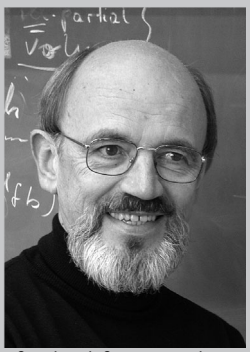

Horst Kisch, born 1942, studied chemistry at the Universität Wien, and completed his PhD in 1969 with Prof. Dr. O. E. Polansky, 1968–1984 at the Max-Planck-Institut für Strahlenchemie in Mülheim a.d. Ruhr. Since 1984 he has been Professor for Inorganic Chemisry at the Universität Erlangen-Nürnberg. His interests include the catalytic activation of 1,2-diazenes and the relationship between charge-transfer character and electrical conductance in metal dithiol/viologen charge-transfer complexes. More recently, semiconductor-catalyzed additions reactions of cyclic olefins to 1,2-diazenes and imines, the photofixation of nitrogen and the development of new semiconductor catalysts for reactions with daylight have formed the focus of his research.

2.1. Primary Processes

Depending on details of the electronic structure, the band-to-band transitions (Figure 1, cases A and D) may be allowed or forbidden, which are generally referred to as direct or

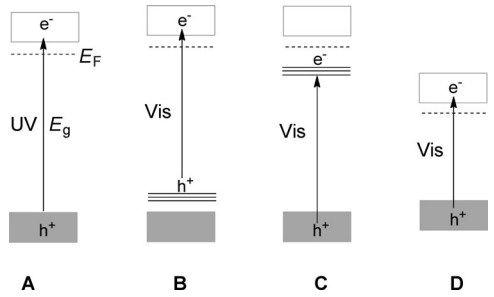

Figure 1. Schematic representation of the absorption of light by an n-type semiconductor crystal. In the case of a p-type material the Fermi level E_F is located close to the upper valence band edge. Shaded and empty rectangles correspond to occupied and empty energy bands, respectively, horizontal lines to localized electronic states. The distance between the Fermi level E_F and the conduction band for most *n*-type semiconductors is in the range 0.1–0.3 eV and depends on the dopant concentration.

indirect transitions. As a result thereof, the absorption coefficients are much larger for direct semiconductors such as cadmium or zinc sulfide than for indirect ones such as titania. Furthermore, the absorption spectrum of a direct semiconductor exhibits a steep onset, whereas an absorption tail and a flatter onset is observed for indirect semiconductors.[12] The valence band in simple binary oxides and sulfides has oxygen and sulfur character, respectively, whereas metal-based orbitals contribute predominately to the conduction band. These energy bands are delocalized throughout the crystal lattice. The bandgap E_g is defined as the energy difference between the edges of the conduction and valence bands and determines the minimum energy necessary for optical excitation. It amounts to 3.2 eV for the frequently used anatase titania crystal phase, thus indicating that only light of wavelengths shorter than 390 nm can be absorbed (Figure 2; corresponds to case A in Figure 1). The corresponding values for cadmium sulfide are 2.4 eV and 520 nm (Figure 2; corresponds to case D in Figure 1).

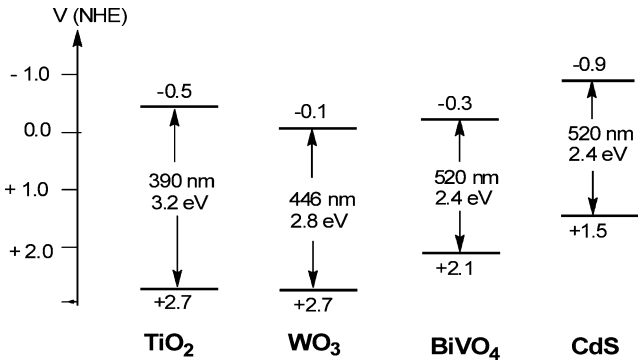

Figure 2. Band-edge positions of some semiconductor powders in contact with neutral water, light absorption onsets, and bandgap energies. TiO_2[13] WO_3,[14] $BiVO_4$,[15] CdS.[16]

The above discussion applies to an idealized semiconductor crystal containing no impurities or surface defects. However, this condition is never met in real practical photocatalysis. As a consequence thereof, new and localized electronic states located within the bandgap, generally called surface states, are always present in a real material. They may also be generated by adsorption of solvent and substrates onto the semiconductor surface. The surface states may act as charge-recombination centers, as well as reactive electron–hole pairs, thus controlling the IFET and, therefore, the photocatalytic activity. Two examples are given in Figure 1 that show two typical locations of such states, which are occupied in case B and unoccupied in case C. Depending on their concentration, they may induce the absorption of visible light, as can occur upon the controlled addition of dopants or surface modifiers. In some cases excitation within this new absorption band results in visible light induced photocatalytic activity of otherwise only UV-active semiconductors such as titania. In these cases, a weak shoulder is usually observable at the low-energy side of the band-to-band absorption, and thus the bandgap is not changed, although this is often claimed in the literature. A bandgap narrowing occurs only in a very few cases, and is evidenced by a shift of the steep onset of the band-to-band absorption (Figure 1, case D). Examples are chromium(III)-doped titania and nitrogen-doped caesium titanates.[17]

Scheme 1 summarizes schematically the primary processes occurring after the absorption of light by a semiconductor powder in contact with an aqueous solution of an electron

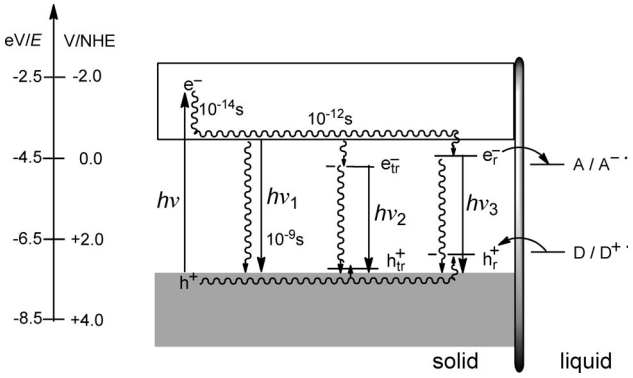

Scheme 1. Primary photoprocesses at a semiconductor/liquid interface. Straight and waved lines correspond to radiative and nonradiative processes, respectively. The thick vertical bar symbolizes the solid/liquid interface. In this scheme, electrons and holes gain stability when moving down and up, respectively. Throughout this Review, all band edge and Fermi potentials refer to a semiconductor in contact with water of pH 7 unless otherwise noted. The depicted band positions apply for titania. The electron energy (eV) is given relative to the vacuum level (0 eV).

donor D and an acceptor A. Dissociation and relaxation of the light-generated exciton affords electrons and holes located energetically close to the corresponding edges of the energy bands. From there they may undergo nonradiative and radiative primary recombination and trapping at nonreactive (e_{tr}^-, h_{tr}^+) or reactive (e_r^-, h_r^+) surface sites. It should be emphasized that the corresponding energy levels are located at the surface and not in the bulk, as may be assumed from the simplified Scheme 1. The depicted life times were taken from

results obtained from colloidal titania.[18] Band bending, which is responsible for charge separation at single-crystal electrodes, is probably not relevant for the powders discussed in this Review, since crystallite sizes in the range of 20 to 100 nm are too small to invoke the presence of a charge-depletion layer. It is known that the incident photon to current efficiency of a titania powder electrode does not depend on the applied potential, which determines the band bending, but on the ease of oxidizing the electron donor.[19] This means, that the efficiency of charge separation is determined by competition between recombination and IFET reactions. Experimental differentiation of the various surface sites may be possible by combining luminescence-quenching with product-inhibition studies, a standard procedure in homogeneous molecular photochemistry (see Section 8.1). The reactive electron–hole pair can undergo the IFET reactions with A and D [Eqs. (14) and (15)] if the corresponding reduction potentials are located at appropriate positions within the bandgap, as depicted in Scheme 1. In some cases, IFET may be coupled with proton transfer (see Sections 6–8). Consecutive reactions of the primary redox products generally afford reduced and oxidized products [Eq. (16)], and only in a few cases can an intermolecular bond formation lead to one unique addition product [Eq. (17)].

$$A + e_r^+ \rightarrow A^{\bullet -} \tag{14}$$

$$D + h_r^+ \rightarrow D^{\bullet +} \tag{15}$$

$$A + D \xrightarrow[SC]{h\nu} B_{red} + C_{ox} \tag{16}$$

$$A + D \xrightarrow[SC]{h\nu} A{-}D \tag{17}$$

Whereas the first case is equivalent to photoelectrochemical reaction schemes, the second case is novel and may include the addition of more than two substrates (see Sections 7 and 8). We have recently proposed to term the first and second reaction modes as semiconductor photocatalysis type A and type B, respectively.[20] It is generally assumed that D and A have to be adsorbed at the semiconductor surface to enable high IFET rates. However, redox transformations of substrates having no contact with the surface at all have also been observed. Rare examples are aerobic oxidation reactions. In this case, the IFET with adsorbed oxygen and water generates short-lived reactive oxygen compounds such as OH and HO_2 radicals that are capable of diffusing to remote substrates.[21]

The simplified Scheme 1 does not show electron-transfer reactions with the material itself that lead to surface destruction and, therefore, to deactivation of the photocatalyst, the so-called photocorrosion process. Whereas titania is quite photostable, zinc and cadmium sulfide in general suffer from photocorrosion to elemental metal and sulfur as a result of redox reactions with the lattice components in the absence of air. Metal and sulfate ions are the final products in the presence of air. The tendency for photocorrosion is often highest for very pure materials, which suggests that surface states of less pure semiconductors not only facilitate the undesired recombination but also the desired interfacial electron transfer in favor of photocorrosion.

When estimating the thermodynamic feasibility of the IFET reactions according to Equations (14) and (15), one has to recall that the reorganization energies χ also have to be considered in addition to the standard reduction potentials A^0_{red} and D^0_{red}.[22] The values of χ are determined by the difference between the standard potential and the maximum of the density of states and are assumed to be about the same for reduction and oxidation (Scheme 2). The energy difference between the reduced and oxidized forms of the redox system is given by 2χ. Reorganization energies may reach values of half an electron volt, depending on the chemical structures of the substrates and solvent. Accordingly, the IFET is thermodynamically allowed when the quasi-Fermi level of reactive electrons ($_nE_F$*) is equal or more negative than the potential ($A^0_{red} + \chi$), while the quasi-Fermi level of reactive holes ($_pE_F$*) must be equal or more positive than the value of ($D^0_{red} + \chi$).[23] This basic aspect is often not included in discussions on the thermodynamic feasibility of an anticipated IFET reaction. Since the reorganization energies are generally unknown, predictions are usually based on the standard reduction potentials A^0_{red} and D^0_{red}. An exception is the photooxidation of thiocyanate at colloidal titania, which has a reorganization energy of 0.6 eV.[23] Since, however, the potentials of the reactive electron–hole pair, that is, the quasi-Fermi levels of the electrons and holes, are also not known exactly—as maximum values the corresponding band edges may be taken—predictions have to be taken with care. The quasi-Fermi level is defined as the Fermi level measured under irradiation.[24] In general, the difference between the two levels is rather small.[13]

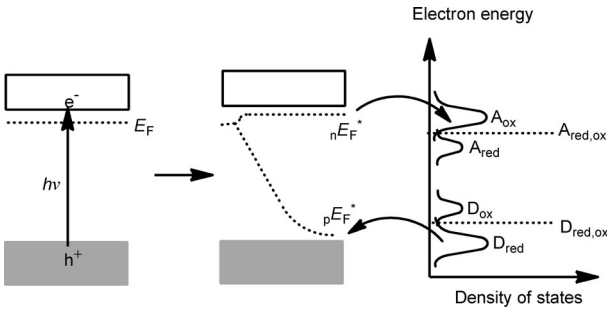

Scheme 2. Thermodynamics of the interfacial electron transfer (IFET) between photogenerated surface electron–hole pairs and dissolved donor D and acceptor A. $_nE_F$* and $_pE_F$* refer to quasi-Fermi levels of electrons and holes, respectively. The density of states is drawn for the case in which the concentrations of A_{ox} and D_{red} are much larger than those of A_{red} and D_{ox}. A_{ox} and D_{ox} are unoccupied electronic states.

In many cases a thermally active redox catalyst is necessary to make the IFET reactions fast enough to compete with the recombination processes. A typical example is cadmium sulfide covered by a few weight percent of metallic platinum (Pt/CdS) to catalyze the reduction of water in the presence of sodium sulfite.[25] Platinization shifts the quasi-Fermi level cathodically from −0.30 V to −0.60 V (at pH 7), thus increasing the driving force of water reduction.[26] No

hydrogen is evolved in the absence of platinum. Typical redox catalysts for oxidative IFET reactions, such as water oxidation, are RuO_2 and IrO_2. Surprisingly, the latter can also photocatalyze the evolution of oxygen in the absence of any sensitizer.[27] The IFET processes are essential for the chemical utilization of light energy. Depending on the nature of the final products [Eqs. (16) and (17)] formed by secondary reactions of the primary redox products $A^{\bullet-}$ and $D^{\bullet+}$, the overall conversion may be an uphill or downhill reaction that corresponds to a storage or a utilization of light energy, as exemplified by water splitting or the exhaustive aerobic oxidation of pollutants.

Aerobic photooxidation reactions catalyzed by semiconductor surfaces are already used in air purification[28] by solar light, whereas the removal of pollutants from water is still a field of basic research. In contrast to conventional air cleaning based on adsorption, which requires a final chemical degradation of the pollutant, photocatalysis removes the pollutant by an exhaustive aerobic photooxidation to generate harmless products such as carbon dioxide and water. The two mechanisms operating in these reactions will now be used to exemplify two basic actions of a semiconductor surface during a photocatalytic reaction (Scheme 3). In direct

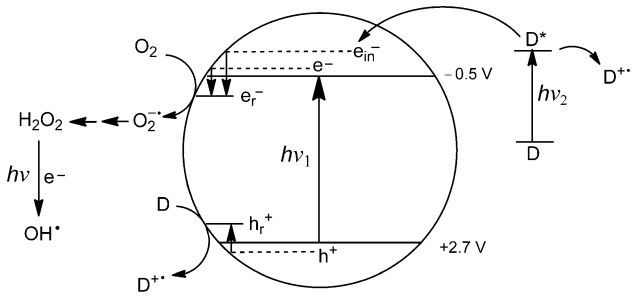

Scheme 3. Schematic representation of the primary processes in direct ($h\nu_1$) and indirect ($h\nu_2$) semiconductor photocatalysis exemplified for titania-catalyzed aerobic photooxidations. The circle symbolizes a large semiconductor crystal or an aggregate of nanocrystals. The two horizontal lines represent the band edges at pH 7.

semiconductor photocatalysis, light ($h\nu_1$) absorbed by the semiconductor and charge recombination is partially prevented by the faster IFET reactions [Eqs. (18) and (19), shown schematically on the left side of Scheme 3]. The oxidation of the pollutant D may occur also via intermediate OH radicals generated by competitive oxidation of water. In indirect photocatalysis, the absorption of light ($h\nu_2$) occurs by the substrate D having an excited state with a reduction potential negative enough for electron injection into the conduction band under formation of the radical cation $D^{\bullet+}$. The resulting spatial separation of the two generated charges slows down the back electron transfer (BET) according to Equation (20), thus enabling successful competition through the reduction of oxygen and oxidative decomposition of $D^{\bullet+}$ by superoxide or its secondary products [Eqs. (18) and (21)]. Thus, no valence band hole is formed in indirect photocatalysis and the semiconductor functions as an electron relay, thereby preventing the undesired back reaction.[29]

$$O_2 + e_r^- \rightarrow O_2^{\bullet-} \quad (18)$$

$$D + h_r^+ \rightarrow D^{\bullet+} \quad (19)$$

$$D^{\bullet+} + e_r^- \rightarrow D \quad (20)$$

$$D^{+\bullet} + O_2^{\bullet-}/HO_2^{\bullet}/OH^{\bullet} \rightarrow C_{ox} \quad (21)$$

In some cases the substrates may interact with the semiconductor surface and induce the appearance of a new absorption band having charge-transfer (CT) character. Typical examples are various aromatic compounds and sulfur dioxide.[30] In the case of aromatic 1,2-diols, such as catechol, stable red chelate complexes are formed. They exhibit a broad absorption band with a maximum at 420 nm that extends down to 600 nm.[31] Thus, in contrast to aliphatic 1,2-diols, aromatic ones can be photooxidized in the presence of titania not only by UV but also by visible light. In this case, excitation also generates a conduction band electron and a donor radical cation [Eqs. (22) and (23)], as discussed

$$SC{-}D \xrightarrow{h\nu_{CT}} SC^{\bullet-}{-}D^{\bullet+} \quad (22)$$

$$SC^{\bullet-}{-}D^{\bullet+} + O_2 \rightarrow SC + D^{\bullet+} + O_2^{\bullet-} \quad (23)$$

above. However, this occurs by an optical electron transfer [Eq. (22)] and not through a photoinduced electron transfer involving the excited state of D (see Scheme 3). Irrespective of this difference in the mechanism of charge generation, in neither case is a valence band hole formed and also the CT mechanism can be classified as indirect semiconductor photocatalysis.

Both direct and indirect photocatalysis transform the initially generated superoxide to reactive oxygen compounds of high oxidative power [Eqs. (24)–(29)] with reduction potentials of 0.94 V ($O_2^{\bullet-}/H_2O_2$), 1.29 V (H_2O_2/H_2O), and 1.90 V ($OH^{\bullet}/OH^-$).[32] They are involved in the thermal degradation steps of the radical cation and can induce autooxidation reactions.

$$O_2^{\bullet-} + H^+ \rightarrow HO_2^{\bullet} \quad (24)$$

$$HO_2^{\bullet} + HO_2^{\bullet} \rightarrow H_2O_2 + O_2 \quad (25)$$

$$O_2^{\bullet-} + HO_2^{\bullet} \rightarrow O_2 + HO_2^- \quad (26)$$

$$HO_2^- + H^+ \rightarrow H_2O_2 \quad (27)$$

$$H_2O_2 + O_2^{\bullet-} \rightarrow {}^{\bullet}OH + OH^- \quad (28)$$

$$H_2O_2 + e_r^- \rightarrow {}^{\bullet}OH + OH^- + O_2 \quad (29)$$

3. Characterization of Photocatalysts

In addition to standard methods for the characterization of heterogeneous catalysts, such as bulk and surface elemental analysis, X-ray powder diffraction (XRD), specific surface area measurements, diffuse reflectance spectroscopy (DRS), emission spectroscopy, and electron paramagnetic resonance,[33] photoelectrochemical experiments, in particular, are of great importance. Only the latter may prove the presence of semiconductor properties and enable a general

heterogeneous photocatalysis mechanism to be excluded, as it does not involve simultaneous reductive and oxidative IFET reactions.[34] Lifetimes of photogenerated charges may be obtained by time-resolved DRS, photoluminescence,[35] and surface photovoltage measurements (Dember voltage). In the last of these, the semiconductor is often embedded in a polymer film with a thickness of a few micrometers. The obtained photovoltage decay curve generally consists of a slow and fast component corresponding to bulk and surface recombination, respectively. The sign of the photovoltage may indicate the presence of an n- or a p-type material.[36] Typical lifetimes of surface charges, relevant for photocatalysis, are in the range of micro- to nanoseconds.

Bandgap values are easily obtained by DRS measurements. In this method, the diffuse reflectance of the powder is recorded relative to a white standard such as alumina or barium sulfate (Figure 3A). The Kubelka–Munk function $F(R_\infty)$ is equivalent to absorbance and is obtained from

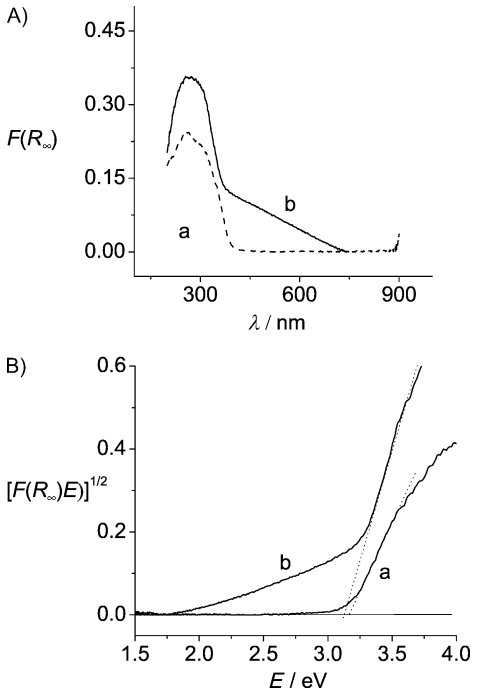

Figure 3. A) Diffuse reflectance spectra of a) TiO_2 and b) TiO_2-C. B) The modified plot (E = energy of exciting light) leads to bandgaps of a) 3.16 eV for TiO_2 and b) 3.11 eV for TiO_2-C.

Equation (30), wherein R_∞ is the diffuse reflectivity [Eq. (31)] of an infinitely thick sample layer, while k and S are the absorption and scattering coefficients, respectively. It should be noted that Equation (30) applies only for a) monochromatic irradiation, b) infinite thick sample layers (which is for most powders reached at about 5 mm), c) low sample concentrations, d) uniform distribution, and e) absence of fluorescence. Although dilution with the white standard improves resolution, this is only rarely done in the literature.[37]

$$F(R_\infty) = (1-R_\infty)^2/2R_\infty = k/S \tag{30}$$

$$R_\infty = R_{\text{sample}}/R_{\text{standard}} \tag{31}$$

To obtain the bandgap a modified Kubelka–Munk function is plotted as function of the energy of the exciting light according to Equation (32).

$$(F(R_\infty)h\nu)^{1/n} \propto h\nu - E_g \tag{32}$$

Extrapolation of the linear part of the resulting curve affords the bandgap (Figure 3B). The number n depends on the nature of the electronic transition and is 1 for a direct and 0.5 for an indirect semiconductor with a crystalline structure.[38] An unambiguous conclusion may not be possible since the extrapolation is associated with a rather large error.[39] Figure 3 exemplifies the procedure for the case of pristine and carbon-modified titania (see Section 5). The often-employed analogous extrapolation of the unmodified Kubelka–Munk function is an incorrect procedure.

The quasi-Fermi level of electrons ($_nE_F$*, Scheme 2) may be obtained from the photocurrent onset[2e,40] or from the light intensity saturation of the photocurrent,[41] both measured with an electrode having the semiconductor as a thin powder layer on conducting glass. When the quasi-Fermi level is located not too far from the pH-independent reduction potential of a dissolved redox couple such as methylviologen (MV^{2+}), the so-called suspension method can be used when the Fermi level is pH-dependent. The latter requirement is usually met for oxidic and sulfidic semiconductors exhibiting a dependence according to Equation (33), wherein the constant k is usually in the range of 0.059 V.

$$E_F(\text{pH}) = E_f(\text{pH}\,0) - k\,\text{pH}_o \tag{33}$$

Thus, the Fermi level is located at more negative potentials in alkaline suspensions than in neutral or acidic ones. According to thermodynamic considerations, the IFET reduction of MV^{2+} is feasible only when the quasi-Fermi level becomes equal (Scheme 4, $pH = pH_o$) or more negative than the methylviologen potential of −0.44 V. This is also recognized visually by the appearance of the blue color of the viologen radical cation upon increasing the pH value. Depending on the reduction potential of h_r^+, it may oxidize

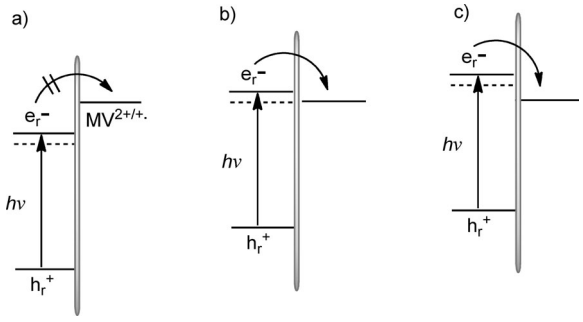

Scheme 4. Schematic representation of the pH dependence of the IFET reduction of methylviologen at a photoexcited semiconductor surface. a) $pH < pH_o$, b) $pH = pH_o$, c) $pH > pH_o$.

water or another donor, or the semiconductor itself (photocorrosion).[13,42] Initially the photocurrent of the powder suspension in water was measured as a function of the pH value with a standard three-electrode setup using a platinum flag as the working electrode. The onset of the photocurrent corresponds to the quasi-Fermi level of electrons. Depending on the irradiation equipment, ${}_nE_F$* values may depend slightly on the light intensity. A cathodic shift of 27 mV was observed for CdS upon a tenfold increase in the light intensity.[13] All values cited in this Review apply to pH 7, as calculated from Equation (33) and are given relative to the normal hydrogen electrode (NHE), unless otherwise stated.

When the photovoltage between the platinum flag and a reference electrode is measured by the suspension method instead of the photocurrent, one obtains a sigmoidal type of voltage versus pH value titration curve.[42a] At the pH value of the inflection point (pH_o), the quasi-Fermi level becomes equal to −0.44 V, the potential of methylviologen. As examples, the titration curves of TiO_2 and the modified material TiO_2-C are depicted in Figure 4. The quasi-Fermi

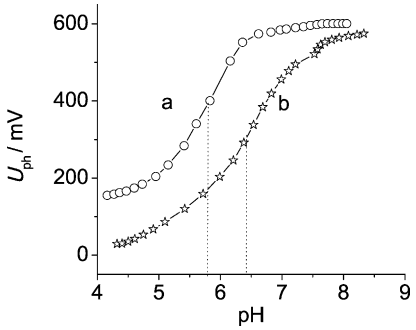

Figure 4. Dependence of photovoltage on pH value of a suspension of a) TiO_2 and b) TiO_2-C under polychromatic irradiation ($\lambda \geq 320$ nm) in a dinitrogen atmosphere.[43]

level of −0.52 V obtained for the former is anodically shifted to −0.48 V in the latter material.[43] As mentioned above, the factor k in Equation (33) has to be known to refer quasi-Fermi levels to the same pH values. For suspensions it can be obtained from the slope of the voltage/pH plot above the inflection point[42a] or from the slope at the onset of photocurrent versus pH value.[13] In our hands neither method exhibited good reproducibility because of considerable voltage fluctuations and very low photocurrents. Alternatively, the pH_o point can be measured not only for one but for a series of pH-independent redox couples.[44] Figure 5 depicts the linear dependence of pH_o values on the reduction potentials of the electron acceptor. From the slopes, k values of 0.050 V and 0.060 V are obtained for titania and a chloroplatinate(IV)-modified material (see Section 5).

Knowing the quasi-Fermi level of electrons also allows the levels of holes to be estimated by adding in the bandgap energy. This rough but helpful procedure is based on the assumption that both levels are located very close to the corresponding band edges (see Scheme 2). This is a reliable approximation, since most of the employed powders represent highly doped n-semiconductors. The position of the

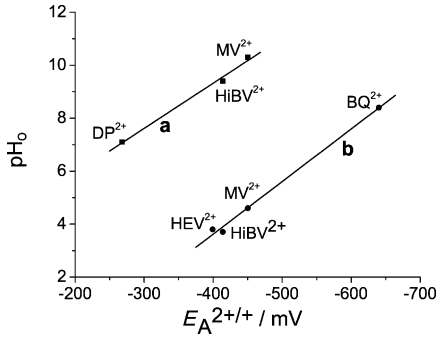

Figure 5. Dependence of the pH_o value of a) untreated titania and b) chloroplatinate(IV)-modified titania on the reduction potential of various bipyridinium electron acceptors. MV^{2+} = methylviologen, $HiBV^{2+}$ = *N*,*N*′-bis(2-methyl-3-hydroxypropyl)-4,4′-dipyridinium, HEV^{2+} = *N*,*N*′-bis(2-hydroxyethyl)-1,1′-dipyridinium, BQ^{2+} = *N*,*N*′-1,4-butandiyl-2,2′-byridinium, DP^{2+} = *N*,*N*′-1,2-ethandiylphenanthrolinium.[44]

Fermi level depends not only on the presence of impurities and modifiers but also on the nature of adsorbed substrates and solvent. Thus, cathodic shifts of up to 1.0 V were reported upon cleaning elemental sulfur and cadmium from the CdS surface of a single-crystal electrode.[45] The Fermi level shifted cathodically by 0.4 V when titania was suspended in acetonitrile instead of water.[46]

Detailed information on the electronic structure of the semiconductor powder and on primary processes at the solid/solution interface can be gained by performing the suspension photovoltage measurements at different wavelengths.[47] This was first illustrated for the experimental determination of surface states in the modified titania photocatalyst TiO_2-N,C, which was obtained by thermal treatment of anatase powders with urea at 400 °C. The spectrum of the slightly yellow powder showed not only the titania-based UV absorption, but also a weak shoulder in the visible region that originates from a surface-bound modifier of the poly(aminotri-*s*-triazine) type sensitizer, abbreviated as "N,C" (see Section 5). TiO_2-N,C can be considered as a core–shell particle with a titania core linked covalently to an "N,C" shell.[48] TiO_2-N,C photocatalyzes visible light driven aerobic oxidation reactions of chlorophenols and formic acid. Photovoltage measurements were performed under polychromatic UV/Vis, UV, and Vis excitation to find out if the novel electronic states responsible for visible light activity are located close to the conduction or close to the valence band (Scheme 5, parts A and B). Irradiation at $\lambda > 300$ nm (UV/Vis) generates e_r^- at a potential of −0.48 V, as obtained from the pH_o value of 6.6. The simultaneously formed $h_{r,v}^+$ should be located in the titania-based valence band, since it is able to oxidize water to the OH radical (Figure 6a, Scheme 5). The same result is obtained when only UV light ($\lambda \leq 400$ nm) is employed, thereby excluding the possibility that the visible part of the exciting light is also relevant. No reduction of methylviologen is observable within the full pH range when TiO_2-N,C is excited with visible light ($\lambda > 420$ nm; Figure 6e). However, in the presence of 2-propanol, formation of the blue methylviologen radical cation is observed and the resulting pH_o and

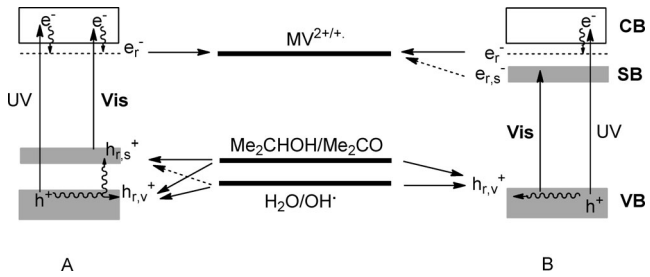

Scheme 5. Wavelength-dependent IFET reactions of TiO_2-N,C at pH_o. Full and dashed arrows indicate observed and unobserved reactions, respectively. Wavy lines symbolize thermal relaxation and surface trapping. Since $h_{r,s}^+$ is centered at the poly(aminotri-*s*-triazine) shell, which may have semiconductor properties as known for pristine polytriazines,[49] corresponding energy levels (SB) are depicted as band-like.

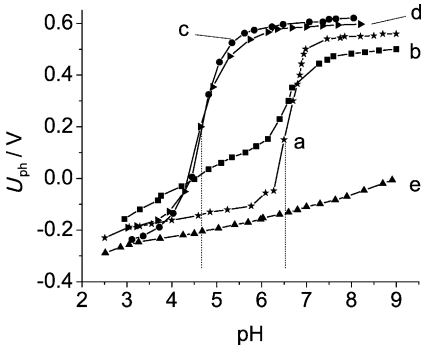

Figure 6. Variation of photovoltage with pH value for an aqueous suspension of modified and unmodified titania suspensions in the presence of methylviologen dichloride; a) TiO_2-N,C, UV/Vis, no 2-propanol, b) TiO_2-N,C, Vis, 2-propanol, c) TiO_2, UV/Vis, 2-propanol, d) TiO_2-N,C, UV/Vis, 2-propanol, e) TiO_2-N,C, Vis, no 2-propanol. Vis: $\lambda \geq 420$ nm, UV/Vis: $\lambda \geq 300$ nm.

${}_nE_F^*$ values are 6.5 and −0.48 V (Figure 6b), respectively, in excellent agreement with UV/Vis excitation in the absence of the alcohol (Figure 6a). This observation suggests that excitation with visible light generates a reactive hole in an "N,C"-localized surface state ($h_{r,s}^+$) that is incapable of oxidizing water but able to oxidize 2-propanol, as shown in Equations (34) and (35) (Scheme 5A). No blue color and no photovoltage change are observed without the addition of MV^{2+} to the TiO_2-N,C suspension in 2-propanol.

$$Me_2CHOH + h_{r,s}^+ \rightarrow Me_2\dot{C}OH + H^+ \quad (34)$$

$$Me_2\dot{C}OH + MV^{2+} \rightarrow Me_2CO + MV^{\bullet+} + H^+ \quad (35)$$

The above results exclude a location of "N,C" electronic states close to the conduction band edge (Scheme 5B). If this was the case, the hole should be generated in the titania valence band and water oxidation should be feasible upon excitation with visible light. The surprising observation that methylviologen is reduced in water upon excitation with UV and UV/Vis light but not with visible light suggests a very weak electronic coupling between titania-based and "N,C"-localized energy levels, since otherwise relaxation $h_{r,v}^+$ to the "N,C" level (formation of $h_{r,s}^+$) should be fast enough to prevent water oxidation.

When the UV/Vis photovoltage measurement is performed in the presence of 2-propanol (10%, v/v), the inflection point is shifted to 4.7, which is about 2.0 units lower than in the absence of the alcohol (Figure 6d). This surprising finding is rationalized by the assumption that the 2-hydroxy-2-propyl radical ($E = -1.39$ V)[50] formed in the IFET reaction according to Equation (34) reduces MV^{2+} in solution [Eq. (35)] and, therefore, induces the potential jump at a quasi-Fermi potential more positive than −0.44 V.[47] An analogous homogeneous reduction of MV^{2+} through an intermediate carbon dioxide radical anion generated by hole oxidation of sodium formate upon UV excitation of colloidal titania is known.[51] Surprisingly, the true inflection point is not shifted upon excitation with visible light in the presence of the alcohol. As a consequence of the lower oxidative power and lower concentration of $h_{r,s}^+$ compared to that of $h_{r,v}^+$, the stationary concentration of the hydroxy-2-propyl radical at $pH \leq pH_o$ may be too low to enable the reduction of MV^{2+}.

This shift of the inflection point because of a secondary electron transfer from a primary oxidation intermediate resembles the well-known current amplification effect observed when alcohols, formic acid, and amines[52] are oxidized at a semiconductor electrode. Accordingly, TiO_2-N,C exhibited a similar shift of the pH_o value when formic acid ($pH_o = 4.4$) instead of 2-propanol ($pH_o = 4.7$) was employed. However, no significant shift was observable with 4-chlorophenol (4-CP) or bromide ions, which also do not exhibit current amplification. The corresponding values are ${}_nE_F^* = -0.49$ V and −0.46 V for UV/Vis/4-CP/MV^{2+} and UV/Vis/Br^-/MV^{2+}, respectively, as compared to ${}_nE_F^* = -0.48$ V measured under UV/Vis irradiation in pure water. These results indicate that the true quasi-Fermi potential may not be obtained in the presence of donors having current amplification properties. A change of the donor and irradiation wavelength should reveal if a real or pseudo-pH_o value was measured. The appearance of a pseudo-pH_o value may also originate from a cathodic shift of the flatband potential induced by adsorption of 2-propanol on the semiconductor surface.[53] However, this can be excluded since the pseudo-pH_o value does not depend on the 2-propanol concentration and since the same real pH_o value is measured upon UV/Vis excitation in the absence of 2-propanol or upon Vis excitation in the presence of the alcohol. This photocatalytic version of the current amplification effect represents a possibility to generate two reactive electrons by the absorption of only one photon. This is especially relevant for multielectron IFET processes such as nitrogen fixation (see Section 6).

The suspension method also works with semiconductor thin films and may be used to test if the semiconductor powder contains a semiconducting impurity. In some cases two inflection points are observable.[54]

4. Reaction Rates and Quantum Yields

The rate of any photoreaction is given by the product of the absorbed photon flux (I_a is number of photons absorbed at a given wavelength per time and volume) and the quantum yield (Φ). Since I_a depends on the intensity of the light source, only the quantum yield, that is, reaction rate divided by I_a, is independent of the intensity and, therefore, can be used to compare the efficiencies of various photoreactions[Eq. (36)]. In addition to the wavelength employed, it has to be specified if the substrate disappearance or product formation rate was measured. With the exception of photoinduced chain reactions, the maximum value of the product quantum yield (Φ_p) is one, which means that each quantum of light absorbed by the reacting system generates one product molecule.[55]

$$\Phi_p = v_p/I_a \tag{36}$$

Whereas the amount of light absorbed by the reacting system can be easily measured for homogeneous solutions, it is extremely difficult for suspensions of powders, as is generally employed in semiconductor photocatalysis.[56] In this case, light is not only absorbed but also scattered and reflected by the suspended semiconductor particles. Up to 13–76% of the light arriving at the powder surface may be lost.[4d,57]

To overcome this intrinsic problem of the quantitative comparison of heterogeneous photoreactions it was proposed to just replace I_a by the easily measurable number of photons of a given wavelength per time and volume arriving at the inside of a flat front window of the photoreactor (incident photon flux I_o). The apparent quantum yield so obtained was termed photonic efficiency [Eq. (37)].[4d,58]

$$\xi_p = \frac{v_p}{I_o} \tag{37}$$

Comparison of the resulting numbers, however, is meaningful only if the fraction of light absorbed is the same in each experiment. This is a rather unlikely assumption, since the amount of scattered and reflected light may change considerably from experiment to experiment. This is a serious problem when comparing photonic efficiencies obtained by various research groups, since different photoreactors are usually employed. However, a comparison is meaningful between a set of reactions performed in the same photoreactor and a standard system, thereby affording "relative photonic efficiencies".[58b,c]

A simpler and more practicable procedure allows the rate of reactions performed in the same photoreactor to be compared. In this case, the reaction rate is measured as a function of increasing photocatalyst concentration. Both for a homogeneous catalysis system[59] (Figure 7) and a heterogeneous one,[57a] the rate initially increases linearly with the photocatalyst concentration (Figure 7, curve A to B), because of the increase in the absorbed photon flux, and then stays constant (in the region of B to C), a region representing concentrations of constant and optimal light absorption. The resulting optimum rate represents a pseudo-photon efficiency that enables a comparison of "photocatalytic activities".[60] In some cases, a rate decrease is observed (in the region from B to D) because of a reduced penetration depth and an increased scattering of the incident light beam.[61] The optimum concentration of the often-employed titania powders with specific surface areas of 50–200 $m^2 g^{-1}$ is in the range 0.5–3.0 $g L^{-1}$, depending on the irradiation system.

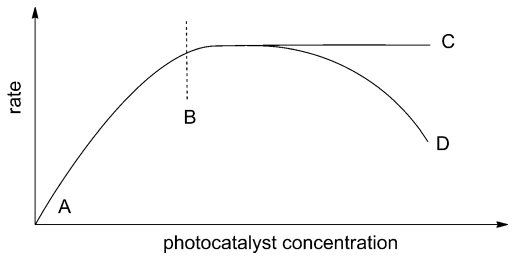

Figure 7. Dependence of reaction rate on photocatalyst concentration.

In general, a semiquantitative comparison of "photocatalytic activities" is meaningful only if the reactions have been conducted in the plateau region of Figure 7. However, this simple requirement is quite often not met and, therefore, the conclusions reported in the literature are often doubtful, especially when there are small differences.[62] A recent proposal coming from the field of thermal heterogeneous catalysis does not present a reliable alternative.[63]

The following qualitative discussion of the parameters influencing the quantum yield illustrates the problems in more detail. Scheme 6 summarizes the most important primary processes that determine the efficiency of charge generation at the solid/solution interface. No band bending has to be considered because of the small size of the crystallites (10–50 nm) making up the powder. The absorption of light generates an electron–hole pair that is delocalized throughout the entire crystal. It may recombine and undergo trapping at unreactive (e_{tr}^-, h_{tr}^+) and reactive (e_r^-, h_r^+) surface sites (Scheme 6, processes 1, 2, 3), followed by nonradiative and radiative charge recombination (processes 4 and 5). IFET from the reactive electron–hole pair affords the primary redox products $A^{\bullet-}$ and $D^{\bullet+}$ (processes 6 and 7) which may suffer back-electron transfer to A and D (process 8) or undergo the desired conversion into final products (processes 9 and 10). By analogy with homogeneous photoreactions, the efficiency of the formation of the reactive electron–hole pair (η_r), the efficiency of the IFET (η_{ifet}), and the efficiency of product formation from the primary redox products (η_p) are given by the ratio of the rate constants for the formation and consumption of the corresponding intermediates present in a quasistationary state [Eqs. (38)–(40), see Scheme 6].

$$\eta_r = \frac{k_3}{k_1 + k_2 + k_3 + k_4} \tag{38}$$

$$\eta_{IFET} = \frac{k_{6,7}}{k_5 + k_{6,7}} \tag{39}$$

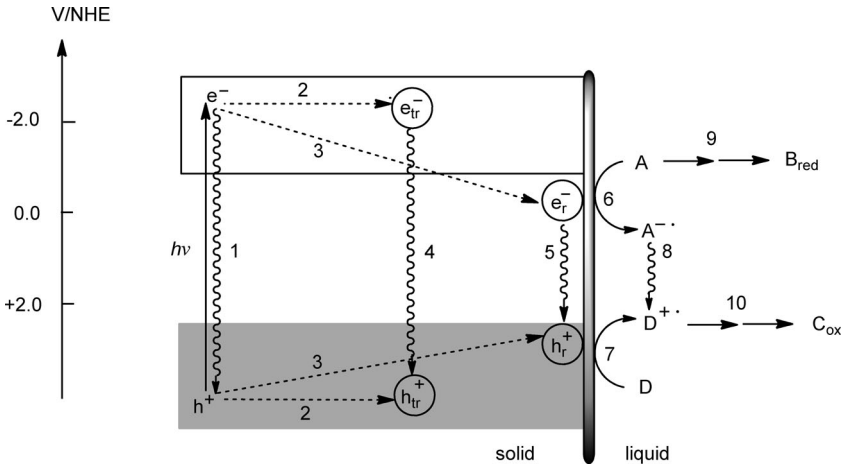

Scheme 6. Schematic description of primary processes occurring during a semiconductor-photocatalyzed redox reaction. For the sake of simplicity, wavy arrows symbolize non-radiative, radiative, and photocorrosion processes. Dashed arrows indicate charge trapping.

$$\eta_p = \frac{k_{9,10}}{k_8 + k_{sb} + k_{9,10}} \tag{40}$$

In Equation (40), the rate constant k_{sb} belongs to the secondary back-electron transfer according to Equations (41)

$$A^{\bullet -} + h_r^+ \rightarrow A \tag{41}$$

and (42).

$$D^{\bullet +} + e_r^- \rightarrow D \tag{42}$$

The efficiency of the overall reaction, that is, the quantum yield of product formation (Φ_p), can then be formulated as the product $\eta_r \eta_{ifet} \eta_p$ [Eq. (43)].

$$\Phi_p = \eta_r \eta_{ifet} \eta_p \tag{43}$$

Thus, Φ_p depends on the rate constants of various elementary reactions, and it is difficult to correlate its variations with one unique elementary process. However, the efficiency of product formation from the primary redox products (η_p) should only weakly depend on small changes in the intrinsic semiconductor properties, whereas the efficiencies of formation of the reactive electron–hole pair and of the IFET reactions (η_r and η_{ifet}) may change considerably. Minor alterations during the synthesis of the powder as well as the adsorption of reaction components can strongly affect the photophysical properties of the semiconductor/liquid interface. Furthermore, since the semiconductor powder consists, in general, of micrometer-sized aggregates built up from nanosized crystallites, the detailed nature of the intercrystallite interaction may strongly affect the efficiency of charge generation and, therefore, the value of η_r. The solid/solid interface in anatase/rutile materials may improve charge generation by preventing recombination through an intercrystallite electron transfer (ICET), as supported by EPR spectroscopic measurements.[33b]

It was recently reported that the coagulation of colloidal titania nanoparticles increases the photocurrent density at a platinum electrode upon photoreduction of methylviologen by methanol in the presence of titania nanoparticles. The effect was rationalized by the assumption that an intercrystallite charge transfer might improve the charge separation.[64] However, other effects, such as a faster oxidation of methanol by the reactive hole, can not be excluded. Similarly, colloidal CdS is inactive, whereas micrometer aggregates photocatalyze organic addition reactions (see Section 8).[65] A strong electronic coupling between properly aligned crystallites was proposed to generate an "antenna effect", thereby inducing improved charge separation, in titania covered by a few weight percent of metallic silver and acts as a type of nanocathode (Ag/TiO_2).[66] Similar effects may rationalize the higher yield of superoxide observed upon UV excitation of ZrO_2–TiO_2 nanoparticles networks compared to TiO_2–TiO_2 and ZrO_2–ZrO_2 systems.[67] Very recently, it was proven that thermal electron transfer can take place from small to large ZnO nanocrystals. As a consequence of the quantum size effect, the conduction band edge of the smaller particles is located at a more negative potential compared to the larger particles.[68]

Thus, when comparing photonic efficiencies or optimum reaction rates induced by various substrates, it is not apparent which of the three efficiencies in the multistep reaction is responsible for the observed changes. In most cases it is not even known whether the electron–hole pairs that are sometimes observable by emission spectroscopy are identical with the reactive electron–hole pairs involved in the IFET reactions. In general, good emitters are poor photocatalysts because radiative charge recombination is faster than the IFET process. This relationship, however, does not prove that the emitting electron–hole pairs are identical with the reactive ones, since the latter may be produced via the former. A combination of emission quenching and reaction inhibition studies offers a simple possibility to answer this question (see Section 8.1).

Apparent quantum yields exhibit peculiar intensity dependence: at low intensity they are independent,[69] but at high intensity they increase linearly with the square root of the reciprocal intensity. The latter case is typical for homogeneous and heterogeneous photoreactions, where the recombination of primary products predominates. Temperature affects photocatalytic reactions analogously to homogeneous systems.[70] The slowest chemical reaction step and the adsorption equilibria of substrates and products are the major factors.[71] Typical values of activation energies are 2–4 kcal mol^{-1}, as reported for the CdS-catalyzed photodimerization of *N*-vinylcarbazole.[72]

The specific surface area of the semiconductor powder influences the reaction rate through two opposite effects.[73] Since the number of surface defects usually increases as the surface area increases, the rate of electron–hole recombination increases and, therefore, the reaction rate should

decrease. However, since the concentration of adsorbed substrates per unit volume increases in the same direction, the IFET rate should increase and, therefore, also the reaction rate. Accordingly, the apparent quantum yield can stay constant, increase, or decrease as the surface area increases. The highest quantum yields for the CdS/Pt-catalyzed photoreduction of water by a mixture of sodium sulfide and sulfite are observed at small surface areas of up to $2\,m^2\,g^{-1}$. Above this value, a linear decrease to almost zero at a specific surface area of $6\,m^2\,g^{-1}$ takes place. This low quantum yield stays constant upon further increase to $100\,m^2\,g^{-1}$.[25]

5. Preparation and Properties of Photocatalysts

With a few exceptions, semiconductor powders are easily prepared by standard methods of inorganic chemistry, such as precipitation from aqueous solutions including hydrothermal conditions and subsequent thermal treatment in the presence of air (calcination) at temperatures of 100–600 °C. Co-precipitation and impregnation or ligand-exchange reactions have also been employed in the case of doping and surface modification of metal oxides.

5.1. Pristine Oxides, Nitrides, and Sulfides

Visible light active photocatalysts may be classified according to the d-electron configuration of the metal.[74] The most important cases are d^0 and d^{10} systems, such as WO_3 and CdS. The energies of the valence and conduction bands in these binary compounds are determined by the anion and metal cation, respectively. Thus, when the d^0 oxide Ta_2O_5 ($E_g = 3.9$ eV) is treated with gaseous ammonia at high temperatures, the compounds TaON and Ta_3N_5 are obtained which have bandgaps of 2.4 eV, and 2.1 eV, respectively. The valence band edge decreases from 3.6 V to 2.0 V and 1.6 V within this series, respectively, as a result of the increasing amount of nitrogen, since the N2p orbitals are of higher energy than the O2p orbitals. On the other hand, the energy of the conduction band edge changes only from −0.3 to −0.5 V in the same sequence since the conduction band maintains its Ta5d nature in all three compounds.[75]

Another possibility for introducing nitrogen is the preparation of homogeneous solid solutions between an oxide and nitride. This is nicely demonstrated by the d^{10} system GaN-ZnO, which is obtained by nitriding a mixture of Ga_2O_3 and ZnO with NH_3 at 850 °C.[75] Whereas the two pristine materials do not absorb visible light, the homogeneous solutions thereof exhibit bandgaps from 2.8 to 2.4 eV, which correspond to absorption onsets of 446 to 520 nm. The narrowing of the bandgap is probably due to an N2p–Zn3d repulsion, which results in a cathodic shift of the valence band.[76,77]

The introduction of nitrogen in both the tantalum and zinc oxides results in a shift of the steep bandgap absorption to longer wavelengths (Figure 8, curve c) and not in the formation of a flat absorption shoulder at the low-energy onset (Figure 8, curve b), as is usually observed upon doping and surface modification of titania—another widely applied method for converting a UV-active photocatalyst into a Vis-active one. A bandgap shift is often claimed in the literature, although the depicted spectra clearly indicate the opposite, being a superposition of the almost unchanged steep bandgap part with an absorption shoulder arising from transitions from surface states. Exceptions are vanadium-, chromium-, iron-, and nickel-doped titania prepared by ion implantation[78] and surface-modified titania containing molecular FeO_x species bound to the surface through Fe–O–Ti bonds.[79] Both exhibit a clear bandgap shift (compare Figure 8, curves a and c). In contrast, only a weak absorption shoulder (Figure 8, curve b) is observable when the FeO_x species is replaced by amorphous FeO(OH) particles.[80]

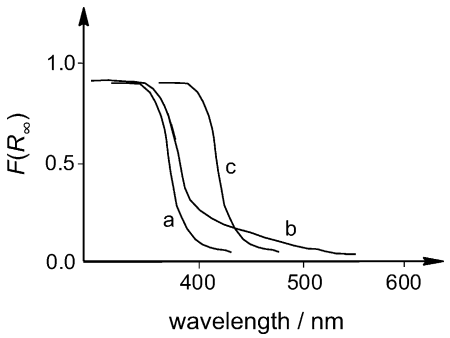

Figure 8. Diffuse reflectance spectra of a) a pristine semiconductor, b) a semiconductor modified by introducing intra-bandgap states, and c) a semiconductor modified by shift of the band edges.

Tungsten oxide is an n-type semiconductor that absorbs visible light of wavelengths below 446 nm (2.8 eV). The conduction and valence band edges are located at −0.1 V and +2.6 V, respectively (Figure 2). Accordingly, reduction of water is thermodynamically not allowed, whereas oxidation to oxygen is feasible in the presence of silver ions.[81] $BiVO_4$ is another n-type material active in the oxidation of water by silver salts in visible light.[82] The tetragonal and monoclinic crystal modifications exhibit bandgaps of 2.9 eV and 2.4 eV, respectively.[83] Conduction and valence band edge positions of the monoclinic phase are at −0.3 V and 2.1 V, respectively.[15]

Of the metal sulfides, the d^{10} compound cadmium sulfide, usually prepared from cadmium sulfate and sodium sulfide or thiourea in the absence of air, is the most important photocatalyst. This is due to a favorable position of the band edges at about −0.9 V and +1.5 V, which result in an absorption onset at 520 nm (Figure 2). When the preparation is conducted in the presence of air, traces of cadmium oxide are produced, which inhibit the photocatalytic action but promote photocorrosion, an often-encountered problem in the application of CdS. A water content of 2–3 % is essential for optimum photocatalytic activity.[84]

5.2. Grafted CdS and TiO_2

5.2.1. Grafting onto an Insulating Support

5.2.1.1. CdS Grafted onto Silica

Since photocatalysis is a surface phenomenon and the surfaces of oxidic and sulfidic semiconductors in general contain under-coordinated metal ions and OH/SH groups, modification of the chemical surface is expected to strongly influence the photocatalytic properties. One of the first examples was grafting, that is, forming chemical bonds between the two components of cadmium sulfide and silica to generate, in addition to the undisturbed CdS surface, also a CdS-O-SiO_2 interface.[42b,85] 12 % CdS-O-SiO_2 is prepared by first stirring a suspension of SiO_2 in an aqueous solution containing 12 wt % cadmium sulfate followed by the addition of sodium sulfide, and then washing and drying the yellow powder at ambient temperature. Surprisingly, the bandgap of 12 % CdS-O-SiO_2 is larger by 0.20 eV than the value of 2.40 eV known for pristine CdS. Furthermore, the quasi-Fermi level of electrons is also cathodically shifted from −0.38 V to −0.59 V. A mechanically prepared mixture of the two components does not produce these significant changes in the optical and photoelectrochemical properties. Similarly, grafting of titania onto silica also leads to a bandgap widening of about 0.20 eV, and in this case an anodic shift of the quasi-Fermi level by 0.20 eV.[86] Clearly, these grafted oxides are linked together by Cd–O–Si and Ti–O–Si bonds, thereby inducing an electronic semiconductor–support interaction (SEMSI effect) which leads to a considerable change in the intrinsic semiconductor properties. As a consequence thereof, the photocatalytic activity of 12 % CdS-O-SiO_2 in an organic addition reaction is increased by factor of about 10 over that of pristine CdS (see Section 8.2). In contrast, 13 % TiO_2-O-SiO_2 is less active by a factor of 0.4 in the oxidative photodegradation of 4-chlorophenol (4-CP) compared to unmodified TiO_2.[86] The photoreduction of carbon dioxide to formate at 17 % CdS-O-SiO_2 is about six times faster than that with unsupported CdS.[87] This opposite effect of grafting CdS and TiO_2 on SiO_2 is in accord with time-resolved photovoltage measurements. A multiexponential decay is observed after laser excitation at 337 nm when the modified powders are embedded in an organic polymer matrix. This decay consists of a fast surface (nanosecond) and slow bulk (microsecond) component. The decay constant of the fast process decreases from $11 \times 10^6\ s^{-1}$ for CdS to $2 \times 10^6\ s^{-1}$ for 12 % CdS-O-SiO_2, which corresponds to an increase in the charge-carrier lifetime from 90 ns to 500 ns,[85] thus accelerating the IFET reactions. In contrast, the lifetime of the light-generated charges in 13 % TiO_2-O-SiO_2 is shortened below the detection limit of 40 ns.[86]

5.2.1.2. CdS Grafted onto Alumina

Similar effects as for silica, although weaker, are observed in CdS-grafted alumina.[88] Instead of the fivefold increase in the lifetime of the charger carriers mentioned above, only a twofold increase is indicated by time-resolved photovoltage measurements. The relative initial rate of addition of cyclopentene to *N*-phenylbenzylideneamine (see Section 8.3) increases from 1.00 for pristine CdS to 1.04, 1.50, and 3.50 for 30 % CdS-O-Al_2O_3, 20 % CdS-O-Al_2O_3, and 9 % CdS-O-Al_2O_3, respectively. The quasi-Fermi level of electrons does not change.

5.2.2. Grafting onto a Semiconducting Support

The reduction of bicarbonate by sodium sulfite with visible light is significantly improved when various amounts of CdS are grafted not onto an insulator such as silica but onto another semiconductor such as ZnS.[87] An unexpected effect was found upon irradiation with unfiltered (both UV and Vis) light. Whereas grafting of 10, 20, and 30 % onto ZnS does not significantly change the rate of formation of formate compared to the unmodified metal sulfides, a loading of only 5 % induces an approximately 80-fold increase. The same effect is observed upon monochromatic irradiation at 365 nm. This surprising result can be rationalized by assuming that an ICET from ZnS to the conduction band of CdS occurs, enabled by the Zn–S–Cd bonds formed during the grafting procedure (Scheme 7, step A). As a consequence thereof, the

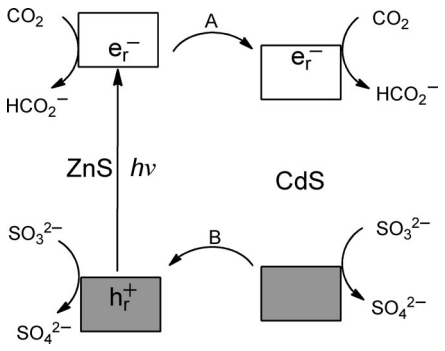

Scheme 7. Proposed mechanism of increased photoinduced charge separation at the grafted semiconductor couple 5 % CdS-S-ZnS. The band edges of ZnS and CdS are located at −1.8/+1.8 V and −0.9/+1.5 V, respectively.

reduction of bicarbonate should also occur at the CdS sites. However, since pristine CdS exhibits only a vanishing activity, "hot electrons" may be involved, as indicated in Scheme 7 by the position of e_r^-. Alternatively, or additionally, an ICET may occur from the CdS valence band to the hole in ZnS (Scheme 7, step B; the generated hole is neutralized through the oxidation of sulfite). As a result, recombination is decreased and the efficiency of the charge separation should increase. This conclusion is justified since it is very unlikely that the efficiency of the IFET to bicarbonate in the grafted powder is different from that in the pristine sulfides. Mechanical mixtures of ZnS and 5 % CdS do not exhibit the same effect. A similar "interparticle electron transfer" was invoked for so-called "coupled" CdS/TiO_2 and similar systems to explain the increased reaction rates in the photooxidation reactions of organic pollutants. However, all these materials were prepared just by grinding.[89] In contrast, α-Fe_2O_3, WO_3, and CdS were deposited onto ZnO also by impregnation methods.[90]

5.3. Metal Halides and Metal Oxides Grafted onto Titania

As a result of its photostability, nontoxicity, and good photocatalytic activity, titania became the most important semiconductor photocatalyst.[91] However, according to its rather large bandgap of about 3.20 eV, light of wavelengths shorter than 400 nm is necessary to enable direct semiconductor photocatalysis. This means that only about 3% of the solar light arriving at the Earth's surface can be utilized and, therefore, practical applications such as the cleaning of air require the use of UV lamps. However, the much larger visible part of sunlight (about 45%) may also induce photocatalysis when titania is surface-modified by dyes and transition- or main-group elements. Although sensitization by organic dyes is an efficient method in photoelectrochemical devices operating in the absence of oxygen, it is not suited for photocatalytic aerobic oxidation reactions since the photogenerated reactive oxygen compounds generally attack not only the substrate but also the dye. Exceptions are a few C-, and N,C-modified titania powders having photostable titania–sensitizer surface complexes (see Section 5.4). In general, a surface complex having only inorganic ligands and a transition metal in a high oxidation state is expected to be more stable than a complex having organic ligands. Since the surface of titania contains under-coordinated titanium atoms and about 3–6 OH groups per nm^2, it may act as a mono- and bidentate ligand (Figure 9 A–C) as well as a titanium coordination center (Figure 9 D–F).[31c]

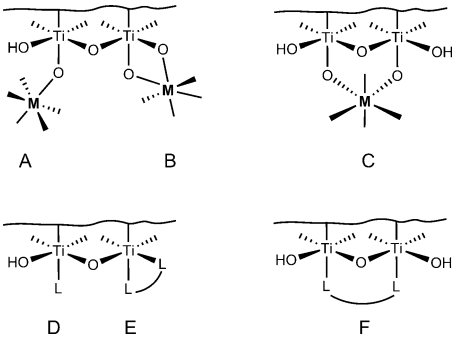

Figure 9. Titania surface as a ligand (A, B, C) or central metal (D, E, F).

5.3.1. Titania–Chloroplatinum(IV) Surface Complexes

Stirring a suspension of anatase hydrate in an aqueous solution of $H_2[PtCl_6]$ in the dark results in maximum amounts of up to 4.0 wt% being adsorbed.[44,92] Subsequent heat treatment at 200°C affords yellowish powders, referred to in the following as $PtCl_4$-O-TiO_2. Simple grinding of anatase hydrate with $PtCl_4$ results in powders of lower photocatalytic activity and lower stability. $PtCl_4$-O-TiO_2 has a specific surface area of 260 $m^2 g^{-1}$ and consists of about 200 nm large aggregates composed of 2–4 nm sized anatase crystallites. Chemical bonding of the chloroplatinate to the titania surface is evidenced by the stability of $PtCl_4$-O-TiO_2 upon stirring it in 0.01 M potassium fluoride. It is known that fluoride irreversibly chemisorbs onto titania through replacement of surface OH groups;[93] apparently, it is not able to also cleave the $PtCl_4O$-Ti and Cl_4Pt-OTi bonds. However, desorption occurs upon decreasing the pH value. These and other observations show that a surface complex of composition [TiO_2]-O-$PtCl_4L^{n-}$, $L = H_2O$, OH^-, $n = 1,2$, is formed during the preparation [Eq. (44)]. In the corresponding photochemical desorption experiments ($\lambda \geq 455$ nm) with 4.0% $PtCl_4$-TiO_2 suspended in water no desorption occurred within 24 h.

$$[TiO_2]\text{-}OH + PtCl_5L^{n-} \rightarrow [TiO_2]\text{-}O\text{-}PtCl_4L^{n-} + HCl \quad (44)$$

The diffuse reflectance spectra of titania and 4.0% $PtCl_4$-O-TiO_2 are compared in Figure 10. The pronounced absorption of the modified material in the visible region is, by analogy with the solution spectrum of $Na_2[PtCl_6]$, tentatively assigned to a metal-centered transition of the platinum(IV)-chloride component. The steep increase in the absorption of the modified sample below 400 nm originates from the bandgap transition of TiO_2. The bandgap energy for an indirect crystalline semiconductor is obtained by extrapolation of the linear part of the plot of $(F(R_\infty)h\nu)^{1/2}$ versus $h\nu$. In the case of 4.0% $PtCl_4$-O-TiO_2 it amounts to 3.21 eV, which is slightly smaller than the value of the employed unmodified titania (3.27 eV). The absorption of these materials extends down to 620–650 nm, and corresponds to about 2.0 eV.

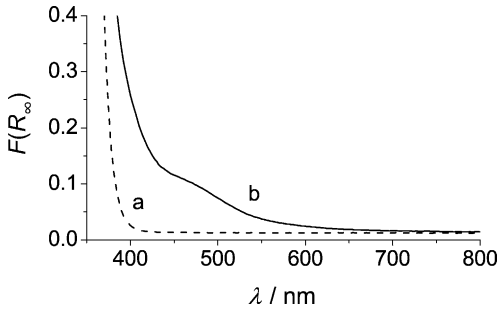

Figure 10. Diffuse reflectance spectra of a) titania and b) 4.0%$PtCl_4$-O-TiO_2.

The quasi-Fermi levels of the powders were measured by the suspension method to locate the approximate redox potentials of the reactive electron–hole pair. The dependence of the photovoltage on the pH value is summarized in Figure 11 for unmodified titania and for a series of $PtCl_4$-O-TiO_2 materials. From the inflection point (pH_o), the corresponding quasi-Fermi potentials at pH 7, as obtained from Equation (33) taking $k = 0.059$ V, are determined as −0.54 V, −0.49 V, −0.43 V, and −0.28 V for TiO_2 containing 0%, 1%, 2%, and 4% platinum, respectively. The reproducibility of the quasi-Fermi potential measurements was in the range of ±0.02 V. Since the onset of the TiO_2 part in the diffuse reflectance spectrum remains nearly constant for the various samples, the bandgap is not altered upon increasing the platinum chloride content.

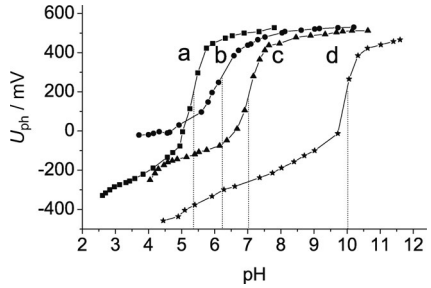

Figure 11. Photovoltage recorded for a) titania and $PtCl_4$-O-TiO_2 suspensions with b) 1.0%, c) 2.0%, and d) 4.0% platinum in 0.1 M KNO_3 in the presence of $(MV)Cl_2$ irradiated with polychromatic UV + Vis light. The position of the inflection point pH_o is marked by a dotted line.

5.3.2. *Titania–Halogenorhodium(III) Surface Complexes*

Pink and dark yellow powders are obtained when the preparation of $PtCl_4$-O-TiO_2 is carried out with the chlorides and bromides of rhodium(III), respectively, instead of hexachloroplatinate(IV).[94] These surface complexes are surprisingly stable. No dissolved rhodium complex was detectable by UV/Vis absorption spectroscopy after stirring an aqueous suspension of 4.0% $RhCl_3$-O-TiO_2 and 4.0% $RhBr_3$-O-TiO_2 for one day in the dark or under irradiation with visible light. Neither powder suffered desorption of the complex even after stirring for five days in the dark in 0.5 M KF. Thus, one can conclude that the Rh^{III} center is covalently bound to titania through a bridging oxygen ligand. This higher stability than $PtCl_4$-O-TiO_2 may reflect the fact that the metal–oxygen bond in the case of rhodium is stronger by 40 kJ mol^{-1} than that of platinum. The chloride ligands are completely displaced in strongly alkaline suspension, as also observed for 4.0% $PtCl_4$-O-TiO_2. From the amount of chloride produced in this experiment, a composition of $[RhCl_3(H_2O)_2$-O-$TiO_2]^-$ was proposed.

The diffuse reflectance spectra clearly indicate new absorption shoulders at 400–500 nm and 500–700 nm (Figure 12). The absorption at about 500 nm compares well with the lowest metal-centered transition of $[RhCl_6]^{3-}$ observed in hydrochloric acid at 518 nm. A strong increase in the absorption at wavelengths shorter than about 550 nm suggests that it does not originate exclusively from the second metal-centered transition that occurs in $[RhCl_6]^{3-}$ at 410 nm

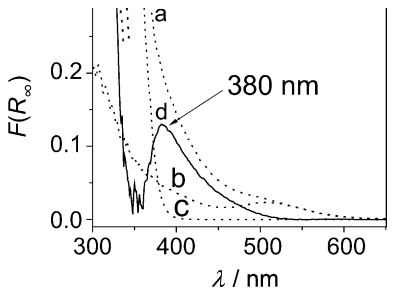

Figure 12. Diffuse reflectance spectra of a) 2.0% $RhCl_3$-O-TiO_2, b) 2.0% $RhCl_3$-O-SiO_2, and c) TiO_2. Spectrum d = a − (b + c).

with about the same intensity as the 510 nm band. Instead it may arise from a rhodium-to-titanium charge-transfer transition (MMCT). This is corroborated by the fact that the silica analogue 2.0% $RhCl_3$-O-SiO_2 does not exhibit a strong absorption increase at $\lambda \leq 550$ nm, most likely because it does not have a low-lying conduction band (Figure 12, curve b). An unsymmetrical absorption band is observed in the corresponding difference spectrum at a maximum of about 380 nm. In the case of 2.0% $RhBr_3$-O-TiO_2, a similar comparison with 2.0% $RhBr_3$-O-SiO_2 afforded the MMCT maximum at approximately 390 nm.

As observed for $PtCl_4$-O-TiO_2, an increase in the metal-complex loading does not significantly influence the bandgap but shifts the quasi-Fermi level anodically by about 0.20 V (see Table 1). Recently, it was reported that the halogenides of Ru^{III}, Ir^{IV}, and Au^{III} are also able to form visible light active titania photocatalysts.[95]

Table 1: Bandgap energies and quasi-Fermi potentials of electrons.

Photocatalyst	E_{bg} [eV][a]	${}_nE_F$*[pH 7, NHE] [V][a]
TiO_2	3.29	−0.54
0.5%$RhCl_3$-O-TiO_2	3.26	−0.53
1.0%$RhCl_3$-O-TiO_2	3.25	−0.48
2.0%$RhCl_3$-O-TiO_2	3.22	−0.46
5.0%$RhCl_3$-O-TiO_2	3.21	−0.34
2.0%$RhBr_3$-O-TiO_2	3.10	−0.32

[a] Reproducibility is ±0.05 eV. [b] Reproducibility is ±0.02 V.

5.3.3. *Metal Oxide Grafted Titania*

Depending on the detailed experimental conditions of the impregnation method discussed above for the preparation of grafted semiconductor powders, the physical and photochemical properties of the obtained materials may be quite different. A good example is the grafting of iron oxide species onto titania. When the impregnation of titania (0.05% Fe relative to rutile TiO_2) is performed with a solution of aqueous iron(III) chloride at pH 2 and 90 °C followed by thermal treatment at 110 °C, the grafted iron species are best described as amorphous FeO(OH) particles.[80] The absorption shoulder at 410–580 nm in the diffuse reflectance spectrum is assigned to a CT transition from the titania valence band to an FeO(OH)-localized surface state at about 0.5 eV below the conduction band edge (See Figure 1C and Figure 8b). The bandgap of 3.00 eV is not changed. In contrast, the use of $[Fe(acac)_3]$ (acac = acetylacetonate) in an anatase suspension in EtOH/*n*-hexane at room temperature and calcination at 500 °C generates an (FeO_x)-O-TiO_x surface complex that does not exhibit an absorption shoulder but exhibits a shift in the bandgap (see Figure 1D and Figure 8c) of about 0.40 eV. It was proposed that this shift originates from an iron-localized small energy band that overlaps with the titania valence band.[79,96]

Titania (rutile) grafted with copper oxide can be prepared as described above but replacing iron(III) chloride by copper(II) chloride and performing the heat treatment at 110 °C. As observed for Fe(OH)-O-TiO_2, CuO-O-TiO_2 also

exhibits a similar CT band at about 450 nm.[97] The electronic structure of both materials differs significantly from the halogenometallate–titania systems (Figure 1B) discussed above, since the new energy states are located close to the conduction band edge (Figure 1C).

5.3.4. Miscellaneous

In addition to binary systems, ternary types of grafted photocatalysts have also been reported. A very recent example is the CdS-O-TiO_2-O-WO_3 hybrid material prepared by precipitating CdS onto TiO_2-WO_3. The special combination was selected since the three semiconductors have band-edge positions well suited for interparticle electron transfer. Furthermore, a selective excitation of only one component is feasible, as indicated in Scheme 8.[98] Upon excitation at $\lambda \geq$ 495 nm, the reduction of $PMo_{12}O_{40}^{3-}$ by methanol is five and two times faster than that of CdS and of the binary systems, respectively. Surprisingly, physical mixtures of two semiconductor powders may also exhibit positive effects. For example, bismuth vanadate and Pt/$SrTiO_3$:Rh suspended in a solution of an electron relay (Fe^{3+}/Fe^{2+}, IO_3^-/I^-) are able to split water with visible light. A mechanism analogous to the Z-scheme of photosynthesis has been proposed.[99]

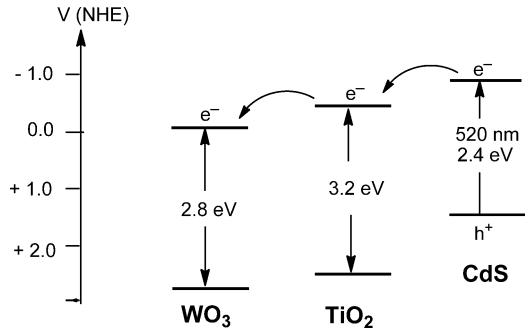

Scheme 8. Schematic description of postulated interparticle electron transfer in the hybrid CdS-O-TiO_2-O-WO_3.

5.4. Nonmetal "Doped" Titania

In addition to metals, nonmetals such as carbon, nitrogen, and sulfur have also been introduced into titania to achieve visible light activity. In most cases the nature of the dopant or modifier is unknown. Carbon and nitrogen "doping" in particular have received great attention in the last 10 years.[100] These beige-brown and slightly yellow powders may be prepared by simple precipitation/calcination procedures or more easily just by calcining titania in the presence of organic carbon or nitrogen compounds at temperatures of 200–600 °C. An example is the modification with thiourea, which was reported to afford a sulfur-doped titania with the dopant in the oxidation state + VI.[101] However, it was shown that the presence of sulfate is not responsible for visible-light activity since the material became more active after washing it with water.[102] In many cases it was also unknown whether true doping or surface modification was the reason for the visible-light activity. As two typical case studies we illustrate these problems for so-called nitrogen- and carbon-modified titania.

5.4.1. Nitrogen-Modified Titania

"N-doped" titania (TiO_2-N) has received great attention.[103] It has been prepared by three major methods: Sputtering and implantation techniques, calcination of TiO_2 under N-containing atmospheres generated by nitrogen compounds such as ammonia and urea, and by sol–gel methods with N-containing reagents.[103a] Despite the many proposals based more on theoretical than experimental results, the nature of the incorporated nitrogen species in most photocatalysts remains an open question. NO_x and various other nitrogen oxide species were proposed by Sato,[104] our research group,[102,105] and others.[106] Nitridic and amidic (NH_x) groups have also been proposed.[107] The simultaneous presence of nitrogen in differing oxidation states was even postulated.[108] Oxygen vacancies and color centers could also be responsible for the visible-light activity.[109] Depending on the preparation method and nitrogen source, the various TiO_2-N powders most likely contain diverse nitrogen species and, therefore, have different photocatalytic activities. A significant example is the unique difference between TiO_2-N prepared from ammonia[100] and urea.[107] Only the material obtained from the latter photocatalyzes the visible-light mineralization of formic acid to carbon dioxide and water, whereas ammonia-derived TiO_2-N is inactive. In an attempt to unravel the nature of the nitrogen species formed from urea, we investigated in detail the chemical and physical properties of the corresponding nitrogen-modified titania and compared it with the photocatalyst obtained from ammonia.[48,107,110]

Slightly yellow nitrogen-modified titania was prepared by calcining a 1:2 (wt/wt) mixture of titania and urea at 400 °C in a rotating flask. Elemental analysis revealed the presence of nitrogen (0.78%) and carbon (0.40%), and therefore these powders are abbreviated in the following as TiO_2-N,C. According to powder X-ray diffraction analysis, all the powders retained the anatase structure of the starting material and consist of 10–13 nm sized crystallites. Electron microscopy indicated that the latter form micrometer-sized aggregates. A specific surface area of 180 $m^2 g^{-1}$ was measured by N_2 absorption. The new materials exhibit a bandgap-narrowing of 0.16–0.33 eV and a slight anodic shift of the quasi-Fermi level of 0.05–0.08 V compared to unmodified titania. This shift may be due to a higher positive surface charge induced by protonation of the more basic TiO_2-NH groups compared to the Ti-OH present in pristine titania (see below). TiO_2-N,C induced a very efficient visible-light mineralization of formic acid ($\lambda \geq 455$ nm).[111]

Since heating urea at 300–420 °C affords ammonia and isocyanic acid, this gas mixture was simulated by heating the isocyanic acid precursor cyanuric acid in the presence of ammonia and titania at 400 °C. The resulting material also efficiently photocatalyzed the mineralization of formic acid. It is also known that isocyanic acid in the presence of silica

surface OH groups is catalytically converted into melamine in the same temperature range by cyclotrimerization of cyanamide. Melamine could be produced analogously at the titania surface [Eqs. (45)–(47)].

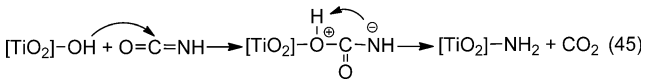

$$[TiO_2]-OH + O=C=NH \rightarrow [TiO_2]-O-C(=O)-NH \rightarrow [TiO_2]-NH_2 + CO_2 \quad (45)$$

$$[TiO_2]-NH_2 + H-O-C\equiv N \rightarrow [TiO_2]-OH + H_2N-C\equiv N \quad (46)$$

$$6(NH_2)_2CO \xrightarrow{400\,^\circ C,TiO_2} C_3H_6N_6 + 6\,NH_3 + 3\,CO_2 \quad (47)$$

In fact, when melamine instead of urea was used, TiO_2-N,C was again produced. Since melamine is converted into white-beige melem and yellow melon at 400 °C, it appeared likely that both are present in TiO_2-N,C (Figure 13). Accordingly, TiO_2-N,C can also be prepared by thermal treatment of a prefabricated yellow melem/melon mixture with titania at 400 °C. Grinding the melem/melon mixture with titania at room temperature produced only an inactive material.

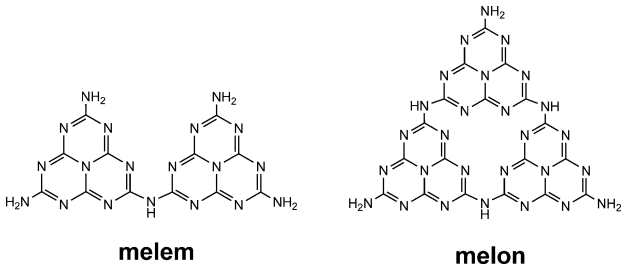

Figure 13. Two major condensation products of melamine produced at 350–500 °C in the absence of titania.[112]

From these results, it follows that a key step in the modification process is the titania-catalyzed formation of melamine from urea. Subsequent condensation affords a mixture of polytriazine amines, predominantly melem and melon. Thereafter, condensation between the *s*-triazine amino and titania OH groups generates Ti–N bonds (Scheme 9). Thus, the visible light absorbing triazine derivative becomes chemically bound to the semiconductor. Accordingly, the modification is not successful when titania is dehydroxylated before use by heating it in vacuo at 400 °C. Further support for the presence of a Ti–N bond comes from the reaction of TiO_2-N,C with sodium hydroxide at 100 °C, which produces cyameluric acid, ammonia, and a white powder (Scheme 10) that is inactive in the degradation of formic acid in visible light. It is known that the amino groups in melem can be replaced by OH groups through nucleophilic attack of hydroxide to generate cyameluric acid.[113]

The diffuse reflectance spectrum of TiO_2-N,C displays a weak shoulder in the range 400–450 nm (Figure 14). From a comparison with the spectrum of a melem/melon mixture one can conclude that the visible absorption in TiO_2-N,C does not origin from a local excitation of the polytriazine component but rather from a CT transition from the sensitizer to the titania conduction band.

The chemical results discussed above clearly indicate that the same photocatalyst is obtained irrespective of whether urea or melem/melon is used as the modifier. In the latter case, higher concentrations of the sensitizer generate not only a titania–sensitizer surface complex but a thin layer of a crystalline melon-type material, as evidenced by the presence of an otherwise unobserved XRD peak at a 2θ value of 27.4°. This can be assigned to the stacked aromatic system of carbon nitrides. Graphitic carbon nitride obtained by heating cyanamide at 650 °C photocatalyzes the reduction and oxidation of water by alcohols and silver salts in visible light, respectively.[49,114]

In summary, these findings indicate that so-called nitrogen-doped titania when prepared from urea and titania at 400 °C produces a poly(amino-tri-*s*-triazine) sensitizer that is chemically bound to the semiconductor. Therefore, and in contrast to previous reports, the visible-light photocatalytic activity of "N-doped" or "N-modified" titania prepared from urea does not originate from the presence of nitridic, amidic, and nitrogen oxide species or color centers.

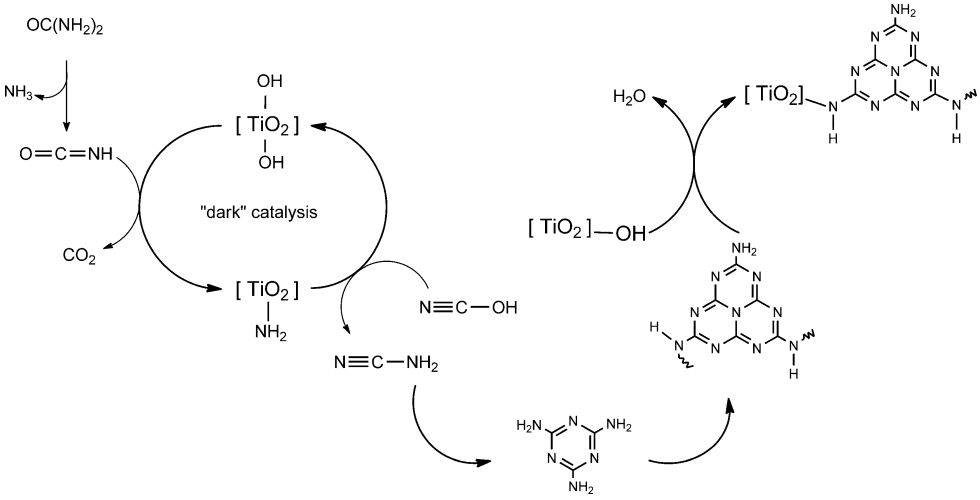

Scheme 9. Proposed mechanism of urea-based titania modification.

5.4.2. *Carbon-Modified Titania*

Carbon-modified titania (TiO_2-C), initally prepared from $TiCl_4$ and tetrabutylammonium hydroxide,[43] has since become a technical product because of its easy preparation

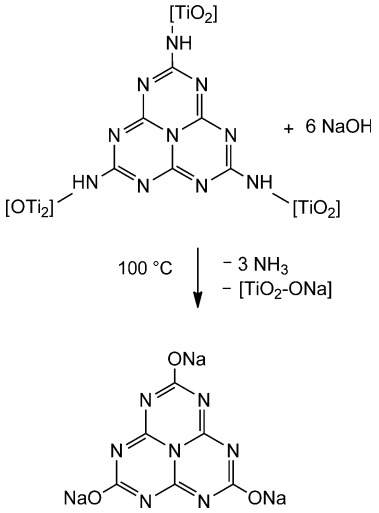

Scheme 10. Nucleophilic displacement of cyameluric acid from TiO_2-N,C.

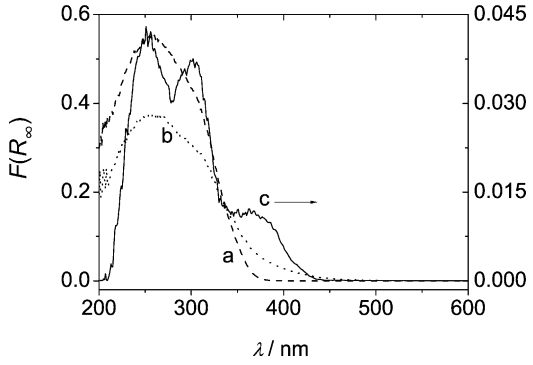

Figure 14. Diffuse reflectance spectra of a) TiO_2, b) TiO_2-N,C, and c) melem, melon. All samples were diluted with $BaSO_4$. Note the different scales of the left and right axes.

by calcining titania at 250–500 °C in the presence of an organic compound as the carbon source.[115] Many reports concerned with this type of modification with solid, liquid, or gaseous carbon sources have since been published.[116] Alternatively, the organic substituent in a titanium alcoholate may also serve as the carbon precursor after hydrolysis and thermal treatment.[116e,117] All these so-called "C-doped" titania materials exhibit a weak absorption shoulder at 400–800 nm, the intensity of which increases with increasing carbon content.[43,117a] In the case of TiO_2-C, the absorbance steadily increases as the carbon content increases to 0.03 %, 0.42 %, and 2.98 %, whereas the reaction rate of the oxidation 4-chlorophenol with visible light exhibits a maximum at 0.42 %.[43]

In general, the C1s binding energy, as readily determined by XPS analysis, was considered the diagnostic tool for the type of carbon species present. From the determined values of 284.8–285.7 eV,[43,116c,118] the presence of elemental carbon and graphitic or coke-like carbon was proposed.[117a,118f] However, since the binding energies of carbidic carbon (281.8–284.3 eV)[116a,118a,b,e,119] and aromatic ring carbon atoms (284.3–284.7)[120] fall in the same range, the assignments are ambiguous. Binding energies of 288.6 and 288.9 eV were proposed to arise from structural fragments such as Ti-O-C[116c] and Ti-OCO.[121] Density functional theory calculations suggest that substitutional (of lattice oxide) and interstitial carbon atoms are present.[122] EPR spectroscopic analysis of anatase powders prepared from alcoholates as carbon source showed a symmetric paramagnetic signal at $g = 2.005$, which was assigned to an aromatic coke-like species.[117a] Although the intensity increased upon irradiation with visible light, it could not be concluded beyond doubt that the corresponding radical is involved in the photocatalysis process since the concentration of radicals was about five to six orders of magnitude lower than the total carbon content.[118c] In contrast to this, it was proposed that in carbon-modified titania prepared from gaseous cyclohexane this paramagnetic signal arises from an electron trapped at an oxygen vacancy.[116f]

Most of these carbon-modified anatase materials are active in visible-light photooxidations of various organic pollutants such as 4-chlorophenol,[43,116b,118d] 2-propanol,[118a] gaseous benzene,[116f] and nitrogen oxides.[116a,e,117c] It was generally proposed that the presence of some carbon species in titania is necessary for the observation of visible light activity. However, another suggestion was that not carbon species but oxygen vacancies, generated only in the presence of a carbon source, were responsible.[109a,b] Simple chemical experiments were thus conducted with the commercial visible-light photocatalyst VLP of anatase structure to differentiate between these two contrary proposals.[43,123]

Heating an alkaline suspension of beige VLP powder at 90 °C afforded a homogeneous brown extract ($SENS_{ex}$) and an almost white residue (VLP_{res}). When VLP_{res} was resuspended in the $SENS_{ex}$ solution at 90 °C and subsequently calcined at 200 °C a slightly brownish powder VLP_{reas} (reassembled) was isolated that exhibited the same photocatalytic acitvity in the visible-light mineralization of 4-chlorophenol as the starting VLP. Furthermore, XPS analysis of VLP_{reas} and VLP revealed no significant differences, as indicated by the C1s binding energies of 284.8, 286.5, and 288.4 eV for VLP_{reas} and 284.8, 286.3, and 288.8 eV for VLP. The peaks at 286.5 and 286.3 eV were tentatively assigned to a bidentately bound arylcarboxylate. All atempts to isolate a pure compound from $SENS_{ex}$ failed. Further evidence for the success of the reassembling procedure was obtained by measuring the quasi-Fermi level of electrons ($_nE_F$*) in the three relevant powders (Figure 15). VLP and VLP_{reas} exhibited the same result, which was in this case one unique $_nE_F$* value of −0.50 V (NHE), whereas −0.56 V was obtained for VLP_{res}. The latter value suggests that the powder remaining after extraction consists of unmodified anatase, in accordance with the XRD data, whereas the anodically shifted value is characteristic of carbon-doped titania.[43]

The results summarized above suggest that the alkali extract $SENS_{ex}$ contains carboxylic groups, which undergo esterification with titania surface hydroxy groups during the reassembling reaction. This is corroborated by FTIR analysis of the brown residue obtained from $SENS_{ex}$ after the removal of water from the basic solution (pH 12). The sample exhibited intense peaks at 1580 and 1420 cm^{-1} (KBr), which

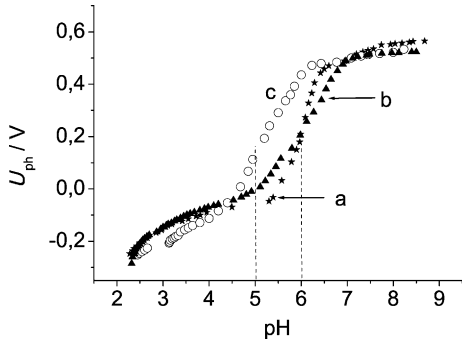

Figure 15. Variation of photovoltage with pH value for the suspension of various photocatalysts in the presence of methylviologen dichloride. a) VLP, b) VLP_{reas}, c) VLP_{res}. Dashed lines indicate pH values of inflection points from which the quasi-Fermi level can be calculated.

were assigned to asymmetric and symmetric stretching vibrations of an arylcarboxylate group. The corresponding values of, for example, free sodium benzoate are 1552/1414 cm^{-1} (KBr). Unfortunately, no corresponding peaks could be obtained in the FTIR spectra of VLP and VLP_{reas}, either when measured conventionally or by the ATR technique. This failing suggests that the sensitizer is present as a thin surface layer of too low a concentration to be detected by FTIR spectroscopy. The fact that the significant carbon peaks at 286.3 eV and 288.8 eV in the XPS spectrum completely disappear after sputtering with argon for 3 min, which is sufficient to remove a 4 nm thin surface layer, corroborates this explanation.

The results summarized above indicate that the visible-light activity of VLP and probably of many previously reported so-called "C-doped" titania powders does not originate from the presence of lattice carbon atoms or oxygen defects as is generally reported. Although the present findings do not exclude the presence of defects in the commercial photocatalyst VLP, there is no experimental evidence that they are involved in the visible light induced charge separation.

6. Nitrogen Fixation

After photosynthesis, nitrogen fixation is the second most important chemical process in nature. The mild reaction conditions of the enzymatic reaction, compared to the Haber–Bosch process, stimulated numerous investigations on the synthesis and thermal reactivity of N_2–transition-metal complexes. Relevant examples are the reductive protonation to generate ammonia with concomitant oxidation of the central metal ion, oxidative alkylation with alkyl halogenides to afford alkyldiazenido complexes,[124] and successive addition of methyllithium and trimethyloxonium tetrafluoroborate to generate a 1,2-dimethyldiazene complex.[125] Comparably few studies were published on photofixation, especially at simple inorganic photocatalysts. The first report dealt with the UV irradiation of humidified titania powder doped with iron oxide in a closed system. A few micromoles of ammonia and molecular oxygen were produced, and their origin from dinitrogen and water was proven by isotopic labeling studies.[126] No ammonia was formed when nitrogen was bubbled through an aqueous suspension of the irradiated powder. It was proposed that nitrogen is reduced to ammonia at the titanium centers via diazene and hydrazine intermediates. The oxidation of surface Ti-OH was suggested as the primary step of water oxidation. The most active photocatalyst was obtained from powdered anatase doped with 0.2% Fe_2O_3 by heating for three hours at 1000 °C. This treatment caused a partial conversion into rutile, thereby producing crystals with diameters from 0.1 to 0.3 μm. Higher iron contents resulted in inactive materials.

Subsequent work by other authors confirmed these results, although the nature of the reducing agent was unknown in most cases since oxygen was only rarely identified.[127] In general, ammonia concentrations were in the range 1–10 μM and excitation by UV light was necessary. Even in the absence of any dopant, an electrochemically formed titania layer was reported to generate ammonia upon UV irradiation.[128] These partly contradictory results induced adverse discussions which culminated in the proposal that all the previously reported yields of ammonia originate from traces of this gas present in the laboratory air.[129] However, this possibility can be easily excluded by working with $^{15,15}N_2$.[126] Furthermore, as discussed in Section 5, it is well known that the photocatalytic properties of semiconductor powders are strongly influenced by the composition of the crystal phase, crystal size, and the presence of impurities. The controversial results, therefore, most likely stem from the intrinsic difficulties in controlling the calcination of powder mixtures. It seemed meaningful, therefore, to use the more easily controllable sol–gel method. In a first attempt, we prepared nanostructured thin films of iron titanates with various Fe/Ti ratios. In contrast to the previously employed titania powders containing only 0.2% iron, the most active films have an Fe/Ti ratio of 1:1 and are also able to fix nitrogen with visible light.[54,130]

6.1. Film Preparation and Characterization

The thin films were prepared from an alcoholic solution of anhydrous iron(III) chloride and titanium tetraisopropylate in ratios of Fe/Ti = 1:1 or 1:2 by dip-coating glass slides, followed by hydrolysis in humid air and annealing at 600 °C. No photoactive film was obtained when hydrous iron chloride was employed or the films were annealed at 500 °C or 700 °C. Electron microscopy images of the iron titanate film obtained from a 1:1 metal ratio indicated the presence of a nanostructured matrix of about 300 nm thickness. It contains 15–20 vol% cubic crystals with an average diameter of 150 nm. The ratio of Fe/Ti/O was determined by energy-dispersive X-ray (EDX) analysis as 1:1:3.5 for both the matrix and the crystals. This composition suggests that the compound $Fe_2Ti_2O_7$ is present. It was previously obtained only as an intermediary phase by heating ilmenite minerals ($FeTiO_3$) in oxygen at 700 °C.[131] The XRD spectra also suggest the presence of traces of pseudobrookite (Fe_2TiO_5) and anatase. In the Mössbauer spectrum of the 1:1 film, the doublet at $\delta =$

0.462 mm s^{-1} (relative to α-Fe; $\Delta E_Q = 0.910$ mm s^{-1}) indicates the presence of a hexacoordinated Fe^{III} center. The UV/Vis spectrum of titania (Figure 16, curve a) is red-shifted down to

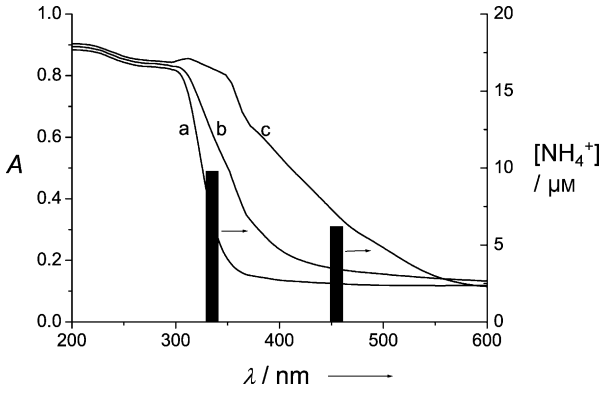

Figure 16. UV/Vis absorption spectra of various films and wavelength dependence of ammonia formation. a) TiO_2, b) Fe/Ti = 1:2, c) Fe/Ti = 1:1. The height of the two vertical bars indicates ammonia concentrations when cut-off filters were employed at $\lambda \geq 335$ and $\lambda \geq 455$ nm for irradiation of the 1:1 film.

600 nm upon increasing the Fe/Ti ratio of the starting metal compounds from 1:2 to 1:1 (Figure 16, curves b and c, respectively). Since the $Fe_2Ti_2O_7$ film produced the highest amount of ammonia, all the results discussed in the following refer to this material and to the use of EtOH (75 vol%) as the reducing agent unless otherwise noted.

The anodic photocurrent observed upon irradiation of an $Fe_2Ti_2O_7$/ITO (ITO is indium tin oxide, a conducting glass) electrode at wavelengths of 320–640 nm suggests the presence of an n-type semiconductor (Figure 17, curve a). The addition of methanol to the electrolyte results in an increase in the photocurrent by a factor of about 3 (at 380 nm, Figure 17, curve b), an effect known in photoelectrochemistry as current amplification (see Section 3). This effect is based on electron injection of the CH_2OH radical, formed by the initial hole oxidation, into the semiconductor conduction band. When the film was calcined at 700 °C, 500 °C, or lower temperatures, the resulting electrode did not exhibit current amplification in the

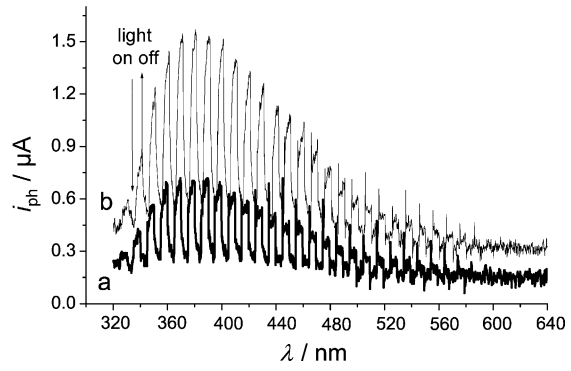

Figure 17. Photocurrent action spectrum of the $Fe_2Ti_2O_7$/ITO electrode a) before and b) after the addition of methanol. The applied potential was 0.5 V versus Ag/AgCl.

presence of methanol and the film was inactive in nitrogen photofixation. Photoelectrochemical measurements of the quasi-Fermi level of electrons were performed by recording the photovoltage of the iron titanate film on glass as a function of the pH value in the presence of methylviologen. The plot of photovoltage versus pH value surprisingly exhibited two inflection points: $pH_o(1)$ and $pH_o(2)$ at pH 4.5 (±0.2) and pH 8.6 (±0.2), respectively (Figure 18A). The first and second inflection points correspond to quasi-Fermi levels of

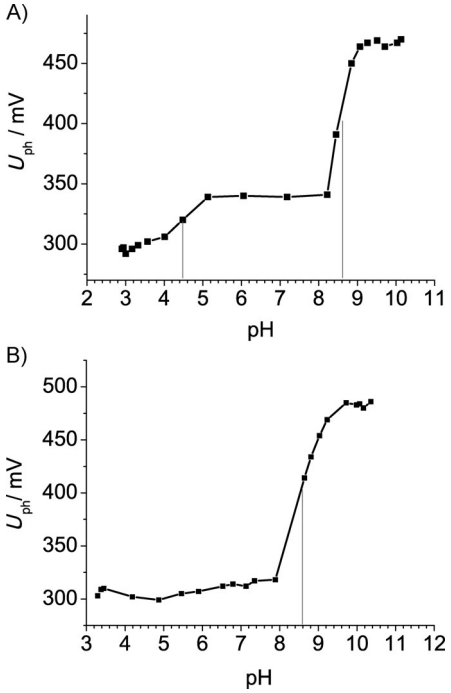

Figure 18. Photovoltage versus pH value recorded for the $Fe_2Ti_2O_7$ film in 0.1 M KNO_3 in the presence of 1 mM methylviologen dichloride. Irradiation A) without filter and B) through a 455 nm cut-off filter.

−0.60 V and −0.32 V, respectively. The first level can be assigned to traces of anatase, as also evidenced by XRD analysis. When a cut-off filter of 455 nm was inserted into the exciting light beam, the first inflection point disappeared, whereas the second was still present at the same pH_o value of 8.6 (Figure 18B). Under these irradiation conditions, the titania component cannot be excited and, therefore, the photovoltage must originate from the $Fe_2Ti_2O_7$ phase. These conclusions are also supported by spectroelectrochemical experiments.[54] Such a wavelength-dependent photovoltage measurement offers an easy method for testing the composition of a semiconducting thin film or powder.

6.2. Formation of Ammonia, Hydrazine, and Nitrate

Irradiation ($\lambda \geq 320$ nm) of the iron–titania films in EtOH/H_2O solutions was performed under N_2 bubbling or in a closed system after saturation with N_2. The maximum background concentrations of ammonia were 2 μM. Corrected ammonia concentrations of 3–17 μM were observed, depend-

ing on the solvent composition. No significant amounts of ammonia formed in the absence of EtOH. Acetaldehyde was detected after 90 min of irradiation and reached a concentration of 13 mM after 24 h. Ammonia is also produced upon excitation with visible light ($\lambda \geq 455$ nm, Figure 16), thus resulting in the absorption of light by the traces of titania becoming impossible. Excitation of an analogously prepared titania-free iron oxide film with visible light did not produce ammonia.

Experiments performed in a closed $^{15,15}N_2$ atmosphere followed by addition of excess $(^{14}NH_4)_2SO_4$ and subsequent oxidation of ammonia with sodium hypobromite generated $^{29}N_2$, as indicated by the intense signal at $m/z = 29$ (Figure 19).

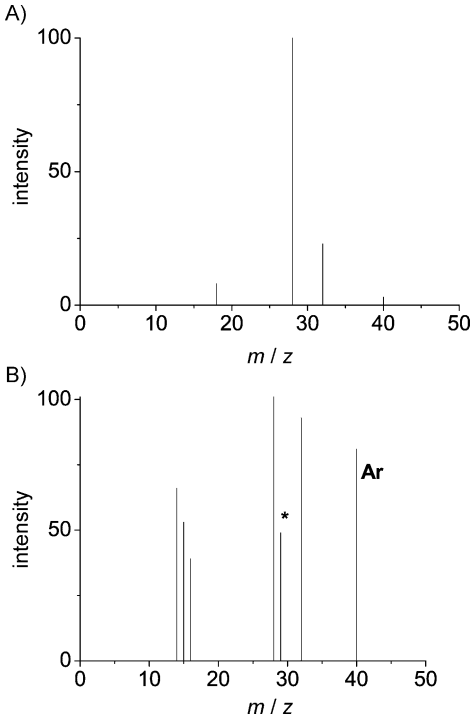

Figure 19. Mass spectra of gas samples obtained from hypobromite oxidation of the reaction solution after 4 h irradiation time. Gas phase in Schlenk tube A) before and B) after filling with product gas.

The same result was obtained when ethanol was replaced by humic acid as the reducing agent.[132] These results prove that the ammonia detected after irradiation originates from the reduction of dinitrogen and not from some unknown impurities.

Complete inhibition of ammonia formation was observed upon bubbling with a mixture of $N_2/CO = 10:1$. The effect is reversible; the same film induced ammonia formation after it had been washed with water. It is known that carbon monoxide inhibits the enzymatic fixation of nitrogen. Ethanol may be replaced by the naturally occurring reducing agent humic acid (see Figure 20, curve e). Figure 20 shows the time dependence of the ammonia concentration under various reaction conditions. Lines (a)–(c) show that the ammonia concentrations never exceeded values of 2 μM in all the blank experiments. However, the formation of ammonia under N_2

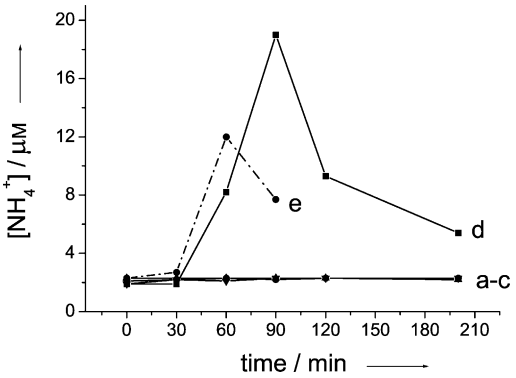

Figure 20. Ammonia formation as a function of irradiation time in EtOH (75 vol%, (a)–(d)). a) Solution with immersed film prior to nitrogen bubbling and irradiation, b) subsequent nitrogen purging in the dark, c) irradiation under argon bubbling, d) irradiation under N_2. e) irradiation under N_2 in the presence of 10^{-2} g L^{-1} of aqueous humic acid in ethanol-free water.

bubbling started after an induction period of 30 min and passed through a maximum of 17 μM at 90 min of irradiation time (Figure 20, curve d). The ammonia concentration decreased by about 60% on using air instead of nitrogen purging.

As shown by Figure 21 (curve a), the photoreduction has a rather long induction period of about 30 min, which suggests formation of the true photocatalyst or of a mutual reaction

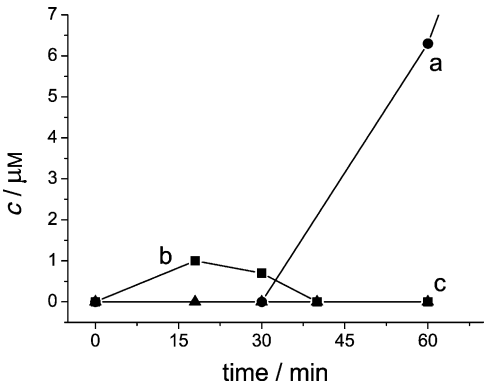

Figure 21. Concentrations of a) ammonia and b) hydrazine under N_2 (b) and under Ar (c).

intermediate such as hydrazine. In fact, small amounts of hydrazine are produced during the first 15–30 min, with a concentration maximum at about 20 min (Figure 21, curve b). This result clearly suggests that nitrogen is photoreduced to hydrazine in the induction period. No hydrazine was detectable when nitrogen was replaced by argon. To test if the further reduction of hydrazine occurs thermally or photochemically a 15 μM solution of hydrazine was employed as a substrate. Whereas the photoreaction produced a 25 μM solution of ammonia after 90 min, the thermal reactions, conducted at 50 °C and room temperature, did not exceed the blank value of 2 μM (Figure 22). These results suggest that

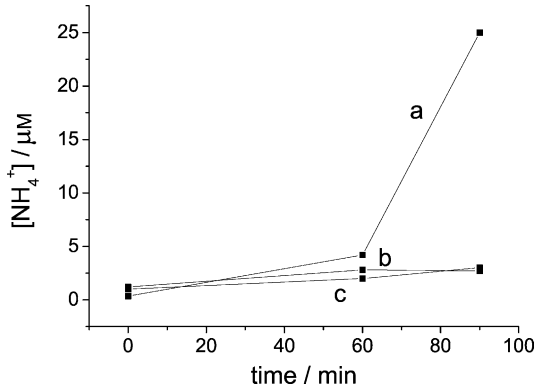

Figure 22. Formation of ammonia from hydrazine in the presence of the iron titanate film upon a) irradiation or stirring in the dark at b) 50 °C and c) at room temperature.

during the nitrogen reduction process hydrazine is also reduced to ammonia photochemically.

The disappointing decrease in the ammonia concentration after 90 min irradiation time (Figure 20, curve d) suggests a deactivation of the iron titanate film or a consecutive reaction, such as oxidation to nitrate, as known from the UV excitation of titania.[133] Since the photoactivity of a used film after repeated washing with water decreased by only 15%, a deactivation of the photocatalyst is rather unlikely. Furthermore, no iron ions were detectable in the solution after 24 h of irradiation. These observations suggest that the primary product ammonia may be oxidized to nitrite/nitrate by traces of oxygen introduced during nitrogen bubbling. Whereas only traces of nitrite were detectable, the nitrate concentration reached 45 μM in the film and 7 μM in solution (Figure 23). When the nitrogen was substituted by air, the total concentration of nitrate was 30 μM. Nitrate was formed in appreciable amounts only when ammonia reached its maximum concentration. This observation suggests that nitrate is produced via intermediary ammonia and not by a mutual direct oxidation of nitrogen. In accordance with this conclusion is the fact that no nitrite/nitrate was generated in the absence of EtOH. To find out if the oxidation of the initially produced ammonia is a photochemical or thermal process, a solution of ammonium chloride of comparable concentration was stirred at 50 °C in the dark in the presence

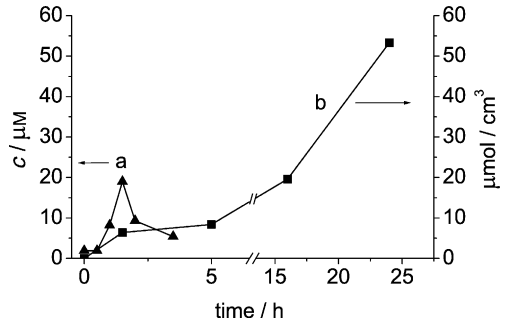

Figure 23. Concentration of ammonia in solution (a) and total nitrate concentration (b) as a function of irradiation time.

of the iron titanate film. Surprisingly, nitrate formation was observable, thus indicating the presence of a thermal process. No nitrate was produced in the absence of the film.

6.3. Role of Chloride Ions

Prolonged washing of the iron titanate film with water produced chloride ions, which suggests that hydrolysis of Fe–Cl bonds during the film preparation was incomplete. The remaining film was inactive, even upon addition of 20 or 40 μM sodium chloride solution. In agreement with this observation is the result that an iron titanate film produced from iron chloride hydrate is inactive. This dominating role of chloride ions suggests that in the oxidative primary step chloride, not ethanol, is oxidized [Eq. (48)]. The resulting adsorbed chlorine atom then oxidizes ethanol to the hydroxyethyl radical [Eq. (49)] followed by re-formation of the reactive surface iron chloride species [Eq. (50)].

$$h_r^+ + [Fe^{III}Cl]_s \rightarrow [Fe^{III}]_s^+ + Cl_{ads} \quad (48)$$

$$Cl_{ads} + CH_3CH_2OH \rightarrow CH_3CHOH + Cl^- + H^+ \quad (49)$$

$$[Fe^{III}]_s^+ + Cl^- \rightarrow [Fe^{III}Cl]_s \quad (50)$$

This unprecedented role of surface Fe–Cl bonds differs from titania-photocatalyzed oxidation reactions in the presence of hydrated chloride ions. In this latter case, both inhibiting and accelerating effects were observed.[134] When anhydrous iron(III) bromide is used as the starting material instead of the corresponding chloride, the resulting film is a little less active, in agreement with the lower oxidation potential of a bromine atom. About the same activity is also obtained when the film is prepared from iron(III) acetylacetonate, thus suggesting that ethanol oxidation can also proceed in the absence of an Fe–X bond (X = Cl, Br), either via an initially formed acetylacetonyl radical or through direct reaction with the reactive hole.

6.4. Mechanism

On the basis of the experimental results presented above, a semiconductor photocatalysis mechanism has been proposed for this unique nitrogen photofixation process (Scheme 11). Absorption of a photon by the $Fe_2Ti_2O_7$ phase generates a reactive electron–hole pair trapped at iron and oxygen surface centers. The hole oxidizes ethanol to the hydroxyethyl radical directly or indirectly through Equations (48)–(50). Subsequently the hydroxyethyl radical injects an electron into the conduction band to afford acetaldehyde as the oxidation product, analogous to the current amplification effect (Figure 17). As already noted, films that do not exhibit this effect also do not induce ammonia formation. Thus, the absorption of one quantum of light generates the two electrons necessary for the crucial first reaction step: the proton-coupled two-electron reduction of N_2 to diazene, which is known experimentally as the primary reduction

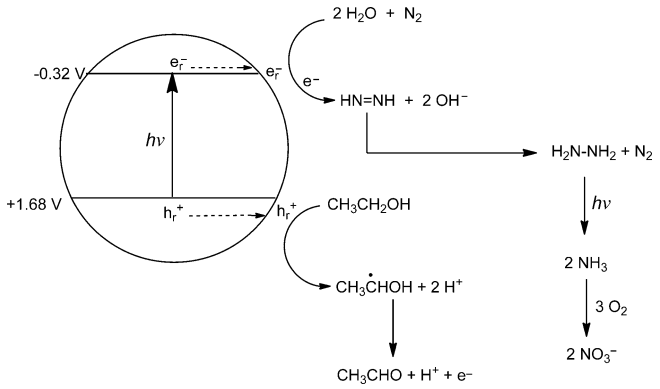

Scheme 11. Simplified mechanistic scheme of the visible-light photofixation of nitrogen to nitrate. The upper and lower horizontal lines represent conduction and valence band edges, respectively.

product in homogeneous model systems of biological nitrogen fixation.[126,135] It is emphasized that this is a likely proposal without any firm experimental evidence. Disproportionation of this short-lived intermediate produces N_2 and hydrazine, the latter of which is subsequently photoreduced to ammonia. The following oxidation of ammonia to nitrate by traces of oxygen is the thermally catalyzed final reaction step.

Humic acid can also act as a reductant instead of ethanol, as shown in Figure 20. Since humic acids are ubiquitous in nature and $Fe_2Ti_2O_7$ phases may be formed through solar oxidative weathering of ilmenite, this novel nitrogen photofixation may be an example of a light-driven non-enzymatic nitrogen fixation under natural conditions. It should be possible to induce solar photocatalysis at semiconducting mineral surfaces in future environmental research. An impressive example is the solar reduction of nitrogen at rutile-containing desert sands.[136]

7. C–H Activation

The activation and functionalization of alkanes is one of the major challenges in chemistry.[137] The only industrially applied process is the photosulfoxidation of liquid alkanes by sulfur dioxide and oxygen in the presence of UV light [Eq. (51)].

$$R{-}H + SO_2 + 1/2\,O_2 + h\nu \rightarrow RSO_3H \quad (51)$$

The linear alkanesulfonic acids resulting from the linear C_{16-20} alkanes are used as biodegradable surfactants. The alkane activation step consists of hydrogen abstraction from the alkane by triplet-excited sulfur dioxide. Subsequent addition of SO_2 to the generated alkyl radical affords an alkylpersulfonyl radical, which undergoes a further hydrogen abstraction to produce another alkyl starter radical and the persulfonic acid (Scheme 12). Fragmentation and hydrogen abstraction [Eqs. (52) and (53)] produce the alkanesulfonic acid.[138]

$$RSO_2\text{-}O\text{-}O\text{-}H \rightarrow RSO_2\text{-}O^{\bullet} + OH^{\bullet} \quad (52)$$

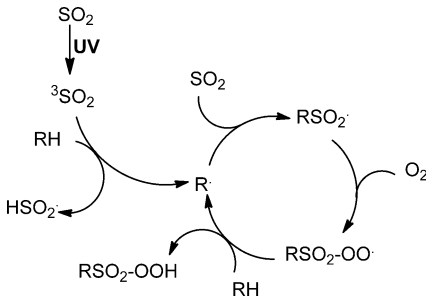

Scheme 12. Basic reaction steps in UV-induced photosulfoxidation of alkanes.

$$RSO_2\text{-}O^{\bullet} + R\text{-}H \rightarrow RSO_3H + R^{\bullet} \quad (53)$$

Accordingly, the overall reaction is a photoinduced radical chain reaction and product formation continues even after turning off the light. In general, regioisomeric alkyl radicals are formed in the hydrogen abstraction step, except in the case of adamantane photosulfoxidation in the presence of hydrogen peroxide, which affords 1-adamantanesulfonic acid regioselectively.

Since hydroxyl and hydroperoxyl radicals are generated at the semiconductor surface in the presence of oxygen [Eqs. (18), (24)–(29)], they may also undergo hydrogen abstraction with an alkane and induce a similar chain reaction. Accordingly, suspensions of various titania powders in *n*-heptane were irradiated with visible light ($\lambda \geq 400$ nm) under an atmosphere of $SO_2/O_2 = 1{:}1$ (v/v). Surprisingly, the formation of *n*-heptanesulfonic acid was observed not only with modified titania that absorbed visible light, but also with the unmodified sample. This finding suggested the formation of a charge-transfer complex between titania and one of the reaction components. In fact, exposure of P25 to sulfur dioxide results in the powder obtaining a yellowish coloration, as is also evident from a broad absorption maximum in the diffuse reflectance spectrum at 410–420 nm (Figure 24).

Product formation stopped after 6 h of irradiation time under the given experimental conditions. However, separating the catalyst powder and washing it with methanol restored the activity. The photocatalyst still retained its original activity after repeating this procedure three times (Figure 25). This behavior suggested that the reaction is

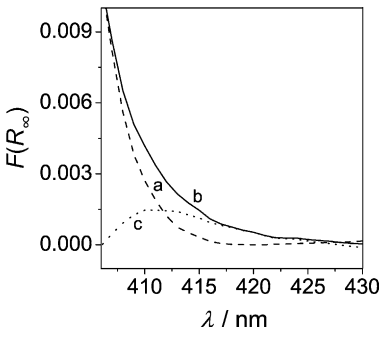

Figure 24. Diffuse reflectance spectra of the titania sample P25 in a) the absence and b) presence of SO_2. Curve (c) corresponds to the difference spectrum of (b) − (a).

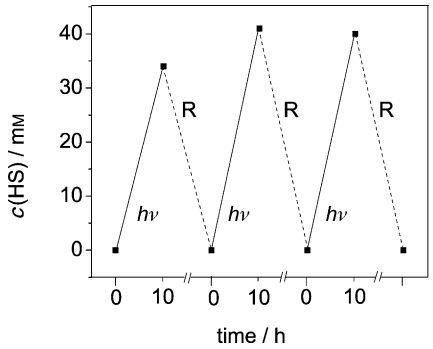

Figure 25. Sequential photosulfoxidation of *n*-heptane. $\lambda_{irr} \geq 400$ nm. HS = *n*-heptanesulfonic acid, R = regeneration.

inhibited by strong product adsorption and that washing desorbs the sulfonic acid. Accordingly, no product was formed when heptanesulfonic acid was added to the suspension prior to irradiation. A similar deactivation and activation was observed during photooxidation of sulfur dioxide in the presence of gaseous *n*-heptane at UV-irradiated titania.[139] Product formation was also inhibited when small amounts, such as 0.3 vol%, of water were present in the suspension. This may be due to blocking the reactive surface centers for oxidation of the heptane by preferential adsorption. When the irradiation was stopped after 2 h, which resulted in a product concentration of 15 mM, and the reaction left for three days in the dark at room temperature, the product continued to form and resulted in 50 mM sulfonic acid. However, product formation did not continue when the radical scavenger hydroquinone was present during the dark phase. All these observations suggest that the new photosulfoxidation is a radical chain reaction. However, the alkyl starter radical is generated not by the UV excitation of sulfur dioxide but through visible-light absorption of the TiO_2/*n*-heptane/SO_2/O_2 system. A proposed mechanism for the generation of alkyl radicals is shown schematically in Scheme 13.

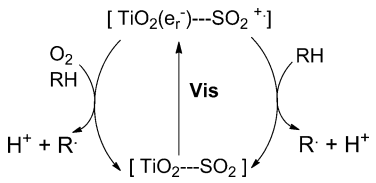

Scheme 13. Postulated mechanism of visible light induced generation of alkyl radicals.

Excitation of the charge-transfer complex by visible light generates a reactive conduction band electron [$TiO_2(e_r^-)$] and an adsorbed sulfur dioxide radical cation. Oxygen reduction by $TiO_2(e_r^-)$ produces superoxide, whereas the adsorbed radical cation may oxidize the alkane to the alkyl radical and a proton. A reduction potential of about 1.8 V is estimated for the latter reaction step. Superoxide may also generate an alkyl radical through protonation to the hydroperoxyl radical by adsorbed water or surface OH groups [see Eqs. (24)–(29)] and subsequent hydrogen abstraction from the alkane. The alkyl radical thus produced is expected to initiate a radical chain reaction as formulated for the stoichiometric photosulfoxidation by UV light [Scheme 12, Eqs. (52) and (53)]. The complete inhibition observed in the presence of only 10 vol% 2-propanol, which should be oxidized much faster than the alkane and which is also an efficient OH radical scavenger, is in agreement with the mechanistic proposal.

The general applicability of the presented C–H activation is demonstrated by the successful photosulfoxidation of cyclohexane and adamantane. In the latter case, glacial acetic acid was employed as a solvent. In summary, this novel visible light induced C–H activation can be classified as a semiconductor photocatalysis type B reaction, which extends the two-substrate addition [Eq. (17)][20] to the three-substrate addition scheme A + B + C = D.

8. C–C and C–N Coupling

Following the early work of Kraeutler and Bard on the TiO_2-catalyzed photo-Kolbe reaction,[140] many studies appeared concerning photocatalytic organic reactions in the presence of colloidal or suspended semiconductor particles. They include *cis–trans* isomerizations,[69b,141] valence isomerizations,[142] substitution and cycloaddition reactions,[72,143] oxidations,[144] and reductions.[145] In general, UV excitation was indispensable and in all cases well-known compounds were formed, which were not isolated but only identified by spectroscopic methods. One reason for this is that photocorrosion of the semiconductor photocatalyst often prevents its use in preparative chemistry. This is very true of colloidal metal sulfide semiconductors, which are photochemically too unstable for synthetic processes.[65,146] The pseudo-homogeneous nature of their solutions did, however, enable classical mechanistic investigations.

The structures of almost all the products can be rationalized within the mechanistic scheme of semiconductor photocatalysis type A. In general, the organic substrate is involved in the oxidative part of the reaction. This means that the reactivity of the initially formed radical cation determines the kind of products finally formed. Typical reactions of radical cations are deprotonation, bond cleavage, and electron transfer.[147] In addition to deprotonation, radical cations may also be transformed to the corresponding radicals by cleavage of C–C, C–H, and other bonds.

All the reactions mentioned above neither lead to novel products nor do they introduce new aspects to organic synthesis. In contrast, the reactions discussed in the next two sections afford new compounds that can be isolated on a gram scale. The major part is concerned with addition reactions, which represent atom-economic processes. They demonstrate that semiconductor photocatalysis may be a valuable new method for preparative chemistry. Recent reviews on organic photochemistry also mention the use of semiconductors as photocatalysts.[4b,9c,148]

8.1. C–C Coupling through Semiconductor Photocatalysis Type A

Irradiation of an aqueous suspension of ZnS or platinized CdS (Pt/CdS) in 2,5-dihydrofuran (2,5-DHF) with UV or visible light affords a few liters of hydrogen and gram quantities of hitherto unknown dehydrodimers in yields of 60% (Scheme 14).[4c,146a,149] The initially evolved hydrogen gas

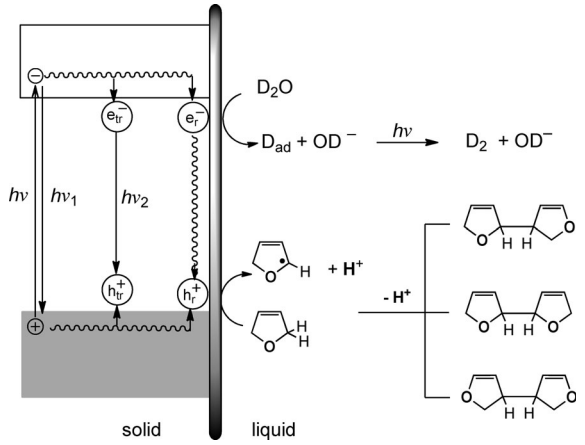

Scheme 14. Anaerobic photodehydrodimerization of 2,5-dihydrofuran ($2e^-/2h^+$ process). Band edges are positioned at −1.8 V and +1.8 V or −0.9 V and +1.5 V for ZnS and CdS, respectively.

contains about 90% D_2 when D_2O is employed, but no reaction occurs in the absence of water. Colloidal zinc or cadmium sulfide and high-purity single crystals do not catalyze the reaction. The structure and statistical ratio of the three regioisomeric dehydrodimers suggest that the products are formed by dimerization of an intermediate dihydrofuryl radical. The formation of hydrogen and dehydrodimers can be rationalized within the scheme of semiconductor photocatalysis type A (Schemes 1 and 14). In the reductive reaction step, water is reduced to hydrogen [Eq. (54)], whereas in the oxidative part 2,5-DHF is oxidized to the allylic dihydrofuryl radical and a proton [Eq. (55)].

$$2\,e_r^- + 2\,H_2O \rightarrow H_2 + 2\,OH^- \tag{54}$$

$$2\,h_r^+ + 2\,RH \rightarrow 2\,R^{\bullet} + 2\,H^+ \tag{55}$$

3-Hydroxytetrahydrofuran, the product of the addition of water to a mutual 2,5-DHF radical cation, could not be detected. According to this basic reaction scheme, although water is reduced, it is not consumed, since it is reformed as indicated by the sum of Equations (54) and (55). In fact, the water concentration did not decrease, although about two liters of hydrogen were produced. The net reaction can, therefore, be summarized according to Equation (56).

$$2\,RH \xrightarrow[H_2O]{h\nu,\,ZnS} H_2 + R{-}R \tag{56}$$

Further support stems from the observation that the initially observed D_2 content of 90% drops to 40% after evolution of one liter of hydrogen, whereas the sum of HD and H_2 increases from 10% to 60%.

From these results it is apparent that the formation of D_2 from D_2O in "sacrificial" systems is a necessary but not a sufficient criterion for "permanent" water reduction. This result is of basic importance, since the consumption of water was never proven in the many reactions dealing with "sacrificial" photochemical hydrogen production. Typical examples are the use of primary and secondary alcohols as reducing agents, which also generate protons according to Equation (57). The radical R_2COH is strongly reducing and may inject an electron into the conduction band, thereby generating R_2CO and a proton (see Section 3). As net reaction, absorption of one photon produces R_2CO and hydrogen from the alcohol.

$$h_r^+ + R_2CHOH \rightarrow R_2C^{\bullet}OH + H^+ \tag{57}$$

Since the dehydrodimers were previously unknown, this reaction is the first example of the preparation of a novel compound through semiconductor photocatalysis. The analogous products were obtained from 3,4-dihydropyran (3,4-DHP), 3-methyl-2,3-dihydropyran (3-MeDHP), and cyclohexene, which were isolated in yields of 30–60%. The saturated ether tetrahydrofuran is also dehydrodimerized, whereas 1,4-dioxane does not react. In situ prepared zinc sulfide photocatalyzes the same reactions, but exhibits a different chemoselectivity, since 1,4-dioxane is also dehydrodimerized.[150]

Substrate adsorption, quenching, inhibition, and kinetic studies were conducted for the ZnS-catalyzed photodehydrodimerization of 2,5-DHF to unravel the detailed mechanism. A plot of the amount of 2,5-DHF adsorbed (n_{eq}) against the residual concentration in solution exhibits two saturation plateaus at $n_{eq(max)}$ values of 2.8×10^{-3} and 65×10^{-3} mol g^{-1}. The first plateau is due to formation of a mixed solvent–solute surface monolayer, while the second corresponds to multilayer adsorption. Assuming that the formation of the monolayer can be described by competitive adsorption between water and 2,5-DHF, the data can be analyzed according to the Hiemenz model.[151] The average area occupied by 2,5-DHF in the surface–solute monolayer obtained from this model is 10.2 Å^2. This value agrees well with the 9.1 Å^2 calculated for 2,5-DHF adsorbed edge-on onto the ZnS surface. From the surface density of zinc sites (11.4×10^{-6} mol m^{-2}) in cubic zinc sulfide[152] and the specific surface area (100–170 m^2 g^{-1}) of the ZnS employed, the surface concentration of 2,5-DHF in the saturated monolayer is estimated to be in the range (1–2) × 10^{-3} mol g^{-1}. This good agreement with the experimental value of 2.8×10^{-3} mol g^{-1} suggests that each zinc site is occupied by one 2,5-DHF molecule. The rather small downfield shift of $\delta = 1.5$ ppm in the ^{13}C NMR spectrum for the C(sp^3) atoms of adsorbed 2,5-DHF suggest that the oxygen atom does not interact directly with zinc sites but rather indirectly through hydrogen bonding to coordinated water.

Emission quenching and product inhibition studies were performed to find out if emissive (e_{tr}^-, h_{tr}^+) and reactive (e_r^-, h_r^+) electron–hole pairs are identical. The addition of zinc or cadmium sulfate slightly increases or does not alter the two emission bands at 366 nm and 430 nm of an aqueous suspension of ZnS. 2,5-DHF has no significant influence. In

contrast to the emission, the reaction is strongly inhibited when cadmium or zinc salts are added. This observation indicates that the emitting and reacting surface sites are different. A Stern–Volmer plot of the reduced reaction rate as a function of the initial concentration of the inhibitor affords a straight line only when the concentration of adsorbed ions (n_{eq}) is employed (Figure 26). From the corresponding slopes,

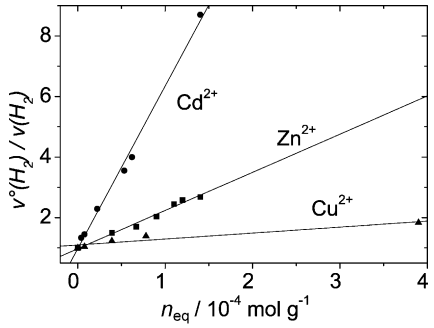

Figure 26. Stern–Volmer plot for the ZnS-photocatalyzed dehydrodimerization of 2,5-DHF.

Stern–Volmer constants of $13\times10^3\,\text{M}^{-1}\,\text{s}^{-1}$ and $50\times10^3\,\text{M}^{-1}\,\text{s}^{-1}$ are calculated for Zn^{2+} and Cd^{2+}, respectively. Copper(II) ions exert only a very weak effect. The inhibition by Cd^{2+} ions proceeds through competitive IFET [Eq. (58)], since the formation of elemental cadmium is observable even at the very low concentration of 3.9×10^{-6} mol g^{-1}; complete inhibition occurs at 6×10^{-4} mol g^{-1}. This differs significantly from the effect of zinc ions, in which the expected elemental zinc[153] could not be detected, even at the high concentration of 0.8 mol g^{-1}. Therefore, zinc ions either prevent the formation of the reactive electron–hole pair or efficiently promote its radiationless deactivation (Scheme 1).

$$2\,e_r^- + Cd^{2+} \rightarrow Cd \tag{58}$$

Inhibition studies with various metal ions reveal that Fe^{2+} and Ni^{2+} ions accelerate the reaction up to a concentration of about 0.7×10^{-3} M, but inhibit the reaction at concentrations above 2×10^{-3} M and 6×10^{-3} M, respectively. At a given surface concentration of these ions ($n_{eq}=3\times10^{-5}$ mol g^{-1}), there is no simple relationship with the reduction potential of the metal ion. However, the reaction rate increases approximately linearly with the electrochemical exchange current density of hydrogen evolution at the corresponding metal electrode.[154] This strongly suggests that the reduction of water at the photoexcited ZnS/M_{ad}^{2+} surface occurs at small metal islands generated by photoreduction.

From these results, the primary events at the semiconductor surface can be summarized as depicted schematically in Scheme 14. The electron–hole pair generated by the absorption of light has a lifetime of 0.1–20 ns and either recombines through radiative or nonradiative processes or is trapped at emitting (e_{tr}^-, h_{tr}^+) or reacting surface (e_r^-, h_r^+) sites. Whereas the former are detected by their emission at 440 nm, the latter could not be observed directly, but their existence is confirmed through the inhibition experiments. The reduction of water is most likely located at surface states formed by photogenerated zinc metal islands. Three pathways may be considered for the formation of the 2,5-dihydrofuryl radical in the oxidative part of the reaction. Firstly, hydrogen abstraction by a surface sulfur radical. Although such radicals have been detected at zinc sulfides, this reaction path is rather unlikely since THF is also dehydrodimerized, but does not undergo H abstraction with sulfur-centered radicals in homogeneous solution.[155] Secondly, a stepwise formation through an initially formed radical cation followed by deprotonation. Thirdly, a dissociative IFET, in which electron transfer and deprotonation proceed in a concerted manner (Scheme 14). All experimental evidence is in favor of the concerted pathway.

Assuming a redox potential of 1.6–2.0 V for the reactive hole and considering the oxidation potential of 2.6 V for 2,5-DHF, oxidation to the radical cation is endergonic by at least 0.6 eV. Furthermore, there is no simple relationship between the apparent product quantum yields and the redox potentials of the various ethers. On the other hand, a similar estimation for the concerted process of a dissociative electron transfer [Eq. (59)] reveals that the reaction is exergonic by at least

$$RH \rightarrow R^{\bullet} + H^+ + e^- \tag{59}$$

0.9 eV.

Since the driving force of this reaction is the difference between the free enthalpy of C–H bond homolysis and the potential of the hydrogen electrode, the former value should be decisive when comparing apparent quantum yields of various substrates. Figure 27 shows the relationship between the quantum yield and calculated bond dissociation energy of

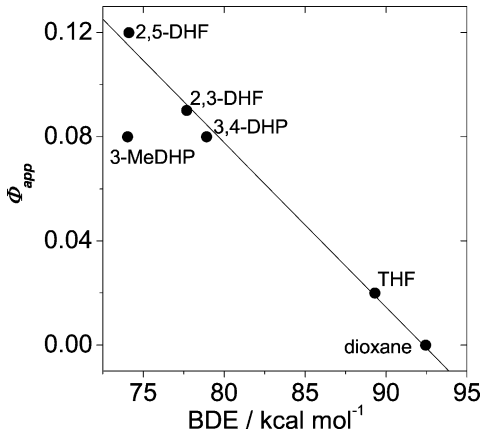

Figure 27. Dependence of apparent product quantum yield on calculated bond dissociation energy of the allylic C–H bond of unsaturated ethers and cycloolefins as well as the α-CH bond in tetrahydrofuran and 1,4-dioxane.

the corresponding C–H bond.[146a] The expected increase with decreasing bond strength favors the concerted oxidation pathway. The deviation of 3-MeDHP most likely arises from steric hindrance of the radical C–C coupling step by the methyl group adjacent to the radical center.

Once formed, the allylic radicals may suffer disproportionation, addition to double bonds, electron transfer, and dimerization, as are well known from their chemistry in homogeneous solution. Surprisingly, the latter pathway is followed to about 90%, as indicated by a complete material balance. This unexpected high chemoselectivity strongly suggests that C–C coupling does not proceed via fully solvated radicals but in the H_2O/2,5-DHF surface layer. This is corroborated by the quadratic dependence of the initial rate on the amount of adsorbed 2,5-DHF, which is characteristic of a heterogeneous catalytic dimerization by a modified Langmuir–Hinshelwood mechanism, which affords readily desorbable products.[156] C–C coupling between radicals adsorbed in the H_2O/2,5-DHF surface layer is further supported by competition experiments with THF. Although the unsaturated ether reacts only ten times faster than the saturated one, no THF dehydrodimers or cross-products are detected when THF is present in tenfold excess over 2,5-DHF. The expected products are observed only at a 500-fold higher concentration.

In summary, one can conclude that hydrogen formation and C–C coupling occur through subsequent absorption of two photons ($2e^-/2h^+$ process). The question arises why the C–C homocoupling between two like radicals is so highly favored over C–H heterocoupling with an adsorbed hydrogen atom to reform 2,5-DHF (no deuterated 2,5-DHF was detectable in the presence of D_2O). One possibility is that the first electron does not produce an adsorbed hydrogen atom, but is stored at the metallic zinc or Pt/CdS center, and water is subsequently reduced in a two-electron step. Another possibility is that the adsorbed hydrogen atom may not undergo coupling to the dihydrofuryl radical because of unknown kinetic barriers. Therefore, it seemed worthwhile to replace water by an organic acceptor which could produce a more-stable one-electron reduction intermediate, perhaps capable of undergoing the postulated heterocoupling with the one-electron oxidation intermediate. The following section illustrates that this concept led to the discovery of a novel type of linear photoaddition reaction.

8.2. C–N Coupling through Semiconductor Photocatalysis Type B

The addition of azobenzene to a running ZnS- or Pt/CdS-catalyzed photodehydrodimerization experiment with 2,5-DHF results in complete inhibition of hydrogen evolution. Instead, the novel allylhydrazine **3c**, a linear addition product of 2,5-DHF to azobenzene, and small amounts of hydrazobenzene (**4**) are formed (Scheme 15).[65,146b,157] When all the azobenzene is consumed and some excess 2,5-DHF is still present, hydrogen evolution restarts. The use of CdS or CdS grafted onto silica (CdS-O-SiO_2) allows the reaction to be conducted with visible light. The photoaddition exhibits a significant solvent dependence. No reaction occurs in dry *n*-hexane or THF, but the addition of water or methanol results in the reaction becoming as fast as in pure methanol.

No photoaddition but efficient photocorrosion occurs when colloidal CdS is employed. Scheme 15 summarizes the

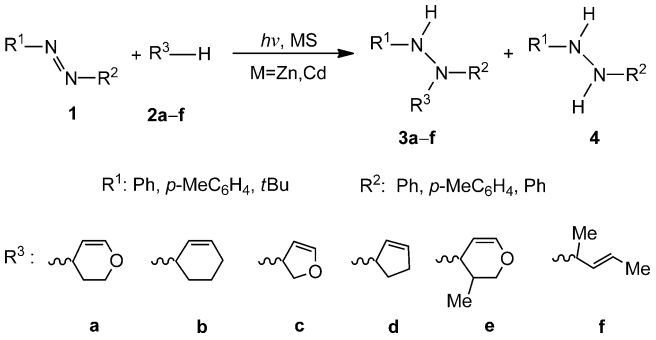

Scheme 15. Linear addition of cyclic allyl/enol ethers and olefins to 1,2-diazenes in methanol.

addition of olefins **2a–f** to 1,2-diazenes **1**to afford hitherto unknown allylhydrazines **3a–f** on a gram scale. As a consequence of the poor crystallization properties, the yields of the isolated products are only 10–40%, whereas the HPLC yields are about two times larger.

When either the 1,2-diazene[158] or the olefin[159] is substituted by electron-withdrawing groups, the same reaction type is observable when the substrates are irradiated in homogeneous solution in the absence of a photocatalyst. However, these reactions are of very limited preparative utility. Surprisingly, only the synthesis of a few other allylhydrazines have been reported in the literature by conventional thermal procedures.[160]

From the discussion at the end of the previous section and the experimental results presented above, a simplified reaction scheme can be drawn (Scheme 16). Since the presence of

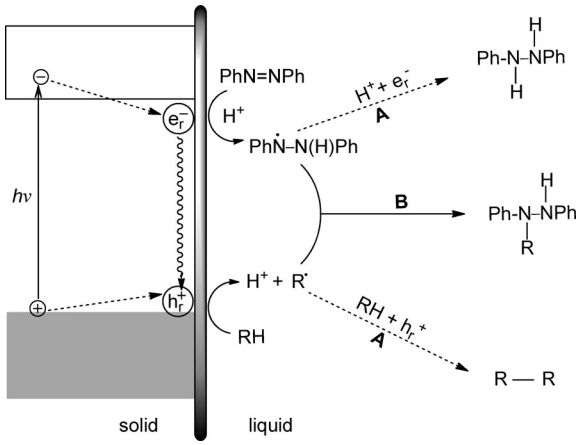

Scheme 16. Simplified mechanistic scheme for the CdS- or ZnS-photocatalyzed addition of cyclic unsaturated ethers or olefins to 1,2-diazenes ($1e^-/1h^+$ process).

the diazene completely inhibits hydrogen evolution and the reaction proceeds only in protic solvents or in the presence of water, the reductive IFET is formulated as a proton-coupled reduction of the diazene to a hydrazyl radical [Eq. (60)].

$$ArN{=}NAr + e_r^- + H^+ \rightarrow ArN^{\bullet}{-}N(H)Ar \qquad (60)$$

The oxidative IFET is assumed to proceed as described for the photodehydrodimerization. Heterocoupling of the hydrazyl and allyl radicals affords the allylhydrazine (path B). Thus, formation of the addition product is a $1e^-/1h^+$ process, whereas the by-products are formed by a $2e^-/2h^+$ process, irrespective of whether the hydrazobenzene derivative **4** is formed by subsequent disproportionation or reduction of the hydrazyl radical [Eqs. (61) and (62)].

$$2\,ArN^{\bullet}-N(H)Ar \rightarrow ArN(H)-N(H)Ar + ArN{=}NAr \quad (61)$$

$$ArN(H)-NAr + e_r^- + H^+ \rightarrow ArN(H)-N(H)Ar \quad (62)$$

The energetic relationships between the band positions and redox potentials are summarized in Figure 28. Formation of the hydrazobenzene product is strongly favored when platinized zinc or cadmium sulfide is used as the photocatalyst. In both cases the rate decreases considerably and hydrazobenzene becomes the major product. It is known that the presence of platinum favors multielectron processes.[161]

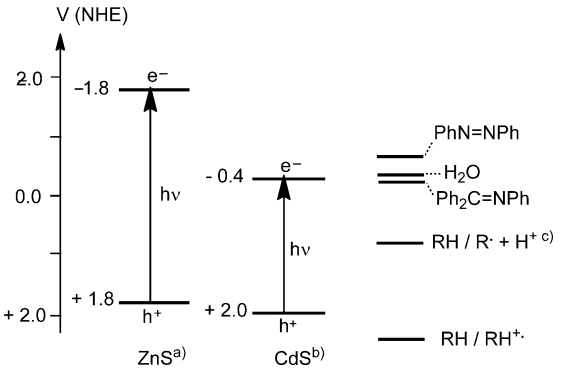

Figure 28. Metal sulfide band edge and substrate redox potential positions. a) Single crystal, b) self-prepared powder, c) RH = 2,5-DHF.

Substrate adsorption studies were conducted with CdS in methanol, the solvent employed in the photoaddition reaction. From the maximum surface concentration of $0.4\times10^{-3}\,mol\,g^{-1}$ found for 2,5-DHF and the maximum number of $1.54\times10^{-3}\,mol\,g^{-1}$ calculated for the Cd^{2+} surface concentration in cubic CdS,[162] it follows that 2,5-DHF adsorbs at about every fourth Cd^{2+} center, in agreement with a parallel orientation. The maximum surface concentration $n_{eq(max)}$ for azobenzene of about $1.00\times10^{-5}\,mol\,g^{-1}$ is two orders of magnitude lower, whereas the adsorption constants are much higher. It is estimated that in the case of CdS only every 220th Cd^{2+} site interacts with an azobenzene molecule, which corresponds to a surface coverage of only about 0.7%. This value suggests that the more polar methanol ($\mu = 1.7$ D) competes efficiently with the less-polar *trans*-azobenzene ($\mu_{trans} \cong 0$ D) for adsorption sites at the polar CdS surface. It seems likely that interaction between surface Brønsted acid sites[157] and the basic nitrogen lone pairs of electrons is the driving force for adsorption.

Apparent quantum yields of allylhydrazine formation (Φ_{app}) were measured at 366 nm, the wavelength at which the absorption of light by the diazene is minimized. The Φ_{app} value for the system CdS/olefin/1,2-diphenyldiazene/MeOH increases from 0.02 (2,5-DHF) over 0.03 (cyclohexene) and 0.04 (3,4-DHP) to 0.05 (2,3-DHF). As also observed for the ZnS-catalyzed photodehydrodimerization, there is no simple relationship with the redox potentials of the olefins.

The postulated C–N heterocoupling requires diffusion of the two radicals either in the solvent/solute surface layer or in the bulk solution. In both cases one expects that the reaction rate should decrease upon increasing the solvent viscosity by application of high pressure. This proposal was tested by conducting the CdS-O-SiO_2-catalyzed photoaddition of 2,5-DHF to azobenzene at pressures ranging from 0.1 to 120 MPa.[157] Both the formation rates of the addition and reduction products **3c** and **4** ($R^1 = R^2 = Ph$) decrease with increasing pressure (Figure 29). From a plot of ln(rate) versus pressure, activation volumes $\Delta V^{\neq}$ of $+17.4 \pm 3.4$ and $+15.8 \pm 2.3\,cm^3\,mol^{-1}$ for **3c** and **4**, respectively, are obtained. However, since the dielectric constant also increases with increasing pressure, the observed effects may originate from a change in this property.[163] To differentiate between these two possibilities the rates were measured in a series of alcohols for which the viscosities and dielectric constants change in an opposite fashion. Whereas the rates again decrease with increasing viscosity, they increase when plotted as a function of increasing dielectric constant. This indicates that the rate decrease at higher pressure is a viscosity effect.

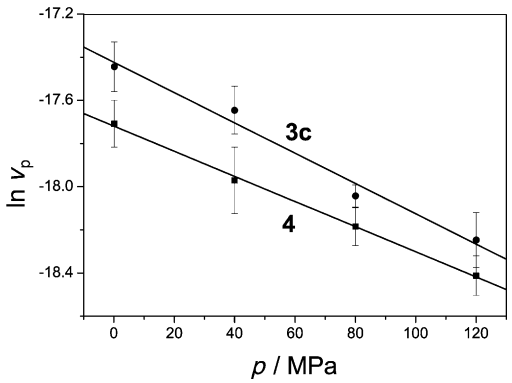

Figure 29. Dependence of the formation rates of **3c** and **4** on applied pressure.

It is unlikely that the activation volume is connected with substrate adsorption and product desorption[164] or with the IFET steps. Usually, interfacial collision rates depend on molecular mass but not on diffusion rates.[165] Most likely, the activation volume measured for the formation of **3c** originates from the diffusion of the intermediary radicals to each other or from the subsequent C–N coupling step itself. The latter case can be excluded since bond formation between neutral organic species in homogeneous solution has, in general, a negative activation volume.[166] The only exception is radical recombination in the termination step of polymerizations.[167] These reactions possess $\Delta V^{\neq}$ values in the range of $+13$ to $+25\,cm^3\,mol^{-1}$, which are composed of the large and positive contribution of the diffusion and the small and

negative part of radical C–N coupling. Hence, the activation volume found for **3c** most likely originates primarily from diffusion of the intermediate radicals to each other and only to a minor part from C–N coupling (see also Section 8.3) and, therefore, should resemble the activation volume for the viscous flow of methanol. The fact that the latter value of $+8\ cm^3\,mol^{-1}$ [166d] is significantly smaller, suggests that the radicals do not diffuse in the bulk homogeneous solution but in the solvent/solute surface layer. The latter should have a higher viscosity and consequently the activation volume should become more positive. The small activation energies of $2.8 \pm 0.3\ kcal\,mol^{-1}$ and $2.5 \pm 0.2\ kcal\,mol^{-1}$ observed for **3c** and **4**, respectively, are in accordance with this interpretation. Since the same activation parameters were also found for the formation of the reduction product **4** as for **3c**, the disproportionation pathway [Eq. (61)], which involves radical diffusion, is favored over the secondary reduction step [Eq. (62)]. However, the latter may be partly involved, as suggested by the slightly smaller pressure effect as compared to **3c**.

8.3. C–C Coupling through Semiconductor Photocatalysis Type B

According to the proposed mechanism for this novel photoaddition reaction, other substrates capable of forming radicals upon CdS-photoinduced one-electron oxidation or reduction should undergo similar C–C coupling reactions. The expected reactions were observed when the 1,2-diazene was replaced by an aromatic imine.[20,84,107,157,168] Trisubstituted imines **5** afford the new homoallylamines **7a–g** in yields of 30–75% (Scheme 17).

When a disubstituted imine (**8a–d**) is employed instead of the trisubstituted one, in addition to the homoallylamine (**9**), the hydrodimer (**10**) of the imine, that is, the dimer of an anticipated α-aminobenzyl radical, is also isolated (Scheme 18). The observation that the hydrodimer is produced only from the disubstituted imine and not from the trisubstituted one parallels the electrochemical reduction, which affords hydrodimers from aldimines but not from ketimines.[169] Thus, product formation can be rationalized by assuming that the allylic radical generated in the oxidative IFET as discussed above, undergoes C–C heterocoupling with the α-aminodiphenylmethyl radical produced according to Scheme 19. In no cases could a product arising from C–N heterocoupling be observed. Thus, in contrast to potential thermal routes, which usually involve the use of organometallic reagents,[170] the reaction is regioselective and much easier to perform.

When the CdS surface is alkylated with 3-bromopropyltrimethoxysilane the resulting powder is completely inactive. However, it becomes very active when the imine is substituted by its iminium salt. This indicates that the surface OH and SH groups of cadmium sulfide protonate the imine to render its redox potential more positive.[168c] The reductive IFET is, therefore, formulated according to Equation (63).

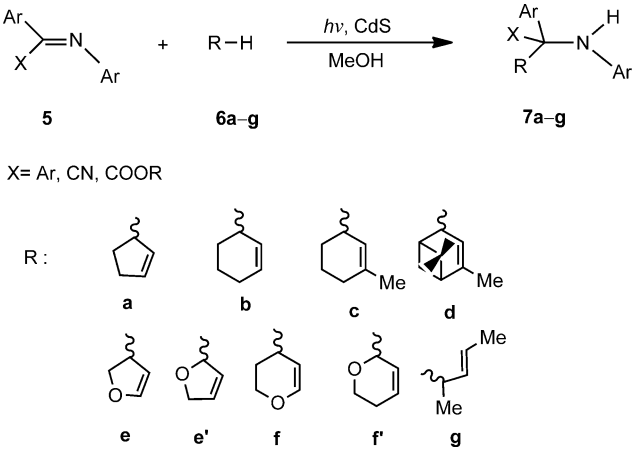

Scheme 17. Linear addition of cyclic allyl/enol ethers and olefins to trisubstituted imines. Imine hydrodimers **10** are formed as by-products (see Scheme 18).

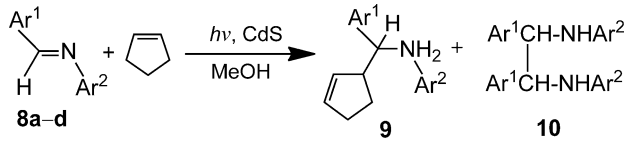

	a	b	c	d
Ar^1	4-ClC_6H_4	2,6-$Cl_2C_6H_3$	4-ClC_6H_4	4-$MeOC_6H_4$
Ar^2	4-ClC_6H_4	C_6H_5	3,5-$Me_2C_6H_3$	4-MeC_6H_4
9[a]	60	40	55	80
10[a]	20	10	40	--

Scheme 18. Linear addition of cyclopentene to disubstituted imines. [a] Yield of isolated product.

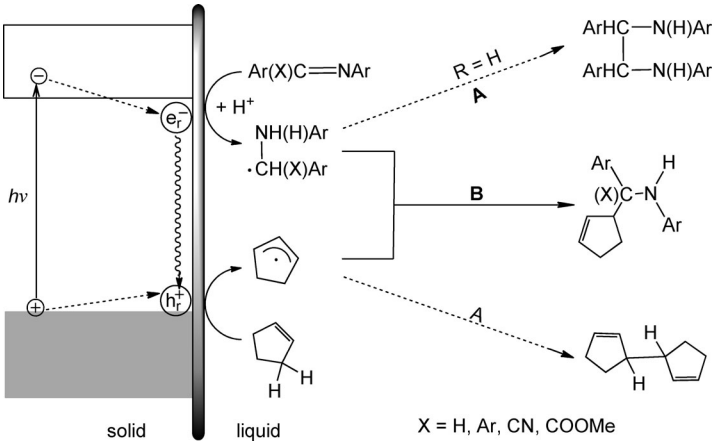

Scheme 19. Simplified mechanistic scheme for the CdS-photocatalyzed addition of cyclopentene to imines.

$$[Ar_2C{=}N(H)Ar]^+ + e_r^- \rightarrow Ar_2C^{\bullet}{-}N(H)Ar \qquad (63)$$

As observed for 2,5-DHF, the imine **8a** also exhibits an adsorption isotherm that indicates the presence of mono- and

multilayer adsorption. A maximum surface concentration of 20×10^{-7} mol g^{-1} can be estimated from the former. Application of the Hiemenz model suggests that only 1–2% of the surface is covered by **8a**, which is in competition with the solvent. The results resemble those obtained for the adsorption of azobenzene. Assuming a size of 8 $Å^2$ for methanol, one arrives at the conclusion that methanol is present in a 500-fold excess over the imine in the methanol/imine surface monolayer. As expected, methanol should adsorb much more strongly onto the hydrous CdS surface.[171] Therefore, it is rational that **8c** does not influence the photocurrent of a CdS electrode, whereas methanol induces a doubling of the current.[172]

Control experiments with **8a** showed that hydrodimers were also formed in the absence of olefins, but the reaction rates were decreased by about 90%. Whereas the reductive reaction step can proceed as depicted in Scheme 18, the solvent must be involved in the oxidative step since no significant oxidative photocorrosion occurs. Accordingly, irradiation of CdS in a solution of **8a** and different alcohols transforms the imine at different rates, and the corresponding addition products **11a–e** and hydrodimers **12a–e** are isolated (Scheme 20). With the exception of methanol and 2-propanol,

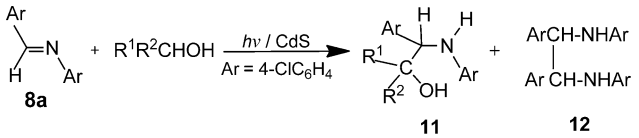

	a	b	c	d	e
R^1	H	Me	Et	Pr	Me
R^2	H	H	H	H	Me

Scheme 20. Addition of alcohols to the Schiff base **8a**.

the products are racemic diastereomeric mixtures which are isolated in low yields (5–20%); they are often mixed with the two-electron reduction product *N*-4-chlorobenzyl-4-chloroaniline. The major product in all reactions is the hydrodimer **12**, obtained in yields of 10% (MeOH), 28% (BuOH), 29% (PrOH), 42% (EtOH), and 60% (*i*PrOH). The structure of **11** indicates that the α-CH bond of the alcohol is added in all cases to the imine, in agreement with the preferred formation of α-hydroxyalkyl radicals. These results show that the solvent can be directly involved in the oxidative step. It is noted that in the presence of olefins no alcohol addition products could be detected by HPLC analysis, even though methanol is present in a 500-fold molar excess. This finding illustrates the high chemoselectivity of the semiconductor/liquid interface.

Increasing the light intensity results in a linear increase in the reaction rate. A saturation effect is observed above an incident intensity of about 10^{18} quanta s^{-1}. This is in accord with other photoreactions catalyzed by semiconductor powders.[69] It is noteworthy that the product ratio of 0.9:1 observed for **9a**/**10a** is not influenced by changing the light intensity. This suggests that the rates of aminobenzyl radical dimerization and addition to the allyl radical exhibit the same dependence on the concentration of the light-generated electron–hole pairs.

The reaction rate increases approximately linearly with the CdS concentration and reaches a plateau at about 3 g L^{-1}. Surprisingly, the ratio of addition to hydrodimer product (**9a**/**10a**) decreases from 2:1 to about 1:1 in the same concentration range. Likewise, the surface concentration of the intermediate radicals should equally decrease and the ratio of α-aminobenzyl to cyclopentenyl radical concentration should not change. Therefore, the product ratio is expected to stay constant. However, a lower concentration of the radicals results in their lifetime increasing, assuming that they undergo only second-order decay reactions. This effect should favor hydrodimerization, which is a $2e^-/2h^+$ process and, therefore, requires that a second radical pair is generated during the lifetime of the first one. Furthermore, one can make the plausible assumption that there is still some weak interaction within a reactive electron–hole pair and, therefore, the distance between the charges in a pair should be smaller than the distance between neighboring pairs. This means that the radical homocoupling most likely requires a longer diffusion path than heterocoupling. Accordingly, a longer radical lifetime should also enable a more efficient diffusion and, therefore, favor formation of the hydrodimer.

Chiral imines were employed in addition reactions with α-pinene to obtain information on the stereochemistry of the radical C–C coupling (Scheme 21). The (+)-menthyl ester affords the C2(*R*)C1(*S*) diastereomer, whereas both diastereomers are produced with the (−)-menthyl ester.[173]

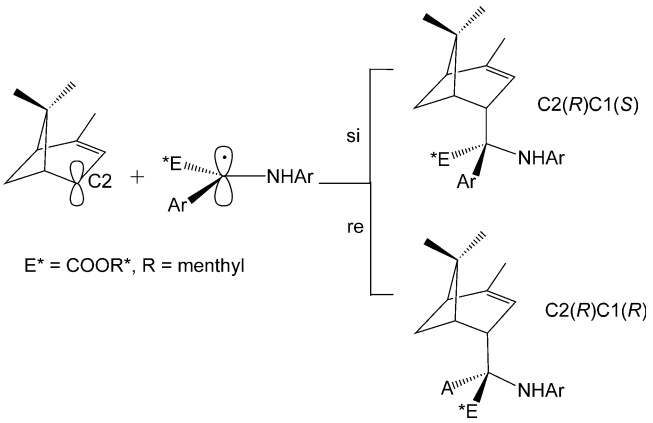

Scheme 21. Diastereoselectivity of C–C coupling.

The aryl group Ar^2 was replaced by the bulky 1-adamantyl group to investigate how steric pressure at the imine nitrogen atom influences the reaction. In this case, CdS-grafted alumina was employed as the photocatalyst. Hitherto unknown homoallyladamantylamines were obtained in yields of 21–85% by using cyclopentene, cyclohexene, and α-pinene and various *N*-adamantylimines (Scheme 22).[174] Unsaturated adamantylamines are of pharmaceutical interest since this class of compounds has antibacterial, antitumor, antipyretic, and anti-inflammatory properties. Some of them were discussed as promising candidates for the treatment of Alzheimer's and Parkinson's diseases.[175]

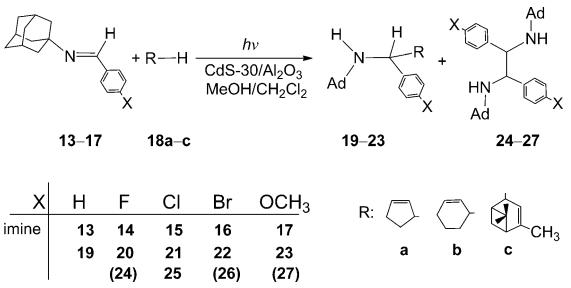

Scheme 22. Linear addition of cyclic olefins to *N*-adamantylimines.

Whereas the diastereoselectivity of C–C heterocoupling is rather low (Scheme 19, path B), the homocoupling between two α-aminobenzyl radicals (Scheme 19, path A) is a diastereospecific process, as exemplified by the hydrodimerization of the *p*-chlorophenyl derivative **15**. According to HPLC and X-ray structural analysis, only diastereomer **25** is formed in the reactions with cyclopentene and α-pinene, whereas **25′** is produced in the case of cyclohexene (Figure 30). Surprisingly, the stereochemistry is controlled by the nature of the olefin, although it is not directly involved in the C–C homocoupling. However, this effect can be rationalized by recalling that the radicals have to diffuse to each other within a solvent/solute surface layer consisting of olefins adsorbed to CdS through hydrogen bonding to surface SH and OH groups. It is expected that steric interaction with the olefin should occur during this diffusion process. Thus, the olefin plays a dual role in being the substrate for the addition and the stereodirecting spectator for the hydrodimerization reaction.

As part of a study to explore the general applicability of the olefin–imine addition reaction for the synthesis of valuable organic compounds, the N-aryl substituent in the imine **5** (X = CN) was replaced by an N-benzoyl group, which may be easily converted into an amino group. The resulting unsaturated amino acids could be of pharmaceutical relevance.[176] Surprisingly, the addition reactions with cyclopentene and cyclohexene in the presence of CdS-O-SiO_2 were completely inhibited in favor of a novel thermal transhydrocyanation of the imine component, and afforded novel malononitriles **31** in yields of 40–50 % (Scheme 23). However, in the presence of CdS, ZnS, or 36 % CdS-S-ZnS this dark

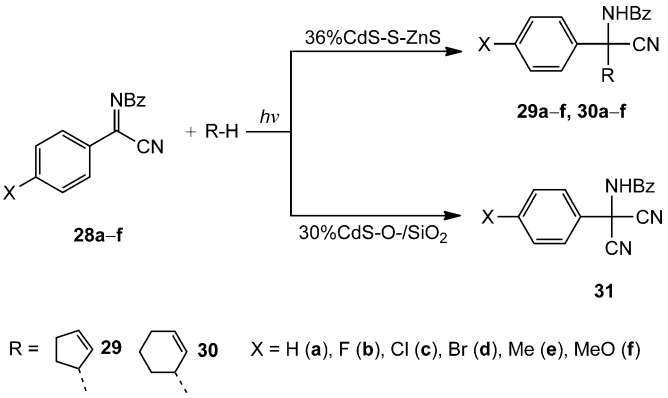

Scheme 23. Support-controlled chemoselectivity in the imine/olefin system.

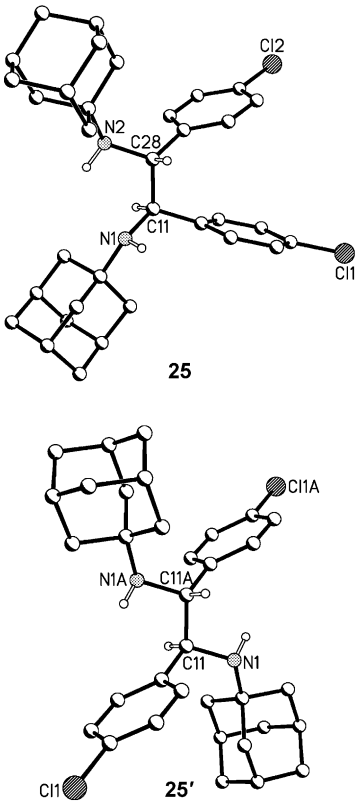

Figure 30. Molecular structures of diastereomers isolated from reactions with imine **15** (nonrelevant hydrogen atoms are omitted for clarity).

reaction was completely inhibited in favor of the desired addition products (65–85 % yield). Unexpectedly, compounds **29** and **30** were unknown in the literature. Whereas complete conversion of **28c** in the presence of 36 % CdS-S-ZnS was already observed after 3 h of irradiation time, 29 h and 19 h were required for self-prepared ZnS and CdS, respectively. Commercially available CdS and ZnS were inactive.

A speculative mechanism for the 36 % CdS-S-ZnS-catalyzed addition reaction is summarized in Scheme 24. This grafted photocatalyst induces reaction rates about six-times higher than pristine CdS. According to time-resolved photovoltage measurements, 36 % CdS-S-ZnS may be considered as a photochemical diode of the type (n-CdS)-S-(p-ZnS).[168e] The increased reactivity is in accord with the longer charge-carrier lifetime of 4 μs, compared to the 3 μs measured for pristine CdS. This slower charge recombination can be rationalized by assuming an intercrystallite electron transfer at the CdS-S-ZnS interface (Scheme 24).

As observed for the radical C–C and C–N coupling reactions, the driving force of the IFET reactions is not the rate-determining parameter. Thus, whereas the reduction potential of the *p*-chlorophenyl-substituted imine **28c** is 150 mV more positive than that of the bromo derivative **28d**, the pseudo rate constants do not differ significantly. To investigate if the rate-determining diffusion of the radicals

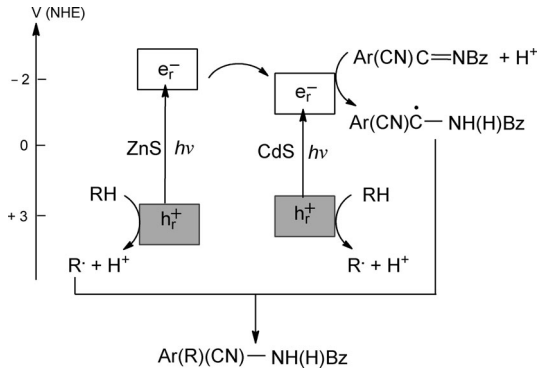

Scheme 24. Photoinduced charge separation facilitated by intercrystallite electron transfer in 36%CdS-S-ZnS. In ontrast to 5%CdS-S-ZnS, wherein ZnS is the major absorber of light (see Scheme 7), both ZnS and CdS are absorbing.

also contains some contribution of the C–C bond formation (see Section 8.2), the addition of cyclohexene and cyclopentene to a series *p*-substituted imines was analyzed in terms of the Hammet Equation [Eq. (64)]. Therein the parameter

$$\log(k_X/k_H) = \sigma\rho \qquad (64)$$

σ is a constant for a given substituent X in the *p*-XC_6H_4 group of the imine, and k_X and k_H are the corresponding rate constants. The value of ρ depends on the specific reaction. In general, positive ρ values indicate that enhanced electron-withdrawing substituents X increase the reaction rate.
A corresponding plot of the left term of Equation (64) versus the σ parameters reveals a linear relationship. Only the fluorophenyl imine **28b** does not follow this general trend. The positive ρ values of $\rho = 1.18$ and $\rho = 1.44$ for cyclopentene and cyclohexene additions, respectively, suggest a nucleophilic attack of the allyl radical at the α-aminobenzyl radical.

9. Summary and Outlook

The unique charge-separating properties of the semiconductor/liquid interface enable micrometer aggregates of nanoscaled semiconductor powders to photocatalyze interfacial electron exchange with dissolved substrates. In most cases the primary products are radicals, which undergo selective formation of chemical bonds in secondary reactions. The high reactivity of such heterogeneous systems is exemplified by the fixation of molecular nitrogen and functionalization of alkanes. The phototocatalytic activity of the semiconductor can be improved by grafting it onto an insulating or semiconducting material. It is likely that the resulting chemical bonds between the crystallites of an aggregate induce an intercrystallite electron transfer, thereby slowing down the undesired charge recombination. Very recent results suggest that such types of hybrid systems are a promising approach for improving the efficiency of charge generation. Clearly, solid-state chemistry should become more involved in this basic aspect of chemical solar energy conversion.

In general, reduced and oxidized products are obtained (semiconductor photocatalysis type A), in complete analogy with electrochemical synthesis. An example is the anaerobic dehydrodimerization of unsaturated ethers in aqueous solution, which produces stoichiometric amounts of hydrogen. The reaction represents a combination of "sacrificial" hydrogen production and organic synthesis. It demonstrates that the formation of D_2 upon using D_2O as the solvent does not prove hydrogen is produced from water, as is generally assumed in the literature for "sacrificial hydrogen production". In a few cases the semiconductor photocatalyzes an addition reaction between two or more substrates to afford a single reaction product (semiconductor photocatalysis type B). This reaction type is unknown in classical electrochemistry. Typical examples are the addition of olefins or unsaturated ethers to 1,2-diazenes or imines and the insertion of O_2 and SO_2 into the C–H bond of alkanes.

The preparatively valuable photoreactions are easily conducted and the heterogeneous photocatalyst can be conveniently separated from the products. They are promising examples of "green chemistry", since they do not produce waste materials and can be driven by solar light. The semiconductor is at least bifunctional in both photocatalysis types. It enables a proper assembly of substrates through adsorption at the surface/solvent layer and it catalyzes photoinduced interfacial electron transfer to and from substrates, often coupled to proton transfer. The resulting primary redox products are radicals, which undergo regio- and stereoselective selective C–C and C–N coupling to the final products. In a formal way, the overall process resembles natural photosynthesis, where the absorption of light also generates reducing and oxidizing centers, which finally induce the synthesis of organic matter through C–C coupling reactions. It is expected that the interdisciplinary nature of semiconductor photocatalysis will stimulate new developments in the fields of chemical solar energy utilization and environmental chemistry.

Received: February 13, 2012
Published online: December 4, 2012

[1] V. Balzani, G. Bergamini, P. Ceroni, *Coord. Chem. Rev.* **2008**, *252*, 2456–2469.
[2] a) H. Gerischer, *Adv. Electrochem. Electrochem. Eng.* **1961**, *1*, 139–232; b) S. N. Frank, A. J. Bard, *J. Am. Chem. Soc.* **1977**, *99*, 4667–4675; c) A. Fujishima, K. Honda, *Bull. Chem. Soc. Jpn.* **1971**, *44*, 1148–1150; d) A. Fujishima, K. Kohayakawa, K. Honda, *J. Electrochem. Soc.* **1975**, *122*, 1487–1489; e) R. Memming, *Semiconductor Electrochemistry*, Wiley-VCH, Weinheim, **2001**; f) S. J. Anz, A. M. Fajardo, W. J. Royea, N. S. Lewis, *Charact. Mater.* **2003**, *1*, 605–636.
[3] a) A. Henglein, *J. Phys. Chem.* **1982**, *86*, 2291–2293; b) D. Bahnemann, A. Henglein, J. Lilie, L. Spanhel, *J. Phys. Chem.* **1984**, *88*, 709–711; c) D. Duonghong, E. Borgarello, M. Graetzel, *J. Am. Chem. Soc.* **1981**, *103*, 4685–4690.
[4] a) S. N. Frank, A. J. Bard, *J. Phy. Chem.* **1977**, *81*, 1484–1488; b) M. A. Fox, M. T. Dulay, *Chem. Rev.* **1993**, *93*, 341–357; c) J. Bücheler, N. Zeug, H. Kisch, *Angew. Chem.* **1982**, *94*, 792–793; *Angew. Chem. Int. Ed. Engl.* **1982**, *21*, 783–784; d) M. R. Hoffmann, S. T. Martin, W. Choi, D. W. Bahnemann, *Chem.*

Rev. **1995**, *95*, 69 – 96; e) D. Meissner, R. Memming, B. Kastening, D. Bahnemann, *Chem. Phys. Lett.* **1986**, *127*, 419 – 423; f) P. Pichat, J. M. Herrmann, J. Disdier, M. N. Mozzanega, *J. Phys. Chem.* **1979**, *83*, 3122 – 3126; g) J. M. Herrmann, J. Disdier, M. N. Mozzanega, P. Pichat, *J. Catal.* **1979**, *60*, 369 – 377.

[5] W. Ostwald, *Die Mühle des Lebens*, T. Thomas, Leipzig, **1911**.

[6] a) A. Fujishima, T. N. Rao, *Pure Appl. Chem.* **1998**, *70*, 2177 – 2187; b) P. Pichat, *Appl. Catal. B* **2010**, *99*, 428 – 434.

[7] a) G. Ciamician, *Science* **1912**, *36*, 385 – 394; b) A. Albini, M. Fagnoni, *ChemSusChem* **2008**, *1*, 63 – 66.

[8] The composition of solar light arriving at the earth surface is approximately 3 % UV, 45 % Vis, and 52 % IR.

[9] a) P. Esser, B. Pohlmann, H.-D. Scharf, *Angew. Chem.* **1994**, *106*, 2093 – 2108; *Angew. Chem. Int. Ed. Engl.* **1994**, *33*, 2009 – 2023; b) G. Palmisano, V. Augugliaro, M. Pagliaro, L. Palmisano, *Chem. Commun.* **2007**, 3425 – 3437; c) M. Fagnoni, D. Dondi, D. Ravelli, A. Albini, *Chem. Rev.* **2007**, *107*, 2725 – 2756; d) S. Protti, M. Fagnoni, *Photochem. Photobiol. Sci.* **2009**, *8*, 1499 – 1516.

[10] J. M. Lehn, J. P. Sauvage, *Nouv. J. Chim.* **1977**, *1*, 449 – 451.

[11] a) T. Daimon, T. Hirakawa, M. Kitazawa, J. Suetake, Y. Nosaka, *Appl. Catal. A* **2008**, *340*, 169 – 175; b) K. Naito, T. Tachikawa, S.-C. Cui, A. Sugimoto, M. Fujitsuka, T. Majima, *J. Am. Chem. Soc.* **2006**, *128*, 16430 – 16431; c) A. Jańczyk, E. Krakowska, G. Stochel, W. Macyk, *J. Am. Chem. Soc.* **2006**, *128*, 15574 – 15575.

[12] M. X. Tan, P. E. Laibinis, S. T. Nguyen, J. M. Kesselman, C. E. Stanton, N. S. Lewis, *Progr. Inorg. Chem.* **1994**, *41*, 21 – 144.

[13] M. D. Ward, J. R. White, A. J. Bard, *J. Am. Chem. Soc.* **1983**, *105*, 27 – 31.

[14] K. L. Hardee, A. J. Bard, *J. Electrochem. Soc.* **1977**, *124*, 215 – 224.

[15] M. Long, W. Cai, H. Kisch, *J. Phys. Chem. C* **2008**, *112*, 548 – 554.

[16] M. F. Finlayson, B. L. Wheeler, N. Kakuta, K.-H. Park, A. J. Bard, A. Campion, M. A. Fox, S. E. Webber, J. M. White, *J. Phys. Chem.* **1985**, *89*, 5676 – 5681.

[17] a) M. Anpo, *Pure Appl. Chem.* **2000**, *72*, 1787 – 1792; b) M. Anpo, S. Kishiguchi, Y. Ichihashi, M. Takeuchi, H. Yamashita, K. Ikeue, B. Morin, A. Davidson, M. Che, *Res. Chem. Intermed.* **2001**, *27*, 459 – 467; c) G. Liu, L. Wang, C. Sun, X. Yan, X. Wang, Z. Chen, S. C. Smith, H.-M. Cheng, G. Q. Lu, *Chem. Mater.* **2009**, *21*, 1266 – 1274.

[18] a) P. V. Kamat, *Chem. Rev.* **1993**, *93*, 267 – 300; b) T. Tachikawa, M. Fujitsuka, T. Majima, *J. Phys. Chem. C* **2007**, *111*, 5259 – 5275.

[19] G. Hodes, I. D. J. Howell, L. M. Peter, *J. Electrochem. Soc.* **1992**, *139*, 3136 – 3140.

[20] W. Schindler, H. Kisch, *J. Photochem. Photobiol. A* **1997**, *103*, 257 – 264.

[21] a) T. Tatsuma, S.-i. Tachibana, A. Fujishima, *J. Phys. Chem. B* **2001**, *105*, 6987 – 6992; b) H. Haick, Y. Paz, *ChemPhysChem* **2003**, *4*, 617 – 620; c) Y. Paz, *Diffus. Defect Data Pt. B* **2010**, *162*, 135 – 162.

[22] a) H. Gerischer, *Surf. Sci.* **1969**, *18*, 97 – 122; b) D. Vanmaekelbergh in *Electron Transfer in Chemistry*, *Vol. 1* (Ed.: V. Balzani), Wiley-VCH, Weinheim, **2001**, pp. 126 – 188.

[23] D. W. Bahnemann, M. Hilgendorff, R. Memming, *J. Phys. Chem. B* **1997**, *101*, 4265 – 4275.

[24] H. Gerischer, *Electrochim. Acta* **1990**, *35*, 1677 – 1699.

[25] J. F. Reber, M. Rusek, *J. Phys. Chem.* **1986**, *90*, 824 – 834.

[26] J. R. White, A. J. Bard, *J. Phys. Chem.* **1985**, *89*, 1947 – 1954.

[27] F. A. Frame, T. K. Townsend, R. L. Chamousis, E. M. Sabio, T. Dittrich, N. D. Browning, F. E. Osterloh, *J. Am. Chem. Soc.* **2011**, *133*, 7264 – 7267.

[28] D. A. Tryk, A. Fujishima, K. Honda, *Electrochim. Acta* **2000**, *45*, 2363 – 2376.

[29] Many authors prefer the term "photosensitized photocatalysis" for such a type of reaction. This is not correct, since according to its definition a sensitizer cannot simultaneously function as substrate.

[30] F. Parrino, A. Ramakrishnan, H. Kisch, *Angew. Chem.* **2008**, *120*, 7215 – 7217; *Angew. Chem. Int. Ed.* **2008**, *47*, 7107 – 7109.

[31] a) Y. S. Seo, C. Lee, K. H. Lee, K. B. Yoon, *Angew. Chem.* **2005**, *117*, 932 – 935; *Angew. Chem. Int. Ed.* **2005**, *44*, 910 – 913; b) S. Manzhos, R. Jono, K. Yamashita, J.-i. Fujisawa, M. Nagata, H. Segawa, *J. Phys. Chem. C* **2011**, *115*, 21487 – 21493; c) W. Macyk, K. Szacilowski, G. Stochel, M. Buchalska, J. Kuncewicz, P. Labuz, *Coord. Chem. Rev.* **2010**, *254*, 2687 – 2701.

[32] All reduction potentials apply to aqueous solutions of pH 7 relative to NHE as defined and summarized by P. Wardman, *J. Phys. Chem. Ref. Data* **1989**, *18*, 1637.

[33] a) D. C. Hurum, A. G. Agrios, S. E. Crist, K. A. Gray, T. Rajh, M. C. Thurnauer, *J. Electron Spectrosc. Relat. Phenom.* **2006**, *150*, 155 – 163; b) G. Li, K. A. Gray, *Chem. Phys.* **2007**, *339*, 173 – 187.

[34] M. Anpo, S. C. Moon, K. Chiba, G. Martra's, S. Coluccia, *Res. Chem. Intermed.* **1993**, *19*, 495 – 519.

[35] a) T. Tachikawa, S. Yamashita, T. Majima, *J. Am. Chem. Soc.* **2011**, *133*, 7197 – 7204; b) T. Tachikawa, A. Yoshida, S. Tojo, A. Sugimoto, M. Fujitsuka, T. Majima, *Chem. Eur. J.* **2004**, *10*, 5345 – 5353; c) A. Furube, T. Asahi, H. Masuhara, H. Yamashita, M. Anpo, *J. Phys. Chem. B* **1999**, *103*, 3120 – 3127.

[36] a) M. Schiller, F. W. Muller, C. Damm, *J. Photochem. Photobiol. A* **2002**, *149*, 227 – 236; b) G. Israel, F. W. Muller, C. Damm, J. Harenburg, *J. Inf. Rec.* **1997**, *23*, 559 – 584.

[37] G. Kortüm, W. Braun, G. Herzog, *Angew. Chem.* **1963**, *75*, 653 – 661; *Angew. Chem. Int. Ed. Engl.* **1963**, *2*, 333 – 341.

[38] J. Tauc, R. Grigorovici, A. Vanuc, *Phys. Status Solidi* **1966**, *15*, 627.

[39] B. Ohtani, O. O. P. Mahaney, F. Amano, N. Murakami, R. Abe, *J. Adv. Oxid. Technol.* **2010**, *13*, 247 – 261.

[40] S. R. Morrison, *Electrochemistry at Semiconductor and Oxidized Metal Electrodes*, Plenum, New York, **1980**.

[41] a) Y. V. Pleskov, V. M. Mazin, Y. E. Evstefeeva, V. P. Varnin, I. G. Teremetskaya, V. A. Laptev, *Electrochem. Solid-State Lett.* **2000**, *3*, 141 – 143; b) R. Beranek, H. Kisch, *Electrochem. Commun.* **2007**, *9*, 761 – 766.

[42] a) A. M. Roy, G. C. De, N. Sasmal, S. S. Bhattacharyya, *Int. J. Hydrogen Energy* **1995**, *20*, 627 – 630; b) H. Weiss, A. Fernandez, H. Kisch, *Angew. Chem.* **2001**, *113*, 3942 – 3945; *Angew. Chem. Int. Ed.* **2001**, *40*, 3825 – 3827.

[43] S. Sakthivel, H. Kisch, *Angew. Chem.* **2003**, *115*, 5057 – 5060; *Angew. Chem. Int. Ed.* **2003**, *42*, 4908 – 4911.

[44] G. Burgeth, H. Kisch, *Coord. Chem. Rev.* **2002**, *230*, 41 – 47.

[45] D. Meissner, I. Lauermann, R. Memming, B. Kastening, *J. Phys. Chem.* **1988**, *92*, 3484 – 3488.

[46] B. Enright, G. Redmond, D. Fitzmaurice, *J. Phys. Chem.* **1994**, *98*, 6195 – 6200.

[47] D. Mitoraj, H. Kisch, *J. Phys. Chem. C* **2009**, *113*, 20890 – 20895.

[48] D. Mitoraj, H. Kisch, *Chem. Eur. J.* **2010**, *16*, 261 – 269.

[49] X. Wang, K. Maeda, A. Thomas, K. Takanabe, G. Xin, J. M. Carlsson, K. Domen, M. Antonietti, *Nat. Mater.* **2009**, *8*, 76 – 80.

[50] a) H. A. Schwarz, R. W. Dodson, *J. Phys. Chem.* **1989**, *93*, 409 – 414; b) P. Neta, J. Grodkowski, A. B. Ross, *J. Phys. Chem. Ref. Data* **1996**, *25*, 709 – 1050.

[51] T. Tachikawa, S. Tojo, M. Fujitsuka, T. Majima, *Langmuir* **2004**, *20*, 9441 – 9444.

[52] a) Y. Maeda, A. Fujishima, K. Honda, *J. Electrochem. Soc.* **1981**, *128*, 1731 – 1734; b) A. J. Bard, *J. Phys. Chem.* **1982**, *86*, 172 – 177.

[53] G. Redmond, D. Fitzmaurice, *J. Phys. Chem.* **1993**, *97*, 1426 – 1430.
[54] O. Rusina, W. Macyk, H. Kisch, *J. Phys. Chem. B* **2005**, *109*, 10858 – 10862.
[55] This is based on the Stark–Einstein law, which states that one quantum of light can convert only one molecule. Higher values are observable only in photoinduced chain reactions, wherein a photogenerated intermediate acts a radical chain carrier.
[56] a) M. L. Satuf, R. J. Brandi, A. E. Cassano, O. M. Alfano, *Ind. Eng. Chem. Res.* **2007**, *46*, 43 – 51; b) G. Sagawe, M. L. Satuf, R. J. Brandi, J. P. Muschner, C. Federer, O. M. Alfano, D. Bahnemann, A. E. Cassano, *Ind. Eng. Chem. Res.* **2010**, *49*, 6898 – 6908.
[57] a) M. Schiavello, V. Augugliaro, L. Palmisano, *J. Catal.* **1991**, *127*, 332 – 341; b) D. F. Ollis, *Top. Catal.* **2005**, *35*, 217 – 223; c) B. Ohtani, *Chem. Lett.* **2008**, *37*, 216 – 229.
[58] a) N. Serpone, R. Terzian, D. Lawless, P. Kennepohl, G. Sauve, *J. Photochem. Photobiol.* **1993**, *73*, 11 – 16; b) N. Serpone, G. Sauvé, R. Koch, H. Tahiri, P. Pichat, P. Piccinini, E. Pelizzetti, H. Hidaka, *J. Photochem. Photobiol. A* **1996**, *94*, 191 – 203; c) H. Tahiri, N. Serpone, R. Le van Mao, *J. Photochem. Photobiol. A* **1996**, *93*, 199 – 203.
[59] H. Einaga, M. Misono, *Bull. Chem. Soc. Jpn.* **1996**, *69*, 3435 – 3441.
[60] The latter term is commonly used and in general is based on the yield or rate of the catalytic photoreaction, which is usually not performed under optimal irradiation conditions.
[61] a) P. Johne, H. Kisch, *J. Photochem. Photobiol. A* **1997**, *111*, 223 – 228; b) D. Curcó, J. Gimenez, A. Addardak, S. Cervera-March, S. Esplugas, *Catal. Today* **2002**, *76*, 177 – 188.
[62] Even when the reactions are performed in the same photoreactor, the reproducibility of the optimum rates is usually in the range of at least ± 10 %. It is noted that the "rate constants" in some publications also depend on the absorbed photon flux and therefore are not constants.
[63] a) T. Maschmeyer, M. Che, *Angew. Chem.* **2010**, *122*, 1578 – 1582; *Angew. Chem. Int. Ed.* **2010**, *49*, 1536 – 1539; b) H. Kisch, *Angew. Chem.* **2010**, *122*, 9782 – 9783; *Angew. Chem. Int. Ed.* **2010**, *49*, 9588 – 9589; c) T. Maschmeyer, M. Che, *Angew. Chem.* **2010**, *122*, 9784 – 9785; *Angew. Chem. Int. Ed.* **2010**, *49*, 9590 – 9591.
[64] N. Lakshminarasimhan, W. Kim, W. Choi, *J. Phys. Chem. C* **2008**, *112*, 20451 – 20457.
[65] R. Künneth, C. Feldmer, F. Knoch, H. Kisch, *Chem. Eur. J.* **1995**, *1*, 441 – 448.
[66] a) C.-Y. Wang, R. Pagel, J. K. Dohrmann, D. W. Bahnemann, *Mater. Sci. Forum* **2007**, *544 – 545*, 17 – 22; b) H. Zhang, G. Chen, D. W. Bahnemann, *J. Mater. Chem.* **2009**, *19*, 5089 – 5121.
[67] a) N. Siedl, M. J. Elser, J. Bernardi, O. Diwald, *J. Phys. Chem. C* **2009**, *113*, 15792 – 15795; b) S. O. Baumann, M. J. Elser, M. Auer, J. Bernardi, N. Husing, O. Diwald, *Langmuir* **2011**, *27*, 1946 – 1953.
[68] R. Hayoun, K. M. Whitaker, D. R. Gamelin, J. M. Mayer, *J. Am. Chem. Soc.* **2011**, *133*, 4228 – 4231.
[69] a) T. A. Egerton, C. J. King, *J. Oil Colour Chem. Assoc.* **1979**, *62*, 386 – 391; b) H. Al-Ekabi, P. De Mayo, *J. Phys. Chem.* **1985**, *89*, 5815 – 5821.
[70] J.-M. Herrmann, *J. Photochem. Photobiol. A* **2010**, *216*, 85 – 93.
[71] J. M. Herrmann, *Catal. Today* **1999**, *53*, 115 – 129.
[72] H. Al-Ekabi, P. De Mayo, *Tetrahedron* **1986**, *42*, 6277 – 6284.
[73] A. Heller, Y. Degani, D. W. Johnson, Jr., P. K. Gallagher, *J. Phys. Chem.* **1987**, *91*, 5987 – 5991.
[74] K. Maeda, K. Domen, *J. Phys. Chem. C* **2007**, *111*, 7851 – 7861.
[75] W.-J. Chun, A. Ishikawa, H. Fujisawa, T. Takata, J. N. Kondo, M. Hara, M. Kawai, Y. Matsumoto, K. Domen, *J. Phys. Chem. B* **2003**, *107*, 1798 – 1803.
[76] S. H. Wei, A. Zunger, *Phys. Rev. B* **1988**, *37*, 8958 – 8981.
[77] This effect should not affect the conduction band edge, as known for ZnO; see Ref. [76].
[78] P. Ji, M. Takeuchi, T.-M. Cuong, J. Zhang, M. Matsuoka, M. Anpo, *Res. Chem. Intermed.* **2010**, *36*, 327 – 347.
[79] H. Tada, Q. Jin, H. Nishijima, H. Yamamoto, M. Fujishima, S.-i. Okuoka, T. Hattori, Y. Sumida, H. Kobayashi, *Angew. Chem.* **2011**, *123*, 3563 – 3567; *Angew. Chem. Int. Ed.* **2011**, *50*, 3501 – 3505.
[80] H. Yu, H. Irie, Y. Shimodaira, Y. Hosogi, Y. Kuroda, M. Miyauchi, K. Hashimoto, *J. Phys. Chem. C* **2010**, *114*, 16481 – 16487.
[81] a) J. R. Darwent, A. Mills, *J. Chem. Soc. Faraday Trans. 2* **1982**, *78*, 359 – 367; b) K. Sayama, K. Mukasa, R. Abe, Y. Abe, H. Arakawa, *J. Photochem. Photobiol. A* **2002**, *148*, 71 – 77.
[82] A. Kudo, K. Ueda, H. Kato, I. Mikami, *Catal. Lett.* **1998**, *53*, 229 – 230.
[83] Y. Sasaki, A. Iwase, H. Kato, A. Kudo, *J. Catal.* **2008**, *259*, 133 – 137.
[84] W. Schindler, F. Knoch, H. Kisch, *Chem. Ber.* **1996**, *129*, 925 – 932.
[85] H. Kisch, H. Weiss, *Adv. Funct. Mater.* **2002**, *12*, 483 – 488.
[86] M. Gärtner, V. Dremov, P. Mueller, H. Kisch, *ChemPhysChem* **2005**, *6*, 714 – 718.
[87] H. Kisch, P. Lutz, *Photochem. Photobiol. Sci.* **2002**, *1*, 240 – 245.
[88] M. Aldemir, PhD Thesis, University of Erlangen-Nürnberg, **2006**.
[89] a) K. R. Gopidas, M. Bohorquez, P. V. Kamat, *J. Phys. Chem.* **1990**, *94*, 6435 – 6440; b) N. Serpone, P. Maruthamuthu, P. Pichat, E. Pelizzetti, H. Hidaka, *J. Photochem. Photobiol. A* **1995**, *85*, 247 – 255.
[90] S. Sakthivel, S. U. Geissen, D. W. Bahnemann, V. Murugesan, A. Vogelpohl, *J. Photochem. Photobiol. A* **2002**, *148*, 283 – 293.
[91] O. Carp, C. L. Huisman, A. Reller, *Progr. Solid State Chem.* **2004**, *32*, 33 – 177.
[92] a) W. Macyk, H. Kisch, *Chem. Eur. J.* **2001**, *7*, 1862 – 1867; b) W. Macyk, G. Burgeth, H. Kisch, *Photochem. Photobiol. Sci.* **2003**, *2*, 322 – 328.
[93] a) H. P. Boehm, M. Herrmann, *Z. Anorg. Allg. Chem.* **1967**, *352*, 156 – 167; b) M. Herrmann, H. P. Boehm, *Z. Anorg. Allg. Chem.* **1969**, *368*, 73 – 86; c) R. Flaig-Baumann, M. Herrmann, H. P. Boehm, *Z. Anorg. Allg. Chem.* **1970**, *372*, 296.
[94] Z.-M. Dai, G. Burgeth, F. Parrino, H. Kisch, *J. Organometal. Chem.* **2008**, *694*, 1049 – 1054.
[95] H. Kominami, K. Sumida, K. Yamamoto, N. Kondo, K. Hashimoto, Y. Kera, *Res. Chem. Intermed.* **2008**, *34*, 587 – 601.
[96] Q. Jin, M. Fujishima, H. Tada, *J. Phys. Chem. C* **2011**, *115*, 6478 – 6483.
[97] a) H. Irie, S. Miura, K. Kamiya, K. Hashimoto, *Chem. Phys. Lett.* **2008**, *457*, 202 – 205; b) M. Liu, X. Qiu, M. Miyauchi, K. Hashimoto, *Chem. Mater.* **2011**, *23*, 5282 – 5286.
[98] H.-i. Kim, J. Kim, W. Kim, W. Choi, *J. Phys. Chem. C* **2011**, *115*, 9797 – 9805.
[99] a) R. Abe, M. Higashi, K. Domen, *ChemSusChem* **2011**, *4*, 228 – 237; b) A. Kudo, Y. Miseki, *Chem. Soc. Rev.* **2009**, *38*, 253 – 278.
[100] R. Asahi, T. Morikawa, T. Ohwaki, K. Aoki, Y. Taga, *Science* **2001**, *293*, 269 – 271.
[101] a) T. Ohno, T. Mitsui, M. Matsumura, *Chem. Lett.* **2003**, *32*, 364 – 365; b) T. Ohno, M. Akiyoshi, T. Umebayashi, K. Asai, T. Mitsui, M. Matsumura, *Appl. Catal. A* **2004**, *265*, 115 – 121.
[102] S. Sakthivel, M. Janczarek, H. Kisch, *J. Phys. Chem. B* **2004**, *108*, 19384 – 19387.
[103] a) X. Qiu, C. Burda, *Chem. Phys.* **2007**, *339*, 1 – 10; b) C. Di Valentin, E. Finazzi, G. Pacchioni, A. Selloni, S. Livraghi, M. C. Paganini, E. Giamello, *Chem. Phys.* **2007**, *339*, 44 – 56.
[104] S. Sato, *Chem. Phys. Lett.* **1986**, *123*, 126 – 128.

[105] a) S. Sakthivel, H. Kisch, *ChemPhysChem* **2003**, *4*, 487 – 490; b) R. Beranek, B. Neumann, S. Sakthivel, M. Janczarek, T. Dittrich, H. Tributsch, H. Kisch, *Chem. Phys.* **2007**, *339*, 11 – 19.

[106] a) Y. Yamamoto, S. Moribe, T. Ikoma, K. Akiyama, Q. Zhang, F. Saito, S. Tero-Kubota, *Mol. Phys.* **2006**, *104*, 1733 – 1737; b) Y. Cong, J. Zhang, F. Chen, M. Anpo, *J. Phys. Chem. C* **2007**, *111*, 6976 – 6982.

[107] H. Kisch, S. Sakthivel, M. Janczarek, D. Mitoraj, *J. Phys. Chem. C* **2007**, *111*, 11445 – 11449.

[108] R. Bacsa, J. Kiwi, T. Ohno, P. Albers, V. Nadtochenko, *J. Phys. Chem. B* **2005**, *109*, 5994 – 6003.

[109] a) N. Serpone, *J. Phys. Chem. B* **2006**, *110*, 24287 – 24293; b) V. N. Kuznetsov, N. Serpone, *J. Phys. Chem. B* **2006**, *110*, 25203 – 25209; c) A. V. Emeline, N. V. Sheremetyeva, N. V. Khomchenko, V. K. Ryabchuk, N. Serpone, *J. Phys. Chem. C* **2007**, *111*, 11456 – 11462; d) V. N. Kuznetsov, N. Serpone, *J. Phys. Chem. C* **2007**, *111*, 15277 – 15288.

[110] D. Mitoraj, H. Kisch, *Angew. Chem.* **2008**, *120*, 10123 – 10126; *Angew. Chem. Int. Ed.* **2008**, *47*, 9975 – 9978.

[111] D. Mitoraj, R. Beranek, H. Kisch, *Photochem. Photobiol. Sci.* **2010**, *9*, 31 – 38.

[112] a) A. G. Koryakin, V. A. Gal'perin, A. N. Sarbaev, A. I. Finkel'shtein, *Zh. Org. Khim.* **1971**, *7*, 972 – 977; b) B. Jürgens, E. Irran, J. Senker, P. Kroll, H. Mueller, W. Schnick, *J. Am. Chem. Soc.* **2003**, *125*, 10288 – 10300.

[113] N. E. A. El-Gamel, L. Seyfarth, J. Wagler, H. Ehrenberg, M. Schwarz, J. Senker, E. Kroke, *Chem. Eur. J.* **2007**, *13*, 1158 – 1173.

[114] a) X. Wang, K. Maeda, X. Chen, K. Takanabe, K. Domen, Y. Hou, X. Fu, M. Antonietti, *J. Am. Chem. Soc.* **2009**, *131*, 1680 – 1681; b) K. Maeda, X. Wang, Y. Nishihara, D. Lu, M. Antonietti, K. Domen, *J. Phys. Chem. C* **2009**, *113*, 4940 – 4947.

[115] J. Orth-Gerber, H. Kisch, U.S. Pat. Appl. Publ., US 20050226761, **2005**.

[116] a) S. Yin, M. Komatsu, Q. Zhang, F. Saito, T. Sato, *J. Mater. Sci.* **2007**, *42*, 2399 – 2404; b) C. Xu, R. Killmeyer, M. L. Gray, S. U. M. Khan, *Appl. Catal. B* **2006**, *64*, 312 – 317; c) W. Ren, Z. Ai, F. Jia, L. Zhang, X. Fan, Z. Zou, *Appl. Catal. B* **2007**, *69*, 138 – 144; d) L. Lin, W. Lin, Y. X. Zhu, B. Y. Zhao, Y. C. Xie, Y. He, Y. F. Zhu, *J. Mol. Catal. A* **2005**, *236*, 46 – 53; e) S. Y. Treschev, P.-W. Chou, Y.-H. Tseng, J.-B. Wang, E. V. Perevedentseva, C.-L. Cheng, *Appl. Catal. B* **2008**, *79*, 8 – 16; f) Y. Li, D.-S. Hwang, N. H. Lee, S.-J. Kim, *Chem. Phys. Lett.* **2005**, *404*, 25 – 29.

[117] a) C. Lettmann, K. Hildenbrand, H. Kisch, W. Macyk, W. F. Maier, *Appl. Catal. B* **2001**, *32*, 215 – 227; b) G. Yu, Z. Chen, Z. Zhang, P. Zhang, Z. Jiang, *Catal. Today* **2004**, *90*, 305 – 312; c) Y.-H. Tseng, C.-S. Kuo, C.-H. Huang, Y.-Y. Li, P.-W. Chou, C.-L. Cheng, M.-S. Wong, *Nanotechnology* **2006**, *17*, 2490 – 2497.

[118] a) H. Irie, Y. Watanabe, K. Hashimoto, *Chem. Lett.* **2003**, *32*, 772 – 773; b) H. Liu, A. Imanishi, Y. Nakato, *J. Phys. Chem. C* **2007**, *111*, 8603 – 8610; c) E. A. Konstantinova, A. I. Kokorin, S. Sakthivel, H. Kisch, K. Lips, *Chimia* **2007**, *61*, 810 – 814; d) Y. Cheng, H. Sun, W. Jin, N. Xu, *Chem. Eng. J.* **2007**, *128*, 127 – 133; e) K. Nagaveni, G. Sivalingam, M. S. Hegde, G. Madras, *Appl. Catal. B* **2004**, *48*, 83 – 93; f) C.-S. Kuo, Y.-H. Tseng, C.-H. Huang, Y.-Y. Li, *J. Mol. Catal. A* **2007**, *270*, 93 – 100.

[119] a) H. Irie, S. Washizuka, K. Hashimoto, *Thin Solid Films* **2006**, *510*, 21 – 25; b) Y. Choi, T. Umebayashi, M. Yoshikawa, *J. Mater. Sci. Lett.* **2004**, *39*, 1837 – 1839.

[120] a) J. Riga, J. J. Pireaux, R. Caudano, J. J. Verbist, *Phys. Scr.* **1977**, *16*, 346 – 350; b) R. Larsson, B. Folkesson, *Chem. Scr.* **1976**, *9*, 148 – 150; c) J. Schnadt, J. N. O'Shea, L. Patthey, J. Schiessling, J. Krempasky, M. Shi, N. Martensson, P. A. Bruhwiler, *Surf. Sci.* **2003**, *544*, 74 – 86.

[121] X. Zhang, M. Zhou, L. Lei, *Carbon* **2006**, *44*, 325 – 333.

[122] C. Di Valentin, G. Pacchioni, A. Selloni, *Chem. Mater.* **2005**, *17*, 6656 – 6665.

[123] a) P. Zabek, J. Eberl, H. Kisch, *Photochem. Photobiol. Sci.* **2009**, *8*, 264 – 269; b) P. Zabek, H. Kisch, *J. Coord. Chem.* **2010**, *63*, 2715 – 2726.

[124] M. Hidai, Y. Mizobe, *Chem. Rev.* **1995**, *95*, 1115 – 1133.

[125] D. Sellmann, W. Weiss, *Angew. Chem.* **1978**, *90*, 295 – 296; *Angew. Chem. Int. Ed. Engl.* **1978**, *17*, 269 – 270.

[126] G. N. Schrauzer, T. D. Guth, *J. Am. Chem. Soc.* **1977**, *99*, 7189 – 7193.

[127] a) E. Endoh, J. K. Leland, A. J. Bard, *J. Phys. Chem.* **1986**, *90*, 6223 – 6226; b) N. N. Lichtin, K. M. Vijayakumar, *J. Indian Chem. Soc.* **1986**, *63*, 29 – 34; c) V. Augugliaro, F. D'Alba, L. Rizzuti, M. Schiavello, A. Sclafani, *Int. J. Hydrogen Energy* **1982**, *7*, 851 – 855; d) M. M. Khader, N. N. Lichtin, G. H. Vurens, M. Salmeron, G. A. Somorjai, *Langmuir* **1987**, *3*, 303 – 304; e) H. Miyama, N. Fujii, Y. Nagae, *Chem. Phys. Lett.* **1980**, *74*, 523 – 524; f) N. N. Rao, S. Dube, Manjubala, P. Natarajan, *Appl. Catal. B* **1994**, *5*, 33 – 42; g) M. I. Litter, J. A. Navío, *J. Photochem. Photobiol. A* **1996**, *98*, 171 – 181; h) P. L. Yue, F. Khan, L. Rizzuti, *Chem. Eng. Sci.* **1983**, *38*, 1893 – 1900; i) M. M. Taqui Khan, D. Chatterjee, M. Bala, *J. Photochem. Photobiol. A* **1992**, *67*, 349 – 352; j) J. Soria, J. C. Conesa, V. Augugliaro, L. Palmisano, M. Schiavello, A. Sclafani, *J. Phys. Chem.* **1991**, *95*, 274 – 282; k) A. Sclafani, L. Palmisano, M. Schiavello, *Res. Chem. Intermed.* **1992**, *18*, 211 – 226; l) L. Palmisano, V. Augugliaro, A. Sclafani, M. Schiavello, *J. Phys. Chem.* **1988**, *92*, 6710 – 6713.

[128] a) K. Hoshino, M. Inui, T. Kitamura, H. Kokado, *Angew. Chem.* **2000**, *112*, 2558 – 2561; *Angew. Chem. Int. Ed.* **2000**, *39*, 2509 – 2512; b) K. Hoshino, R. Kuchii, T. Ogawa, *Appl. Catal. B* **2008**, *79*, 81 – 88.

[129] a) D. L. Boucher, J. A. Davies, J. G. Edwards, A. Mennad, *J. Photochem. Photobiol. A* **1995**, *88*, 53 – 64; b) J. G. Edwards, J. A. Davies, D. L. Boucher, A. Mennad, *Angew. Chem.* **1992**, *104*, 489 – 491; *Angew. Chem. Int. Ed. Engl.* **1992**, *31*, 480 – 482.

[130] a) O. Rusina, A. Eremenko, G. Frank, H. P. Strunk, H. Kisch, *Angew. Chem.* **2001**, *113*, 4115 – 4117; *Angew. Chem. Int. Ed.* **2001**, *40*, 3993 – 3995; b) O. Rusina, O. Linnik, A. Eremenko, H. Kisch, *Chem. Eur. J.* **2003**, *9*, 561 – 565.

[131] S. K. Gupta, V. Rajakumar, P. Grieveson, *Metall. Trans. B* **1991**, *22*, 711 – 716.

[132] O. Linnik, H. Kisch, *Photochem. Photobiol. Sci.* **2006**, *5*, 938 – 942.

[133] P. Pichat, M. N. Mozzanega, J. Disdier, J. M. Herrmann, *Nouv. J. Chim.* **1982**, *6*, 559 – 564.

[134] a) P. Calza, C. Minero, A. Hiskia, E. Papaconstantinou, E. Pelizzetti, *Appl. Catal. B* **2001**, *29*, 23 – 34; b) M. Lewandowski, D. F. Ollis, *J. Catal.* **2003**, *217*, 38 – 46.

[135] a) G. N. Schrauzer, J. G. Palmer, *Z. Naturforsch. B* **2001**, *56b*, 1354 – 1359; b) G. N. Schrauzer, J. G. Palmer, *Z. Naturforsch. B* **2003**, *58*, 820.

[136] G. N. Schrauzer, N. Strampach, L. N. Hui, M. R. Palmer, J. Salehi, *Proc. Natl. Acad. Sci. USA* **1983**, *80*, 3873 – 3876.

[137] a) R. G. Bergman, *Nature* **2007**, *446*, 506; b) T. Gräning, *Nachr. Chem.* **2007**, *55*, 836 – 840.

[138] H. Ramloch, G. Taeuber, *Chem. Unserer Zeit* **1979**, *13*, 157 – 162.

[139] J. Shang, Y. Zhu, Y. Du, Z. Xu, *J. Solid State Chem.* **2002**, *166*, 395 – 399.

[140] B. Kraeutler, A. J. Bard, *J. Am. Chem. Soc.* **1978**, *100*, 5985 – 5992.

[141] a) S. Yanagida, K. Mizumoto, C. Pac, *J. Am. Chem. Soc.* **1986**, *108*, 647 – 654; b) M. Anpo, M. Sunamoto, M. Che, *J. Phys. Chem.* **1989**, *93*, 1187 – 1189; c) S. Kodama, S. Yagi, *J. Phys. Chem.* **1989**, *93*, 4556 – 4561.

[142] a) H. Ikezawa, C. Kutal, *J. Org. Chem.* **1987**, *52*, 3299 – 3303; b) H. Al-Ekabi, P. De Mayo, *J. Phys. Chem.* **1986**, *90*, 4075 – 4080.

[143] a) A. M. Draper, M. Ilyas, P. De Mayo, V. Ramamurthy, *J. Am. Chem. Soc.* **1984**, *106*, 6222 – 6230; b) A. Maldotti, R. Amadelli, C. Bartocci, V. Carassiti, *J. Photochem. Photobiol. A* **1990**, *53*, 263 – 271; c) C. M. Wang, T. E. Mallouk, *J. Am. Chem. Soc.* **1990**, *112*, 2016 – 2018; d) R. A. Barber, P. De Mayo, K. Okada, *Chem. Commun.* **1982**, 1073 – 1074; e) M. Ilyas, P. De Mayo, *J. Am. Chem. Soc.* **1985**, *107*, 5093 – 5099.

[144] a) M. A. Fox, T. L. Pettit, *J. Org. Chem.* **1985**, *50*, 5013 – 5015; b) P. Boarini, V. Carassiti, A. Maldotti, R. Amadelli, *Langmuir* **1998**, *14*, 2080 – 2085.

[145] a) C. Joyce-Pruden, J. K. Pross, Y. Li, *J. Org. Chem.* **1992**, *57*, 5087 – 5091; b) F. Mahdavi, T. C. Bruton, Y. Li, *J. Org. Chem.* **1993**, *58*, 744 – 746; c) B. Ohtani, H. Osaki, S. Nishimoto, T. Kagiya, *J. Am. Chem. Soc.* **1986**, *108*, 308 – 310.

[146] a) G. Hörner, P. Johne, R. Kunneth, G. Twardzik, H. Roth, T. Clark, H. Kisch, *Chem. Eur. J.* **1999**, *5*, 208 – 217; b) R. Künneth, C. Feldmer, H. Kisch, *Angew. Chem.* **1992**, *104*, 1102 – 1103; *Angew. Chem. Int. Ed. Engl.* **1992**, *31*, 1039 – 1040.

[147] a) M. Schmittel, A. Burghart, *Angew. Chem.* **1997**, *109*, 2658 – 2699; *Angew. Chem. Int. Ed. Engl.* **1997**, *36*, 2550 – 2589; b) T. Linker, M. Schmittel, *Radikale und Radikalionen in der Organischen Synthese*, Wiley-VCH, Weinheim, **1998**.

[148] a) M. A. Fox, *Top. Curr. Chem.* **1987**, *142*, 71 – 99; b) S. Marinković, N. Hoffmann, *Eur. J. Org. Chem.* **2004**, 3102 – 3107; c) N. Hoffmann, *Pure Appl. Chem.* **2007**, *79*, 1949 – 1958; d) F. Su, S. C. Mathew, L. Möhlmann, M. Antonietti, X. Wang, S. Blechert, *Angew. Chem.* **2011**, *123*, 683 – 686; *Angew. Chem. Int. Ed.* **2011**, *50*, 657 – 660.

[149] a) W. Hetterich, H. Kisch, *Chem. Ber.* **1988**, *121*, 15 – 20; b) N. Zeug, J. Bücheler, H. Kisch, *J. Am. Chem. Soc.* **1985**, *107*, 1459 – 1465; c) R. Künneth, G. Twardzik, G. Emig, H. Kisch, *J. Photochem. Photobiol. A* **1993**, *76*, 209 – 215.

[150] a) S. Yanagida, T. Azuma, Y. Midori, C. Pac, H. Sakurai, *J. Chem. Soc. Perkin Trans. 2* **1985**, 1487 – 1493; b) S. Yanagida, H. Kawakami, Y. Midori, H. Kizumoto, C. Pac, Y. Wada, *Bull. Chem. Soc. Jpn.* **1995**, *68*, 1811 – 1823.

[151] a) A. W. Adamson, *Physical Chemistry of Surfaces*, *4th ed.*, Wiley, New York, **1982**; b) P. C. Hiemenz, *Principles of Colloid and Surface Chemistry*, *2nd ed.*, Marcel Dekker, New York, **1986**.

[152] Q. Zhang, Z. Xu, J. A. Finch, *J. Colloid Interface Sci.* **1995**, *169*, 414 – 421.

[153] a) L. Spanhel, M. Haase, H. Weller, A. Henglein, *J. Am. Chem. Soc.* **1987**, *109*, 5649 – 5655; b) A. Henglein, *Ber. Bunsenges. Phys. Chem.* **1982**, *86*, 301 – 305.

[154] G. Hoerner, PhD thesis, Universiät Erlangen-Nürnberg, **2000**.

[155] L. Lunazzi, G. Placucci, L. Grossi, *Tetrahedron* **1983**, *39*, 159 – 163.

[156] F. Wilkinson, *Chemical Kinetics and Reaction Mechanism*, Van Nostrand Reinhold, Workinghan, **1980**.

[157] A. Reinheimer, R. Van Eldik, H. Kisch, *J. Phys. Chem. B* **2000**, *104*, 1014 – 1024.

[158] a) G. O. Schenck, H. Formanek, *Angew. Chem.* **1958**, *70*, 505; b) R. C. Cookson, I. D. R. Stevens, C. T. Watts, *Chem. Commun.* **1965**, 259 – 260; c) R. Askani, *Chem. Ber.* **1965**, *98*, 2551 – 2555.

[159] a) I. Rosenthal, D. Elad, *Tetrahedron* **1967**, *23*, 3193 – 3204; b) G. Ahlgren, *J. Org. Chem.* **1973**, *38*, 1369 – 1374; c) I. Ninomiya, T. Naito, *Photochemical Synthesis*, Academic Press, New York, **1989**.

[160] B. H. Al-Sader, R. J. Crawford, *Can. J. Chem.* **1970**, *48*, 2745 – 2754.

[161] R. Memming, *Top. Curr. Chem.* **1988**, *143*, 79 – 112.

[162] D. Chan, J. W. Perram, L. R. White, T. W. Healy, *J. Chem. Soc. Faraday Trans. 1* **1975**, *71*, 1046 – 1057.

[163] a) K. Schäfer, *Landolt-Börnstein*, *Zahlenwerte und Funktionen*, *Vol. 6*, Springer, Berlin, **1969**; b) K. R. Srinivasan, R. L. Kay, *J. Solution Chem.* **1977**, *6*, 357 – 367; c) D. W. Brazier, G. R. Freeman, *Can. J. Chem.* **1969**, *47*, 893 – 899; d) M. G. Gonikberg, *Chemical Equilibria and Reaction Rates at High Pressure*, Israel Program for Scientific Translations, Jerusalem, **1963**.

[164] M. Miyahara, S. Iwasaki, T. Kotera, T. Kawamura, M. Okazaki, *J. Colloid Interface Sci.* **1995**, *170*, 335 – 339.

[165] O. S. Andersen, S. W. Feldberg, *J. Phys. Chem.* **1996**, *100*, 4622 – 4629.

[166] a) T. Asano, W. J. Le Noble, *Chem. Rev.* **1978**, *78*, 407 – 489; b) R. Van Eldik, T. Asano, W. J. Le Noble, *Chem. Rev.* **1989**, *89*, 549 – 688; c) A. Drljaca, C. D. Hubbard, R. Van Eldik, T. Asano, M. V. Basilevsky, W. J. Le Noble, *Chem. Rev.* **1998**, *98*, 2167 – 2289; d) N. S. Isaacs, *Liquid Phase High Pressure Chemistry*, Wiley, Chichester, **1981**.

[167] a) A. E. Nicholson, R. G. W. Norrish, *Discuss. Faraday Soc.* **1956**, *22*, 104 – 113; b) M. Yokawa, Y. Ogo, *Makromol. Chem.* **1976**, *177*, 429 – 436.

[168] a) H. Keck, W. Schindler, F. Knoch, H. Kisch, *Chem. Eur. J.* **1997**, *3*, 1638 – 1645; b) A. Reinheimer, A. Fernandez, H. Kisch, *Z. Phys. Chem.* **1999**, *213*, 129 – 133; c) M. Hopfner, H. Weiss, D. Meissner, F. W. Heinemann, H. Kisch, *Photochem. Photobiol. Sci.* **2002**, *1*, 696 – 703; d) H. C. Pehlivanugullari, E. Sumer, H. Kisch, *Res. Chem. Intermed.* **2007**, *33*, 297 – 309; e) M. Gärtner, J. Ballmann, C. Damm, F. W. Heinemann, H. Kisch, *Photochem. Photobiol. Sci.* **2007**, *6*, 159 – 164.

[169] a) K. Takaki, Y. Tsubaki, S. Tanaka, F. Beppu, Y. Fujiwara, *Chem. Lett.* **1990**, 203 – 204; b) H. Thies, H. Schoenenberger, K. H. Bauer, *Arch. Pharm.* **1960**, *293/65*, 67 – 73.

[170] a) S. J. Jin, S. Araki, Y. Butsugan, *Bull. Chem. Soc. Jpn.* **1993**, *66*, 1528 – 1532; b) B. Mauze, M. L. Miginiac, *Bull. Soc. Chim. Fr.* **1973**, 1832 – 1838; c) R. Arous-Chtara, J. L. Moreau, M. Gaudemar, *J. Soc. Chim. Tunis.* **1980**, *3*, 1 – 11.

[171] A. Mills, G. Williams, *J. Chem. Soc. Faraday Trans. 1* **1987**, *83*, 2647 – 2661.

[172] H. Weiß, H. Kisch, PhD Thesis, University of Erlangen-Nürnberg, **2003**.

[173] S. Kohl, PhD Thesis, University of Erlangen-Nürnberg, **2007**.

[174] M. Aldemir, H. Kisch, *Photochem. Photobiol. Sci.* **2012**, *11*, 908 – 913.

[175] T. Arndt, B. Guessregen, A. Hohl, J. Reis, *Clin. Chim. Acta* **2005**, *359*, 125 – 131.

[176] a) J. Kollonitsch, L. Barash, F. M. Kahan, H. Kropp, *Nature* **1973**, *243*, 346 – 347; b) J. Kollonitsch, L. M. Perkins, A. A. Patchett, G. A. Doldouras, S. Marburg, D. E. Duggan, A. L. Maycock, S. D. Aster, *Nature* **1978**, *274*, 906 – 908.